The Causes and Consequences of Urban Heat Islands*

Tridevi Chakma† Jonathan Colmer John Voorheis

November 1, 2023

Please click here for the latest version.

Abstract

This paper studies the causes and consequences of urban heat islands. Combining new administrative data with a novel proxy for experienced temperature at the neighborhood scale, we show that a hot day increases mortality by six additional deaths per 100,000 for the elderly population living in neighborhoods with a high concentration of impervious surfaces, relative to the median. These patterns hold even within counties and cannot be explained by selection. Moreover, the increase in mortality among elderly Black Americans following a hot day is three times that of elderly White Americans, and half of this disparity can be attributed to Black individuals living in more impervious neighborhoods. We then present suggestive evidence that imperviousness is driven by density zoning policies, and document that the racial incidence of density is reflected in a long historical process since the Great Migration.

*Correspondence: tchakma@g.harvard.edu. Affiliations: Chakma—Harvard Kennedy School, Harvard University; Colmer—Department of Economics, University of Virginia; Voorheis—U.S. Census Bureau. All errors and omissions remain our own. Any opinions and conclusions expressed herein are those of the authors and do not represent the views of the U.S. Census Bureau. The Census Bureau has ensured appropriate access and use of confidential data and has reviewed these results for disclosure avoidance protection (Project 7505723; Disclosure Authorization Numbers CBDRB-FY23-0450, CBDRB-FY23-0520 and CBDRB-FY24-0031).

†I would like to thank Nathan Hendren, Joe Aldy, and Marcella Alsan for their continued guidance and support. I am grateful to the participants of the Occasional Workshop in Environmental and Resource Economics, the Northeast Workshop on Energy Policy and Environmental Economics, the Heartland Environmental and Resource Economics Workshop, the AERE Summer Conference, and the Harvard Economics and Social Policy Seminar for valuable feedback. I gratefully acknowledge financial support from the Washington Center for Equitable Growth and the Harvard Joint Center for Housing Studies. I thank Alexander Sahn for generously sharing zoning data from his paper 'Racial Diversity and Exclusionary Zoning: Evidence from the Great Migration'. Thanks to Nanditha Menon for excellent research assistance.

1 Introduction

Urban neighborhoods—where constructed structures are highly concentrated and greenery is limited—are known to experience higher temperatures than outlying areas in a phenomenon known as the 'urban heat island' effect. Cities replace trees, which naturally cool the air, with impervious structures such as buildings and pavements, which absorb heat and increase local temperatures on hot days. Even within cities, temperatures can vary substantially over a short distance with variations in the built environment (Grimmond 2007). Heat has detrimental effects on health, and the climate crisis is poised to exacerbate the effect of extreme heat on health (IPCC 2021). With 80 percent of the U.S. population living in cities, urban heat could pose a serious public health concern (Census Bureau 2022).[1] Urban heat islands are also a salient environmental justice issue. Using satellite-derived measures of land surface temperature, Benz & Burney (2021) and Hsu et al. (2021) show that disparities in land surface temperature across neighborhoods are correlated with the racial composition and average income of the neighborhood. Using individual-level data, Chakma et al. (2023) document substantial racial disparities in heat exposure, even within the same commuting zone and after conditioning on individual income.

Although scientists have known about urban heat islands for over two centuries (Howard 1818), we do not have a comprehensive understanding of the health effects and drivers of urban heat islands, and their racial incidence. In this paper, we combine new administrative data for the population of the U.S. with a novel proxy for air temperature at the neighborhood-scale to estimate the mortality impacts of heat stress in urban heat islands. Our proxy for localized experienced temperature explicitly accounts for the neighborhood's built environment. We estimate separate mortality effects of exposure to hot days for the Black and White populations, and find significant disparities in outcomes. This motivates subsequent analyses of the role of density zoning, housing market restrictions, and the Great Migration in the creation of urban heat islands characterized by disproportionately Black populations.

There are two key challenges in estimating the mortality effects of urban heat islands—measurement and selection. First, there are no ground truth measures of air temperature ('experienced temperature') at the neighborhood scale across the U.S.. The canonical papers in the environmental economics literature estimate the temperature–mortality relationship at the county level (Deschênes & Moretti 2009, Deschênes & Greenstone 2011, Carleton et al. 2022) or state level (Barreca et al. 2016, 2015), with the notable exception of Heutel

[1]The urban heat island effect does not only occur during the day but also at night, when the difference can be even starker (Zhao et al. 2014). High overnight temperatures place a particularly high physiological burden on the human body, increasing the risk of heat-related illness and death (Thompson 2023).

et al. (2021) who estimate this relationship at the zip-code level. In the U.S. context, the authors proxy for actual air temperature by taking an inverse-distance weighted average of measurements from a sparse network of weather stations.[2] As only 10 percent of the 72,000 Census tracts in the U.S. contain an active weather station in 2019, these interpolations are likely to smooth out local temperature fluctuations. This measurement challenge is further complicated by the fact that the urban built environment increases local temperatures on hot days. Unlike plants and vegetation which naturally cool the air on hot days, the urban built environment is characterized by a high concentration of impervious structures—such as buildings and pavements—that absorb and release the heat into the atmosphere on hot days (Grimmond 2007).

To address this measurement issue, we combine conventional measures of air temperatures imputed from weather stations ('imputed temperature'), with high-resolution satellite-derived data on the urban built environment, which predicts experienced temperatures at the neighborhood-scale on hot days. The urban built environment has multiple components including, but not limited to buildings, roads, parks and trees. We use neighborhood imperviousness—defined as the share of the Census tract's land area that is covered in constructed surfaces, such as buildings and pavements—as a summary measure of the built environment.[3] Our imperviousness data comes from the National Land Cover Database (NLCD) and has a resolution of 30 meters $\times$ 30 meters, which corresponds to around 9 billion grid cells within contiguous U.S.. We aggregate this high-resolution data up to the Census tract level. To allow for the mortality effects of a hot day to vary non-linearly, we rank all Census tracts in the U.S. and construct deciles of imperviousness. We proxy for experienced air temperature at the neigborhood scale based on the Census tract's decile of imperviousness, interacted with daily imputed air temperature from weather stations.[4] Results will be presented for each decile; for simplicity, we refer to Census tracts in the top decile as 'urban heat islands'. We combine these data with newly assembled individual-level micro-data on residential location, demographics and mortality from the Environmental Impacts Frame (Voorheis et al. 2023). This allows us to characterize race- and age- specific mortality on a fine geographic scale, down to the Census tract.[5]

Second, in order to interpret differences in mortality rates in urban heat islands compared

[2]Carleton et al. (2022) estimate the global temperature–mortality relationship at a level equivalent to U.S. counties. The authors use both model-derived and spatially interpolated gridded air temperature data, at a resolution of 0.25–1°, or 27 km to 110 km.

[3]Imperviousness is highly correlated with population density and tree cover, and can be thought of as a summary measure of a multi-dimensional urban built environment.

[4]The existing literature proxies for experienced temperature solely using the latter.

[5]Additionally, unlike recent work using Medicare administrative records, we can accurately characterize all-cause mortality for the entire population, not just the elderly Medicare-eligible population.

to other tracts as the causal effect of higher experienced temperatures, we need to rule out possible selection. Those who live in more impervious Census tracts may have differential baseline health or access to healthcare. To address this, we include a set of high-dimensional fixed effects at the Census tracts by day-of-the-year and state-year levels. This means that we exploit random shocks to daily imputed temperatures at the Census tract-level, on the same day-of-the-year. These fixed effects also absorb mean differences in mortality rates across Census tracts. However, those who live in urban heat islands may be more susceptible to hot days than those living in other tracts, for example, due to differences in underlying conditions or access to healthcare. To rule out this possibility, we implement placebo tests based on all non-hot days, including cold days. We exploit the fact that both extreme cold and extreme heat increase mortality. Because cold weather does not interact with the built environment in a meaningful way, extreme cold should not deferentially increase the death rate in impervious places, unlike extreme heat, which leads to higher temperatures in more impervious neighborhoods. Conditional on fixed effects, if higher mortality rates in the most impervious Census tracts are due to selection, we would expect these differences to persist on cold days, and possibly other non-hot days.

We present comprehensive, neighborhood-scale evidence that a hot day leads to a larger increase mortality in urban heat islands—the top decile of Census tracts ranked by imperviousness—compared to the other tracts. Consistent with the idea that the built environment elevates local experienced temperature in ways that are not captured by the existing network of weather stations, we find that on hot days over 32°C (i.e., 90°F), urban heat islands experience the largest increase in mortality relative to a 17–22°C day (i.e., 62–72°F). On a hot day, the mortality rate for the over-65 population increases by 2.5 deaths per 100,000 in tracts with median imperviousness but by 8.5 deaths per 100,000 in the most impervious tracts. This means that the over-65 populations living in the urban heat islands experience 6 additional deaths per 100,000 on days when temperatures exceed 32°C (i.e., 90°F) compared to those living in communities with median imperviousness. Are these effects driven by differences between impervious and non-impervious counties, or are there meaningful variations within counties? We show that most of this effect operates at a hyper-local scale; within the same county on the same date, the over-65 populations living in the most impervious communities experience 4.5 additional deaths per 100,000 on days when temperatures exceed 32°C (i.e., 90°F), compared to those living in communities with median imperviousness. This suggests that for mortality, hyper-local variations in heat are important.

We implement the placebo tests: although a cold day also leads to elevated mortality, this impact does not vary by neighborhood imperviousness. We also find that mortality does not vary by imperviousness in other non-hot days. These results suggest that the

increase in mortality in the most impervious tracts on hot days is unlikely to be explained by selection alone. We find that a cold day increases the mortality rate for the over-65 population by 2 deaths per 100,000 in communities with median imperviousness, and 1.4 per 100,000 in the most impervious communities. The results are also robust to a number of alternative specifications and explanations. We rule out the possibility that the results are driven by the oldest of the over-65 population living in the most impervious Census tracts. We show that the results hold even in places that experience extreme heat frequently and therefore may exhibit higher adaptation. Furthermore, we show that results cannot be explained by 'harvesting'—a period of high mortality followed by a period of low mortality. We also consider tree canopy cover and population density as alternative measures of the built environment. Consistent with our main results, we find that neighborhoods with the lowest level of tree canopy cover and highest population density see the largest increase in mortality.

The built environment is a complex result of policies and history. This motivates an exploration of the racial incidence of urban heat islands. Relative to White individuals, Black individuals are more likely to live in neighborhoods characterized by a greater share of impervious surfaces, higher density, lower tree canopy, and higher land surface temperatures in summer months (Benz & Burney 2021, Hsu et al. 2021, Chakma et al. 2023). Black individuals also have a lower life expectancy and a higher incidence of chronic diseases for a multitude of reasons, including but not limited to lack of access to healthcare and structural racism (IOM 2003, Arias et al. 2017). It is also possible that Black individuals have differential access to air conditioning. Motivated by this, we first investigate the baseline relationship between imputed temperature and mortality separately for Black and White individuals, ignoring the effects of the built environment. We find that the elderly Black population experience much larger increases in mortality rates compared to the elderly White population on both hot and cold days. Following a hot day, mortality for the over-65 White population increases by 1.9 deaths per 100,000, or 1.8 percent relative to the race-specific mean. In contrast, mortality for the over-65 Black population increases by 5.6 deaths per 100,000, or 6.2 percent relative to the race-specific mean.

To what degree can the racial differences in the temperature and mortality relationship be explained by differences in exposure to higher experienced temperatures, as opposed to differences in underlying health or adaptation? Both the elderly Black and elderly White populations living in the most impervious tracts see the largest increase in mortality on hot days. A decomposition of the effects, inspired by the Kitagawa–Oaxaca–Blinder method, shows that about half of the Black–White gap in mortality on hot days in temperate and continental climates can be attributed to differences in tract imperviousness. These results

suggest that urban built environment may be contributing to racial health disparities.

In light of these results, we examine the determinants of neighborhood imperviousness and its racial incidence that drive these racial health disparities. We examine how historical factors and policies contribute to local variation in imperviousness at the neighborhood scale and, consequently, the location of urban heat islands and who inhabits these neighborhoods. Imperviousness is closely related to urban population and housing density. Economic theory predicts that density is driven by agglomeration and dispersion forces as well as productive amenities that determine the location of economic activity. Across U.S. cities, housing market restrictions disrupt this process. Historically, racial discrimination and institutions have restricted where Black households could live, with potential consequences for density. Since the mid-20th century, land-use regulations have restricted density of housing construction by location (Hsieh & Moretti 2019, Herkenhoff et al. 2018, Ganong & Shoag 2017). At a macro scale, housing supply restrictions affect growth, wealth accumulation, and geographic mobility (Hsieh & Moretti 2019, Herkenhoff et al. 2018, Ganong & Shoag 2017, Deryugina & Molitor 2021). At a micro scale, zoning restricts housing supply and increases housing prices in the neighborhoods where restrictions bind (Kulka et al. 2023, Turner et al. 2014, Song 2021, Shanks 2021, Monarrez & Schönholzer 2022). Such regulations are, at least in part, motivated by a desire for racial segregation and are shown to widen racial inequality (Rothstein 2017, Shertzer et al. 2016, Trounstine 2018, Cui 2022).

We provide suggestive evidence that density zoning regulations affect the local distribution of impervious surfaces, tree cover, and urban heat today. Using four large cities as case studies—Boston, Baltimore, Chicago, and Pittsburgh—we study the effect of density zoning on tree cover, impervious surfaces, and urban heat through a spatial discontinuity design along zoning district boundaries within municipalities. Following Kulka et al. (2023), we focus on zoning boundaries within municipalities, holding constant local policies that could change across municipal borders. We find that density regulations decrease tree cover and increase share of impervious surfaces and, consequently, surface temperature on the side of the boundary with higher regulated density. For the Greater Boston area, we find that tree cover is 5 percentage points (p.p.) lower, and the share of impervious surfaces is 7 p.p. higher on the side of the boundary with higher regulated density. The mean tree cover and share of impervious surfaces across zoning districts are 22 percent and 60 percent, respectively, indicating that the estimated effects are economically significant. Correspondingly, land surface temperature on the side of the boundary with higher regulated density is 0.6°C higher on hot days. We find similar patterns in Baltimore, Chicago, and Pittsburgh, suggesting that these results may generalize across a broader set of cities.

The built environment is also a product of history. To explore this, we use racial com-

position changes induced by the Great Migration to study the long-run determinants of the built environment and its racial incidence. Using racial composition shocks during the Great Migration as a natural experiment, this paper examines the historical origins of differential imperviousness at the neighborhood-scale. During the Great Migration, between 1940 and 1970, four million Black Americans moved from the U.S. South to urban areas in the North and West. Previous literature has shown that the Great Migration transformed the racial demographics of destination cities, prompting White flight from urban neighborhoods, altering the policies of local governments, and changing access to opportunity in destination cities (Boustan 2010, Derenoncourt 2022, Tabellini 2020). These policies could also have affected neighborhood density and urban form in ways that affect the distribution of imperviousness today. Historically, racial discrimination and institutions have restricted neighborhoods that Black households could live in (Ondrich et al. 1998, Rothstein 2017, Li 2023), with potential consequences for density. We show that in response to a city-wide Black population shock, historically Black neighborhoods experience a greater increase in density relative to White neighborhoods. Using parcel-level zoning data, combined with historical neighborhood-level data for Great Migration destination cities, we find that these neighborhoods are more likely to be zoned for higher density land-uses today.

This paper contributes to several strands of the literature. First, we present new quasi-experimental evidence on the hyper-local nature of the temperature–mortality relationship, bringing into sharp focus the role of the built environment in moderating these effects.[6] While there is piecemeal evidence on urban heat islands and mortality,[7] we present the most comprehensive estimates of the mortality effects of urban heat islands on hot days. Second, we contribute to the wider literature on environmental inequality (Banzhaf et al. 2019),[8] and racial health disparities (IOM 2003, Arias et al. 2017, Murphy et al. 2017, Williams & Cooper 2019, Alsan et al. 2019, Bailey et al. 2021). To our knowledge, we are the first to estimate racial disparities in the causal effect of temperature on mortality. Third, this paper contributes towards our understanding of how segregation endogenously affected the creation of urban heat islands and its racial incidence (Cutler et al. 1999, Card et al. 2008, Andrews et al. 2017, Akbar et al. 2019, Shertzer et al. 2016, Li 2023).

[6]See Deschênes (2014) for a review of the empirical literature on temperature, health and adaptation literature.

[7]For a review of the evidence on heat islands and health, see Gronlund (2014).

[8]This literature has mostly focused on the unequal distribution of air pollution and polluting sources (Currie et al. 2020, Colmer et al. 2020, Mohai et al. 2009).

2 The mortality effects of urban heat islands

2.1 Measurement of urban heat islands

Urban heat islands are a hyper-local phenomenon, as temperatures can vary substantially over a short distance with variations in the built environment (Grimmond 2007). To illustrate this, consider an example of two neighborhoods in Middlesex county in the Greater Boston area during a heat wave in 2019. The Inner Belt neighborhood of Somerville, MA, has a tree canopy cover of 13 percent and 92 percent of its land area is covered in impervious surfaces. Three miles west, the neighborhood of West Cambridge in Cambridge, MA has a tree canopy cover of 37 percent and 51 percent of the land area is covered in impervious surfaces. On 29 July 2019, as part of the Urban Heat Island Mapping campaign, volunteers measured the local ambient air temperature across the Greater Boston area by mounting sensors to cars.[9] Data from the campaign show that the ambient temperature in West Cambridge was 32.3°C (i.e., 90.2°F), whereas the temperature in the Inner Belt area was 33.6°C (i.e., 92.5°F). A small increase in temperature can have large health effects on hot days because the temperature–mortality relationship is convex (Carleton et al. 2022, Barreca et al. 2016, Deschênes & Greenstone 2011). Figure 1b presents the average ambient temperature at the tract-level based on the data from the campaign for Cambridge and Somerville, MA. Consistent with the presence of urban heat island effects, the tract-level average ambient temperatures in these two cities on 29 July 2019 correlate strongly and positively with the tract's share of impervious surfaces, as shown in Figure 1a. The correlation between the two is 0.74.[10]

While data from the Urban Heat Island campaign are valuable, they capture static data for a cross-section of neighborhoods often on a single day, as opposed to continuous weather station data, and are only available for a handful of cities.[11] Consequently, these data are not suitable for studying the mortality effects and racial incidence of urban heat islands. There are no ground truth measures of daily air temperature at the neighborhood scale across the U.S.. Canonical papers in the environmental economics literature that estimate the temperature–mortality relationship in the U.S. proxy for experienced temperature by taking an inverse-distance weighted average based on measurements from a sparse network of weather stations (Deschênes & Moretti 2009, Deschênes & Greenstone 2011, Barreca et al. 2016, 2015, Heutel et al. 2021). There are around 72,000 Census tracts in the U.S., and only around 7,200 active weather stations in NOAA's Global Historical Climate Network

[9] Data from the Boston chapter of the campaign is available here.

[10] The correlation between tree canopy cover and ambient temperature in this data is -0.58.

[11] For more details on the Urban Heat Island Mapping Campaign, see here.

('GHCN') database as of 2019. This means that for 9 in 10 Census tracts, air temperatures need to be imputed based on nearby weather stations. Moreover, weather stations are more likely to be located in rural areas or in the outskirts of urban areas, rather than near the densely built urban center. Figure 2 shows weather stations located within 20 miles of Cambridge and Somerville MA. There were no weather stations in either of these cities in 2019. Daily imputed temperature for all tracts in Cambridge and Somerville are based on temperature measurements averaged from the same set of weather stations, with different weights assigned depending on the distance between the weather station and the Census tract's centroid.

Imputed temperatures from weather stations that are located in the outskirts of a city are likely to smooth out local variations in actual temperature and systematically understate temperatures in densely built urban neighborhoods. Cities are built in ways that amplify heat.[12] They replace trees and the natural environment with impervious structures—such as buildings and pavement—built with concrete, brick and asphalt. On hot days, trees and vegetation cool the atmosphere through transpiration, a process in which heat energy is absorbed by the evaporation of water. In contrast, impervious surfaces contribute to higher local temperatures on hot days in two ways. First, these surfaces have a low *albedo*, which increases the amount of energy from solar radiation they absorb.[13] Second, these surfaces do not contain water that can be evaporated, meaning that the absorbed energy is instead released through conduction, convection, or radiation.[14] The combination of these factors means that more impervious neighborhoods in cities are hotter than less densely built areas in the outskirts.

The location of the weather stations outside city centers, combined with the fact that the built environment increases local temperature, suggests that imputing temperature from weather stations will lead to an understatement of local experienced temperatures in highly impervious neighborhoods. Figure 1c shows the Census tract-level imputed temperatures from the weather stations for Cambridge and Somerville on 29 July 2019. There is little spatial variation in imputed temperature at the tract level, indicating that the imputation masks substantial local spatial heterogeneity. Figure 1d presents the measurement error—calculated as the ambient temperature from the Urban Heat Island Mapping campaign, less the imputed temperature—at the Census tract level for Cambridge and Somerville. While

[12]For a textbook treatment of the earth's energy balance and the formation of urban heat islands, see this explanation from NASA.

[13]Albedo indicates what percentage of the incoming solar radiation (sunlight) is reflected by a surface. Darker colored surfaces have lower albedo and thus absorb more heat.

[14]Conduction transfers heat to cooler air that directly touches the hot surface. Convection occurs when air warmed by the surface rises upward, moving heat away from the surface. Infrared radiation is detected as heat, like the warmth felt from a fire.

the average temperature overall is accurate, the measurement errors are positive and large in more impervious neighborhoods. The correlation between the measurement error and imperviousness at the tract level is 0.7. To show that measurement errors are larger in more impervious neighborhoods more broadly, we use ground truth air temperature data from all active weather stations in 2019 for contiguous Unites States. Figure 3a shows the share of Census tracts that contain one or more weather stations in each decile of imperviousness. Over 18 percent of tracts in the least impervious decile contain at least one weather station, whereas less than 1 percent of tracts in the most impervious decile contain a weather station. For each Census tract containing a weather station, we identify other weather stations that are located within a 20-mile radius of the centroid of the Census tract, but located in areas that belong to a different decile of the imperviousness distribution. Using these subset of weather stations, we spatially interpolate the daily air temperature for the impervious Census tracts based on inverse-distance weighting ('imputed temperature'), leaving out the weather stations located inside the Census tract that capture the actual air temperature. Figure 3b presents the mean measurement error, calculated as actual minus imputed air temperature, for Census tracts in each decile of imperviousness. Again, we find that the measurement errors are positive and larger for the most impervious decile of Census tracts.

Motivated by the fact that actual temperatures are systematically higher than imputed temperatures in more impervious neighborhoods on hot days, we construct a novel proxy for experienced temperature at the Census tract-level for the contiguous U.S., combining conventional measures imputed temperature from weather stations with high-resolution satellite-derived data on the urban built environment. On hot days, we expect experienced temperature to be higher than imputed temperature in highly impervious tracts. Because imperviousness can be measured at a hyper-local level, we interact imputed temperatures from weather stations with tract-level imperviousness to construct a better proxy for experienced temperature at the neighborhood scale. Our hypothesis is as follows: the built environment, as measured by neighborhood imperviousness, increases local experienced temperature in highly impervious neighborhoods, which in turn could affect health.

2.2 Data

2.2.1 Experienced temperature

Our proxy for experienced temperature combines data from two sources: high resolution satellite-derived data on the urban built environment from the National Land Cover Database (NLCD) and daily imputed air temperatures calculated from weather stations included in the National Oceanic and Atmospheric Administration's (NOAA) Global Historical Climate

Network.

The urban built environment is multi-faceted, consisting of human-made structures such as buildings and roads, as well as parks and trees. We use neighborhood imperviousness—defined as the share of the Census tract's land area that is covered in impervious surfaces, such as buildings and pavements—as a measure of the built environment. Imperviousness is strongly correlated with other elements of the built environment, such as tree canopy cover and population density, and can be thought of as a summary measure of the urban built environment.[15] We obtain gridded data on imperviousness from the National Land Cover Database (NLCD) for the years 2019, 2016, 2013, 2011, 2008, 2006, 2004, and 2001. Imperviousness is a stock and changes very slowly. Over our sample period, the rank–rank correlation is 0.98. As such, we treat imperviousness as a cross-sectional measure of the urban built environment. The NLCD provides data at a 30 meters $\times$ 30 meters resolution, which corresponds to around 9 billion grid cells within contiguous U.S..[16]

We aggregate this to data to the Census tract level, by taking an average of all grid cells that fall within the Census tract boundary. In the years where NLCD data are not available, we impute tract imperviousness by linearly interpolating between the values calculated from the NLCD. To capture potential non-linearities in the temperature–mortality relationship by imperviousness, we rank all Census tracts in the U.S. by the deciles of imperviousness. Figure A4 presents the distribution of tract imperviousness for the U.S. and the deciles of tract imperviousness. In the bottom decile of the distribution of Census tracts by imperviousness, less than nine percent of the land area is covered in impervious surfaces. In the top decile, more than 70 percent of the land area is covered in impervious surfaces. There is wide variation in the built environment in the top decile of Census tracts. The top decile of Census tracts have a mean imperviousness of 80 percent, with some tracts going up to 98 percent imperviousness.[17] The top decile of Census tracts have a mean tree canopy cover of 13 percent, with tree cover as low as 1 percent in some tracts.

We combine the decile of tract imperviousness with conventional air temperature measures imputed from weather stations. Here, we follow the imputation methods commonly used in the existing literature, although we conduct the analysis at a finer geographical scale (i.e., the Census tract level). Specifically, we obtain daily minimum and maximum temperatures from NOAA's GHCN database for the years 2000–2019, which provides weather

[15]The correlation between imperviousness and tree canopy cover is -0.74. The correlation between log imperviousness and log population density is 0.88. For completeness, we will also present our main result using tree canopy cover and population density as a measure of the built environment, instead of imperviousness.

[16]The accuracy of the 2019 NLCD is close to 90%. https://www.usgs.gov/publications/thematic-accuracy-assessment-nlcd-2019-land-cover-conterminous-united-states.

[17]The standard deviation is 6.4 p.p..

station-level data across the United States. For each Census tract, we construct daily maximum and minimum temperatures as the inverse-distance weighted average of all available maximum and minimum temperatures for stations within 20 miles of the Census tract centroid, following the monitor aggregation method used by Currie & Neidell (2005), Beatty & Shimshack (2014), and Heutel et al. (2021). The daily average imputed temperature is defined as the midpoint of the daily maximum and minimum temperatures. Following the existing literature, we construct discrete temperature bins. We proxy for experienced temperature at the Census tract level by interacting the Census tract's imperviousness decile, with binned daily imputed temperatures.

2.2.2 Mortality

We combine our proxy for localized experienced temperature with new Census tract-level mortality data for the years 2000–2019 constructed from confidential micro-data using the Census Bureau's Environmental Impacts Frame (EIF) (Voorheis et al. 2023). The EIF provides detailed individual-level information on demographics, economic characteristics, and address-level histories for almost every resident in the United States over the past two decades. Importantly, the EIF micro-data infrastructure includes individual-level data on the date of birth, the date of death, race, and the Census tract of residence in the year of death for nearly all residents in the United States.

We aggregate the individual-level mortality data from the EIF by age group and race. This paper is the first to construct mortality rates by age and race from the EIF data. We calculate mortality for three age groups—those below 5 years old, those who are 5 to 64 years old, and those 65 and over. We further divide the over-65 age group into three age bins—age 65–74, 75–84, and over 85. Within each age group and bin, we calculate mortality for all individuals, as well as separately for Non-Hispanic White and Non-Hispanic Black individuals. This results in 18 race-by-age groups. For each Census tract, and for each combination of race and age groups, we tabulate the number of daily deaths and the number of individuals alive in the beginning of the year. Using these tabulations, we calculate daily tract-level mortality rates for a given race-by-age group. Following Heutel et al. (2021), we define the daily mortality rate for each tract and each race-by-age group as those who died within a given time-frame (e.g., three days) of the index date as a fraction of all residents belonging to that age-by-race group who were alive in that tract in the beginning of the year. The daily mortality data for each race-by-age group contains around 450 million observations ($\approx$ 61,500 tracts $\times$ 20 years $\times$ 365 days). We present here the results for the over-65 population, as the elderly are particularly vulnerable to extreme heat. Appendix B presents the results for those under 5 years old and for 5–64 year olds.

2.2.3 Climate zones

For our main analysis, we restrict our sample to Census tracts in temperate and continental climates. 85.2 percent of the U.S. population live in temperate and continental climates, while 12.7 percent live in arid climates. Urban-rural differences in day time temperatures strongly vary by background climate (Zhao et al. 2014). Urban heat island effects are especially pronounced in temperate and continental climates, where the urban built environment replaces trees and forests that naturally cool the air. Some examples of cities in temperate and continental climates include New York, Boston, D.C.. Chicago, Nashville, Atlanta, Jacksonville, Houston, Seattle and San Francisco, among others. In contrast, in arid climates, urbanization replaces deserts, rocky surfaces and shrubs (Chakraborty et al. 2020). These natural surfaces in arid climates have low albedo and do not contain much water and, consequently, they interact with the surface energy balance in a similar way to the built environment.[18] Examples of cities in arid climate include Las Vegas and Phoenix. Results for arid climates are presented in Appendix A.

2.2.4 Definition of key terms

For the purpose of exposition and clarity, we adopt the following definitions.

- *Imperviousness*—share of a Census tract's land area that is covered in impervious surfaces, such as buildings and pavements.
- *Imputed temperature*—the inverse-distance weighted average temperature at the Census tract level, imputed from air temperature measurements at weather stations.
- *Experienced temperature*—the ground truth air temperature at the Census tract level.
- *Hot day*—a day in which the imputed temperature exceed 32°C (i.e., 90°F).
- *Cold day*—a day in which the imputed temperature is between -13°C to -8°C(i.e., 9–18°F).
- *Urban heat islands*—Census tracts in the highest decile of the distribution of Census tract imperviousness.

[18]In Figure A1, we plot the relationship between tract imperviousness and land surface temperature by climate zone. Consistent with the scientific literature, we find that in continental and temperate climates, imperviousness and land surface temperature are strongly correlated (correlation of 0.84), whereas in arid climates, the two are largely uncorrelated (correlation of 0.07). Figure A2a shows the geographic distribution of various climate zones.

2.3 Impact of temperature on mortality: without imperviousness

To provide a point of comparison for our main results and to the existing literature, we first estimate the causal effects of temperature on tract-level mortality using the imputed temperature measures based on weather stations, without accounting for the effects of the built environment on local temperatures.

2.3.1 Empirical strategy

Following the existing literature, we leverage random shocks in daily imputed temperature to identify this effect. Our primary outcome of interest, $mortality_{ajt}$, is the number of deaths per 100,000 in a Census tract j for a given age group a within three days after index date t, scaled by the number of individuals in age group a in tract j who were alive in the beginning of the year. We estimate the following equation:

$$mortality_{ajt} = \sum_{b} \beta_b tempbin^b_{jt} + \alpha_{jd(t)} + \theta_{s(j)y(t)} + \varepsilon_{ajt} \tag{1}$$

The parameters of interest are β_b, the coefficients on the binned daily imputed temperature, $tempbin^b_{jt}$, which takes on the value 1 if the daily imputed temperature in tract j on date t is in bin b. The set of temperature bins include 5°C (i.e., 9°F) bins ranging from $<$ -13°C (i.e., 9°F) to $>$ 32°C (i.e., 90°F), excluding the 17–22°C (i.e., 63–72°F) range as the reference bin. Figure A3 summarizes the distribution of imputed temperature over 2000–2019 across each of the 11 temperature bins. We include state-by-year fixed effects, $\theta_{s(j)y(t)}$, to control for arbitrary annual shocks that may vary by state, such as healthcare policy changes. This also controls for state-level economic conditions and adaptation evolving over time. We include Census tract by day-of-the-year fixed effects, $\alpha_{jd(t)}$, where $d(t)$ is the day-of-the-year corresponding to date t.[19] These fixed effects account for daily seasonal patterns in mortality that may vary at the Census tract-level. All regressions are weighted by the Census tract's population belonging to the age group. Standard errors are clustered by county.

β_b is identified based on variation in daily temperature in tract j across years on a specific day of the year (e.g., July 1). The identification assumption is that for any given day-of-the-year, whether the day is hot in a given year, is random. For example, suppose that 1 July 2003 in tract A is hot, but 1 July 2002 is not. Our specification compares the number of people who died following 1 July 2003 in tract A, with the number of people who died following 1 July 2002 in the same tract. As we hold the Census tract constant over time, we are comparing people living in the same tract in over time.

[19] As an example, 1 July 2003 is a date, whereas 1 July is the day-of-the-year.

2.3.2 Baseline results without imperviousness

Consistent with previous literature, we find a U-shaped relationship, with elevated three-day mortality rates following very cold and very hot days. Figure 4 presents the results from estimating equation 1 for the over-65 population, with three-day mortality rates as the outcome variable. Relative to a day in 17–22°C (i.e., 63–72°F), a day over 32°C (i.e., 90°F) increases the three-day mortality for the population aged 65 and over by 2.4 deaths per 100,000. Similarly, a cold day between -13°C to -8°C (i.e., 9–18 °F) increases the three-day mortality for the over-65 population by 2.2 deaths per 100,000. Notably, cold days between -13°C to -8°C (i.e., 9–18°F) and hot days over 32°C (i.e., 90°F) have similar mortality effects. Mean mortality rate for those aged 65 and over is 65.8 per 100,000. Because mortality rates are highest in the over 65 population, who are most vulnerable to temperature shocks, we focus on results for this age group in this section. Detailed results for the other two age groups are presented in Appendix B.

2.4 The impact of temperature on mortality: with imperviousness

2.4.1 Heterogeneity by imperviousness

We interpret the coefficients on a hot day over 32°C (i.e., 90°F) as the average treatment effect of a generally hot day, as measured by imputed temperatures. Because imputed temperatures are likely to understate the experienced temperatures in neighborhoods with a high concentration of impervious surfaces, this average treatment effect is likely to mask heterogeneity by imperviousness. To illustrate this, we first adopt a simple dichotomous definition of urban heat islands. In section 2.4.2, we relax this definition and present results for each decile. We refer to Census tracts in the top decile of imperviousness as being in urban heat islands, and all other Census tracts as not being in urban heat islands. We estimate equation 1 separately for tracts in the top decile of imperviousness and all other tracts. Figure 5 presents the coefficients on binned imputed temperature for tracts in urban heat islands and tracts not in urban heat islands. We find that the over-65 population living in Census tracts in the top decile see a substantially larger increase in mortality compared to all other tracts on hot days, but not on cold days.

2.4.2 Main specification

The results presented in section 2.4 capture the heterogeneous impact of a hot day in urban heat islands. However, these effects could either be driven by experienced temperatures being higher than imputed temperatures in urban heat islands, or because of selection—those who

live in urban heat islands maybe different from those who do not. To disentangle these two channels, we present results for each decile separately, and examine the effect of temperature on mortality using our proxy for local experienced temperature.

We estimate the following equation:

$$mortality_{ajt} = \sum_{d=1}^{10} \beta_{d,hot} Impervious_j \times \mathbf{1}\{HotDays\}_{jt} + \sum_{d=1}^{10} \beta_{d,other} Impervious_j \times \mathbf{1}\{OtherDays\}_{jt} + \alpha_{jd(t)} + \theta_{s(j)y(t)} + \varepsilon_{jt} \quad (2)$$

where $Impervious_j$ is the decile of the imperviousness distribution that the Census tract belongs to. For simplicity, we refer to Census tracts in the top decile as urban heat islands.

$\mathbf{1}\{HotDays\}_{jt}$ is an indicator variable taking on the value 1 when the daily temperature exceeds 32°C (i.e., 90°F). $\mathbf{1}\{OtherDays\}_{jt}$ indicates when t is not a hot day, and the daily temperature is outside the reference temperature (i.e., 17–22°C, or 63–72°F). The coefficient of interest is $\beta_{d,hot}$, which captures the effect of a day over 32°C (i.e., 90°F) on mortality relative to the mortality rates when the temperature is between 17 and 22°C (i.e., 9–18°F), for the d'th decile of imperviousness. Because experienced temperatures in Census tracts in the top decile of the imperviousness distribution are likely to be higher than imputed temperatures, we expect the mortality effects of a hot day in urban heat islands, i.e., $\beta_{10,hot}$, to be higher than $\beta_{5,hot}$, the mortality effects of a hot day in the tracts with median imperviousness.

We include a set of high-dimensional fixed effects at the Census tracts by day-of-the-year $\alpha_{jd(t)}$ and state-year levels, $\theta_{s(j)y(t)}$. As in the specification in equation 1, the state-year fixed effects control for annual shocks that may vary by state. The tract by day-of-the-year fixed effects isolate random shocks to daily imputed temperature at the Census tract-level, on the same day-of-the-year (e.g., July 1) across year. All regressions are weighted by the Census tract's population belonging to the age group. Standard errors are clustered by county.

2.4.3 Main results with imperviousness

Figure 6 presents the estimates of $\beta_{d,hot}$ from equation 2 for the over-65 population in temperate and continental climates. $\beta_{d,hot}$ captures the effect of a day over 32°C (i.e., 90°F) on mortality rates, relative to a 17–22°C (i.e., 63–72°F) day, for each decile d of imperviousness. For Census tracts in the median (i.e., fifth) decile of imperviousness, a hot day increases mortality rates by 2.5 deaths per 100,000 relative to a 17–22°C (i.e., 63–72°F) day. In contrast, for Census tracts in the 10th decile of imperviousness, a hot day over 32°C (i.e., 90°F) increases mortality rates by 8.5 deaths per 100,000. The effect of a hot day on mortality rates for the top decile of imperviousness, $\beta_{10,hot}$, is significant and statistically different from

the effect of a hot day on mortality rates for any other decile of imperviousness. Compared to tracts in the median decile, the most impervious Census tracts see an additional increase of six deaths per 100,000 on a hot day. Consistent with the idea that local experienced temperatures are higher than imputed temperatures in the most impervious neighborhoods, the effects are concentrated in the most impervious Census tracts in the 10th decile of the national distribution, i.e., the urban heat islands.[20]

2.4.4 Placebo tests

Although $\mathbf{1}\{HotDays\}_{jt}$ is plausibly random in our main specification, imperviousness is not randomly assigned. In order to causally interpret variations in $\beta_{d,hot}$ by deciles of imperviousness as the effect of localized experienced temperature on mortality on hot days, we need to rule out possible selection. Those who live in more impervious Census tracts may have differential baseline health, and therefore be more susceptible to hot days. We address this selection issue in two ways. The high-dimensional Census tract by day-of-the-year fixed effects absorb mean differences in mortality rates due to unobserved characteristics of the tracts (e.g., proximity to hospitals) and the inhabitants (e.g., differences in baseline health). For each of the 61,500 Census tracts in our sample, we include 365 fixed effects for the days of the year, for a total of 22.5 million fixed effects in our main specification. These absorb daily seasonal patterns in mean mortality at the tract-level. However, those who live in urban heat islands may be more vulnerable to extreme heat than those living in other tracts, even after accounting for differences in baseline health. This could be due to differences in underlying conditions that interact with extreme heat (e.g., heart conditions).

To rule out this possibility, we implement a placebo test based on cold days which also interact with similar pre-existing health conditions. To benchmark this placebo analysis, recall that the estimated models without imperviousness indicate that a cold day increases mortality by 2.2. deaths per 100,000, whereas a hot day increases mortality by 2.4 deaths per 100,000 (section 2.3.2). Although cold days and hot days have different physiological effects on individuals, it is plausible that individuals with similar health risks and co-morbidities are susceptible to both temperature extremes. For example, both hot and cold temperatures are associated with causing cardiovascular and respiratory stress, although through different pathways (Huynen et al. 2001, Basu & Samet 2002, Deschênes & Moretti 2009, Barreca et al. 2016). Conditional on the fixed effects, if differences in mortality rates across tracts in different deciles of imperviousness are due to selection, we would expect these differences to

[20] As the temperature–mortality relationship is non-linear, we expect some non-linearity in the effect of imperviousness on mortality on hot days, even if imperviousness increased local temperature linearly. However, it is also plausible that the effect of imperviousness on local temperature is non-linear.

persist on cold days, and possibly on other non-hot days. Therefore, cold days can serve as a potentially valid placebo test.

Specifically, we test whether excess mortality rates vary by deciles of imperviousness on cold days—e.g., days between -13°C to -8°C (i.e., 9–18°F). We implement this placebo test by estimating the effects of a cold day on mortality rates relative to a 17–20°C (i.e., 63–72°F) day by deciles of imperviousness, replacing $\mathbf{1}\{HotDays\}_{jt}$ with $\mathbf{1}\{ColdDays\}_{jt}$. $\mathbf{1}\{ColdDays\}_{jt}$ is an indicator variable taking on the value 1 when the daily temperature is between -13°C and -8°C (i.e., 9–18°F). Here, $\mathbf{1}\{OtherDays\}_{jt}$ indicates when t is not a cold day and the daily temperature is outside the reference temperature (i.e., 17-22°C, or 63–72°F). We repeat this process for other non-hot days, replacing $\mathbf{1}\{HotDays\}_{jt}$ with indicator variables for the other temperature bins. Our hypothesis is that imperviousness affects mortality through its impact on local experienced temperatures on hot days. If imperviousness does not affect mortality on cold and otherwise non-hot days, and selection does not vary by temperature, then we would expect a level shift in mortality rates on cold and non-hot days relative to a 17–20°C (i.e., 63–72°F) day, which would not vary by tract imperviousness.

Figure 6 also presents estimates from the placebo test: the effect of a cold day between -13°C and -8°C (i.e., 9–18°F) on mortality rates relative to a 17–22°C (i.e., 63–72°F) day by deciles of imperviousness. In sharp contrast to the results for hot days, we find that the increase in mortality rates does not vary by tract imperviousness on cold days. For Census tracts in the median decile of imperviousness, a cold day increases mortality rates by 2.1 deaths per 100,000, whereas a cold day increases mortality rates by 1.4 deaths per 100,000 for tracts in the top decile. We find that cold days elevate mortality across the board. This suggests that, conditional on the tract-day and state-year fixed effects, those living in the more impervious tracts are not more vulnerable to cold temperature shocks than those living in less impervious tracts. We calculate coefficients for all non-hot temperature bins, by deciles of imperviousness. Figure 7 presents estimates of the effects of various temperature bins on mortality rates relative to a 17–22°C (i.e., 63–72°F) day by deciles of imperviousness. This figure shows that increases in mortality rates do not vary by tract imperviousness on any days, except on hot days. This suggests that, conditional on the tract-day and state-year fixed effects, the over-65 populations living in the more impervious tracts are not generally more vulnerable to dying. We cannot fully rule out the possibility that those with co-morbidities that only interact with hot temperatures, but not cold temperatures, select into the most impervious tracts. However, given that the over-65 population living in more impervious tracts are not more vulnerable on any non-hot days, we find it implausible that the effects can be explained by selection.

2.4.5 Impact of hyperlocal variations in experienced temperature on mortality

How much of this effect operates at a local level? Are we simply picking up differences between impervious and non-impervious counties, or are there meaningful variations within counties? To address this, we include county-by-date fixed effects in equation 2 in addition to tract by day-of-the-year and state-year fixed effects. This introduces an additional 20 million fixed effects, heavily saturating the data. The county-by-date fixed effects absorb mean differences across counties on a specific date (e.g., 1 July 2023), leaving us with within-county variations in imperviousness and mortality. Figure 8 shows the results from this specification. For Census tracts in the median decile of imperviousness, a hot day increases mortality by 1.1 deaths per 100,000, although this is not statistically significant. In contrast, for Census tracts in the top decile of imperviousness, a hot day increases mortality rates by 5.6 deaths per 100,000 relative to a 17–22°C (i.e., 63–72°F) day. Compared to the median Census tracts, mortality increases by an additional 4.5 deaths per 100,000 on a hot day in the most impervious Census tracts. This suggests that a substantial proportion—around 75 percent—of the variation in mortality is across tracts within the same county.

This result highlights the hyper-local nature of the temperature–mortality relationship, and provides evidence that the spatial variation in the built environment—even within the same county—has consequences for health on a hot day. This is in contrast to the existing literature which estimate the temperature–mortality relationship at the county level (Deschênes & Moretti 2009, Deschênes & Greenstone 2011, Carleton et al. 2022) or state level (Barreca et al. 2016, 2015).[21] Our results indicate that hyper-local variations in temperature are important for mortality.

2.4.6 Additional robustness checks

These results are robust to a number of specifications and alternative explanations.

Age bins above 65. We rule out the possibility that the results are driven by the oldest of the above-65 age group living in the most impervious Census tracts. In Figure A7, we present the results separately for three age bins above 65: ages 65–74, 75–84, and over 85. For each of the three age bins above 65, mortality rates are substantially higher for tracts in the most impervious decile. For Census tracts in the top decile of imperviousness, a hot day increases mortality rates by 3.6, 15.6, and 23.7 deaths per 100,000, respectively, for the 65–74, 75–84, and over-85 age bins. The differences between the median and the top deciles of imperviousness are 3, 10.7, and 25.5 deaths per 100,000, respectively, for the 65–74, 75–84,

[21] Heutel et al. (2021) estimate this relationship at the zip-code level; however, the authors proxy zip-code level temperature using inverse distance-weighted imputations based on weather stations, which do not capture local variations.

and over-85 age bins. Figure A8 presents the estimates of $\beta_{d,hot}$, pooling together the three age bins. For the pooled estimates, we define the three-day mortality rates for each age bin separately, and interact the fixed effects with age bin indicators. We find that the estimates are similar to those from our main specification. A hot day increases mortality by 1.4 deaths per 100,000 for the median tract and 8.1 deaths per 100,000 for tracts in the top decile of imperviousness, meaning that a hot day increases mortality by an additional 6.7 deaths per 100,000.

Adaptation. We examine whether differences in adaptation can explain variation in the temperature–mortality relationship by imperviousness. Curriero et al. (2002), Barreca et al. (2015, 2016) and Heutel et al. (2021) document that the impact of extreme heat on mortality is smaller in places that more frequently experience extreme heat due to increased adaptation; for example, through higher levels of air conditioning penetration. Following Heutel et al. (2021), we categorize the Census tracts into terciles based on their average annual cooling degree days (CDD) over the sample period. CDDs are based on daily average temperatures and are designed to reflect the energy needed to cool a building to a base temperature, typically 18°C (i.e., 65°F). For example, one day with an average temperature of 24°C (i.e., 75°F) represents 10 CDD, corresponding to the temperature being 10°F higher than the base, while a day with temperatures below 18°C (i.e., 65°F) represents 0 CDD. Annual CDD is the sum of daily CDD values across all days in the year, whereas average annual CDD represents the average of this value over 2000–2019. This allows us to identify the warmest third of Census tracts over the sample period. Figure A2b shows the geographic distribution of the terciles of average annual CDD. There are both warmer and cooler places within temperate and continental climates. We consider whether, for tracts that are in the temperate or continental climate zones, the relationship between imperviousness and mortality on hot days varies across warmer and cooler places. Figure A9 presents estimates of $\beta_{d,hot}$ from equation 2 by CDD. We see a similar pattern for tracts in the warmest tercile as well as tracts in the first and second terciles of CDD. However, effect sizes are larger for tracts that are cooler and experience extreme heat less frequently.

Harvesting. We consider whether the imperviousness–temperature–mortality relationship on hot days can be explained by 'harvesting', or short-term mortality displacement.[22] Following Heutel et al. (2021), to test for potential short-term harvesting effects we replace three-day mortality rates with seven- and 28-day mortality rates following the index date as the outcome variable in equation 2. If hot days displace mortality in the seven- and 28-day window that follows, then the point estimates for the effects of temperature on mortality

[22]Harvesting refers to a short period of excess mortality that is followed by a compensating period of mortality deficit.

would be lower for the longer window following a hot day. We find that the point estimates are higher, not lower, when the outcome variable is the seven-day or 28-day mortality rates. Figure A10 shows the estimates of $\beta_{d,hot}$ for the median and top decile from equation 2 where $mortality_{jad}$ represents the seven-day and 28-day mortality rates, respectively. Recall that for Census tracts in the top decile of imperviousness, three-day mortality increases by 8.5 deaths per 100,000 following a hot day. In contrast, a hot day increases the seven-day and 28-day mortality rates for tracts in the top decile by 14.8 and 19.4 deaths per 100,000, respectively, relative to a 17–22°C (i.e., 63–72°F) day. The elevated mortality rates over the longer time frame following a hot day is likely explained by multiple hot days occurring during the longer time frame. We find that a hot day is followed by 1.8 and 3 additional hot days in seven-day and 28-day windows that follow, suggesting that the effect of a hot day scales approximately linearly. The difference between the median and the top decile of imperviousness is 10.2 and 5.5 deaths per 100,000 respectively during the seven-day and 28-day windows following the index day. Results for 28-day mortality are noisy given repeated treatment—heatwaves with multiple hot-days in a row—and dynamic effects—i.e., early-season heatwaves are more deadly than late season heatwaves. Nevertheless, we believe the results presented here suggest that harvesting has limited ability to explain the effects of experienced temperature on mortality in highly impervious tracts on hot days.

Tree canopy cover. We use imperviousness as our summary measure of the urban built environment. Here we consider tree canopy cover as an alternative measure of the built environment. While imperviousness and tree canopy cover are strongly correlated (correlation coefficient = -0.62), the correlation is not perfect. To conduct this analysis, we rank all census tracts in the contiguous U.S. based on tree canopy cover, defined as the share of the tract's area shaded by trees. We replace $Impervious_{jt}$ in equation 2 with deciles of the tree canopy cover distribution that the Census tract belongs to. Here, Census tracts in the bottom decile, with the lowest levels of tree canopy cover, is most likely to exhibit urban heat island effects, i.e. higher experienced temperatures on hot days. Figure A11a shows the resulting estimates of $\beta_{d,hot}$ by deciles of tree canopy cover. We find that the over-65 population living in tracts in the lowest decile of tree canopy cover experience the largest increase in mortality on a hot day. In the median decile, a hot day increases the mortality rate by 0.7 deaths per 100,000, whereas in the bottom decile, a hot day increases the mortality rate by 5.2 deaths per 100,000. The mortality effects of a hot day increase gradually as tree canopy cover declines. In contrast, the increase in mortality rates on cold days does not vary by tree canopy cover. Next, we consider whether tree canopy cover is a better proxy for urban heat islands than imperviousness. To do this, we add an additional control for deciles of tree canopy cover interacted with $\mathbf{1}\{HotDays\}$ in equation 2. Figure A11b shows

the estimates of $\beta_{d,hot}$ from equation 2 for each decile of imperviousness, conditional on this control. We find that controlling for deciles of tree canopy cover interacted with indicators for hot days do not substantially alter the results from our main specification. Conditional on the interaction of tree canopy cover and $\mathbf{1}\{HotDays\}$, a hot day increases the mortality rate by 8.9 deaths per 100,000 in the most impervious Census tracts and 3.5 deaths per 100,000 in the median Census tracts. These results help us rationalize the use of imperviousness as a valid summary measure of the built environment.

Population density. Another alternative measure of the built environment is population density. The intensity of the urban built environment is often a function of population density. Figure A12a shows the effects of a hot day by deciles of population density, replacing $Impervious_{jt}$ in equation 2 with deciles of the tract population density distribution. We find that the mortality effects of a hot day increases with tract population density. For the over-65 population, a hot day increases the mortality rate by 0.3 deaths per 100,000 in the median tracts and by 8.2 deaths per 100,000 in the most densely populated tracts. In contrast, the effects of a cold day do not appear to increase with tract population density. Higher mortality rates in highly impervious tracts on hot days could be explained by population density rather than by imperviousness. To address this, we include an additional control for deciles of tract population density interacted with $\mathbf{1}\{HotDays\}$. Figure A12b shows the estimates of $\beta_{d,hot}$ from equation 2 after the inclusion of this control. Even though population density and imperviousness are strongly correlated, the results do not change substantially. We find that the effect of a hot day is increasing in tract imperviousness. A hot day increases the over-65 mortality by 5.7 deaths per 100,000 in the median tract and 9.6 deaths per 100,000 in the most impervious tracts.

Arid climates. Our main results are based on Census tracts in continental and temperate climate zones. Zhao et al. (2014) show that geographic variations in urban–rural differences in daytime temperatures strongly vary by background climate. Cities surrounded by forests have more pronounced heat islands than do cities in arid environments. In Figure A1, we plot the relationship between tract imperviousness and land surface temperature by climate zone. Consistent with the scientific literature, we find that in continental and temperate climates, imperviousness and land surface temperature are strongly correlated (correlation of 0.84), whereas in arid climates, the two are largely uncorrelated (correlation of 0.07). Figure A2a shows the geographic distribution of various climate zones. Our main results are based on temperate and continental climates. 85.2 percent of the U.S. population live in temperate and continental climates, while 12.7 percent live in arid climates. Here, we estimate equation 2 separately for Census tracts in arid climates. Imperviousness deciles are still based on the national distribution of tract imperviousness. Figure A5 shows the

distribution of population across deciles of tract imperviousness in arid and temperate or continental climate zones; a larger share of tracts in arid climates are in the higher deciles of imperviousness. Figure A6 presents the estimates of $\beta_{d,hot}$ from equation 2 for the over-65 population in arid climates. Unlike in temperate and continental climates, we do not see a large spike in mortality rates for the top decile.

3 The racial incidence of urban heat islands

In this section, we test whether the temperature–mortality relationship varies by race, and whether any racial disparities in the relationship can be attributed to the racial differences in the neighborhood built environment. To our knowledge, we are the first to present causal evidence on heterogeneity by race in temperature–mortality relationship.[23]

3.1 Motivation

Black individuals have a lower life expectancy and a higher incidence of chronic diseases for a multitude of reasons, including but not limited to, lack of access to healthcare and structural racism (IOM 2003, Arias et al. 2017). Differences in adaptation by race, such as differential access to air conditioning, could also lead to differences in heat exposure by race. Furthermore, relative to White individuals, Black individuals are more likely to live in neighborhoods characterized by a greater share of impervious surfaces, where experienced temperatures are higher than those indicated by imputed temperatures on hot days. A priori, these factors suggest that Black individuals may experience a larger increase in mortality than White individuals on a hot day.

Using land surface temperature data as a proxy for localized urban heat, and tract-level demographics data from the American Community Surveys (ACS), the existing literature documents that lower-income neighborhoods and neighborhoods with a higher Black population share are hotter (Benz & Burney 2021, Hsu et al. 2021). Using new Census micro-data infrastructure for the universe of U.S. residents, combined with satellite-derived land surface temperature data at the Census block-level, Chakma et al. (2023) document substantial racial disparities in land surface heat exposure within the same commuting zone, even after conditioning on individual-level income data. As an illustrative example, Figure 9 shows the raw correlation between neighborhood racial composition, imperviousness, and summer temperature within a single city—Detroit. Panel (a) of Figure 9 shows the Black population share at the Census block-group-level in 2019 in the Detroit commuting zone and panel (b)

[23]For a review of observational evidence on racial disparities in heat-related deaths, see Gronlund (2014).

shows the imperviousness of the block-groups in 2019. In panel (c), we present the average land surface temperature in summer 2019.[24] The correlation is apparent in the raw data—the Black population in Detroit is concentrated in areas that are covered in impervious surfaces and have higher summer surface temperature. This pattern generalizes across all Census tracts in our sample. Figure 11b shows the share of the total Black and White population that live in Census tracts belonging to each decile of imperviousness. Around 13 percent of the Black population live in Census tracts in the 10th decile of imperviousness, while less than four percent of the White population live in Census tracts in the 10th decile of imperviousness. Motivated by this, we examine the heterogeneity in the temperature–mortality relationship by race.

3.2 The impact of temperature on mortality by race: without imperviousness

To provide a point of comparison, we start by documenting the baseline relationship between imputed temperature and mortality—ignoring the effects of the built environment on locally experienced temperature—separately for Non-Hispanic White and Non-Hispanic Black individuals. We consider if there is heterogeneity by race in the imputed temperature–mortality relationship both in levels (i.e., deaths per 100,000) and in proportion (i.e., the percent increase in deaths relative to the race-specific baseline) and find substantial heterogeneity in the imputed temperature–mortality relationship by race. Figure 10 presents the results from estimating equation 1 separately for the Non-Hispanic White and Non-Hispanic Black populations over 65. Relative to a 17–22°C (i.e., 63–72°F) day, a hot day over 32°C (i.e., 90°F) increases mortality rates by 1.9 deaths per 100,000 for the Non-Hispanic White population over 65. In contrast, a hot day increases mortality rates by 5.3 deaths per 100,000 for the Non-Hispanic Black population over 65. The coefficients on a hot day are statistically different for the Black and White populations over 65. The Black mortality response to a hot day is higher than the White mortality response by 3.7 deaths per 100,000. The differential response to heat by race cannot be explained by racial differences in baseline mortality alone. Figure A13 presents the estimates for β_b in equation 1, replacing the outcome variable with *proportional* mortality, i.e., three-day mortality rates scaled by the race and age group-specific mean daily mortality rates over the sample period. For the White population, a day over 32°C (i.e., 90°F) increases mortality rates 1.9 percent relative to the

[24] Most evidence of localized urban heat island effects relies on satellite-derived land surface temperature measures, which are available at a fine-scale of geography (Shandas et al. 2019). Land surface temperature data measure how hot the ground is to touch. However, it is unclear whether land surface temperature is an accurate proxy for experienced temperature, which affects health.

mean, whereas the mortality rate increases by 5.1 percent for the Black population.

3.3 The impact of temperature on mortality by race: with imperviousness

Next, we estimate the effect of temperature on mortality using our proxy for experienced temperature, which interacts deciles of imperviousness with imputed temperatures, separately for the White and Black population. Figure 11a presents the estimates of $\beta_{d,hot}$ from equation 2 for the Black and White populations over 65 in temperate and continental climates. For both the Black and White populations over 65, the increase in mortality rates are the highest in the most impervious tracts (i.e., the urban heat islands) on hot days. Figures A14a and A14b present the cold day placebo test for the White and Black population respectively. For each of the Black and White population over 65, the increase in mortality rates does not vary by tract imperviousness on cold days, suggesting that the spike in mortality in the most impervious tracts is unlikely to be driven by selection alone.

For the White population over 65, a hot day increases mortality rates by 2.6 deaths per 100,000 and 6.8 deaths per 100,000, respectively, for tracts in the median and the 10th decile of imperviousness. The estimates for the Black population over 65 are larger. A hot day increases mortality among the elderly Black population by 6.7 deaths per 100,000 and 17.5 deaths per 100,000, respectively, for tracts in the median and the 10th decile of imperviousness. Relative to elderly White individuals living in neighborhoods with similar degree of imperviousness, elderly Black individuals experience larger increases in mortality rates in response to a hot day. These could be due to differences in baseline health or adaptation. For example, air conditioning could play a role in mitigating the temperature–mortality pathway, and differential access to air conditioning by race could result in racial disparities in exposure to heat. In addition, historical factors and pre-existing conditions or co-morbidities could result in the same level of heat having differential impacts by race. For example, differences in the quality and quantity of health care received by Black and White individuals could lead to ex-post differences in mortality even if heat exposure is the same.

3.4 Decomposing racial differences in the impact of temperature on mortality

While elderly Black individuals are more vulnerable to heat than White individuals living in tracts that belong to the same decile of imperviousness, Black individuals are also more likely to live in more impervious Census tracts. Figure 11b shows that the distribution of the

Black and White population across deciles of imperviousness are strikingly different. As local experienced temperatures are greater than those suggested by imputed temperatures in more impervious tracts, Black individuals may have exposure to higher experienced temperature due to differences in the built environment.

To what extent can the racial differences in temperature and mortality relationship be explained by the differences in exposure to imperviousness? We calculate the counterfactual effect of a hot day on Black mortality rates inspired by a Kitagawa–Oaxaca–Blinder style decomposition. Specifically, we calculate the average increase in mortality rates of the Black residents as if they lived in tracts with imperviousness that were drawn from the White distribution of tract imperviousness, as shown in Figure 11b. In practice, this amounts to calculating the weighted average of decile-specific increase in Black mortality in response to a hot day from Figure 11a, using as weights the distribution of neighborhood imperviousness for the White population from Figure 11b. We find that if Black individuals lived in tracts that followed the White distribution of tract imperviousness, Black mortality rate would have increased by 3.5 deaths per 100,000 following a hot day, in contrast to 5.3 deaths per 100,000. The Black–White gap in the temperature–mortality response would have been 1.8 deaths per 100,000, in contrast to 3.7 deaths per 100,000. This suggests that about half of the Black–White gap in the mortality response to a hot day can be attributed to differences in tract imperviousness.

4 The determinants of urban heat islands

Given the racial incidence of urban heat islands, and the consequences for inequalities in mortality, we next turn to examining the determinants of urban heat islands. Why did some neighborhoods develop into urban heat islands while others did not? What drives Black individuals to live in more impervious neighborhoods than White individuals? In sections 4.3 and 4.2, we consider the historical and policy determinants of urban heat islands.

4.1 Motivation

Mechanically, urban heat islands are created through the process of urbanization, but not all neighborhoods are created equal. Even within the same city, temperatures vary substantially over short distances as a function of land cover. Impervious surfaces—such as pavements, roads, and buildings—absorb and retain heat, while tree canopy counteracts higher temperatures. These local variations in temperature matter for mortality. In section 2, we show that on hot days, local imperviousness affects experienced temperature and matters for mor-

tality. Moreover, there are substantial racial disparities in neighborhood imperviousness and experienced temperature within the same city.

What are the causes of spatial variation in imperviousness that drive these local differences in temperature? Urban imperviousness is closely related to urban population density. Figure A15 presents the relationship between log imperviousness—the share of the land area covered in impervious surfaces—and log population density, using data on 11 million Census blocks in 2019. Log imperviousness and log population density are strongly and positively correlated, with a correlation coefficient of 0.88. Economic theory predicts that density is driven by agglomeration and dispersion forces as well as productive amenities that determine the location of economic activity. In this case, urban heat islands are a disamenity associated with proximity to productive amenities. Across U.S. cities, historical institutions and housing market restrictions disrupt this process. Since the mid-20th century, land-use regulations have restricted housing density by location. At a macro scale, housing supply restrictions affect growth, wealth accumulation, and geographic mobility. At a micro scale, zoning restricts housing supply and increases housing prices in the neighborhoods where restrictions bind. We hypothesize that zoning creates discontinuous changes in urban land cover and urban heat. Using a spatial discontinuity design along zoning district boundaries in four cities, we find that density regulations result in decreased tree cover, increased share of impervious surfaces, and, consequently, surface temperature on the side of the boundary with higher regulated density.

Zoning regulations were, at least in part, motivated by a desire for racial segregation (Rothstein 2017, Shertzer et al. 2016, Trounstine 2018, Cui 2022). Historically, racial discrimination and institutions have restricted where Black households could live, with potential endogenous consequences for density. Using the Great Migration as a natural experiment, we show that in response to a city-wide Black population shock, historically Black neighborhoods experience a greater increase in density relative to White neighborhoods. We find that these neighborhoods are more likely to be zoned for higher density land-uses today. We show that historical Great Migration shocks predict increased Black mortality on hot days, but not on moderate days. Taken together, the evidence presented in this section indicates that housing policies interact with migration shocks in ways that affect the distribution of heat-related amenities across urban neighborhoods.

4.2 The policy drivers of urban heat islands: evidence from density zoning regulations

Land-use regulations, which are ubiquitous across U.S. cities, often dictate the density with which housing can be built across parcels of land, in turn affecting the population density and imperviousness at the city block-level. How do land-use regulations affect the distribution of urban density and imperviousness? Using four cities as case studies—Greater Boston, Chicago, Pittsburgh, and Baltimore—we examine whether urban land-use changes discontinuously along zoning boundaries. We leverage a spatial discontinuity design along zoning district boundaries, with pixel-level (i.e., 30 meters $\times$ 30 meters) satellite-derived data on imperviousness, tree cover, and land surface temperature as outcome variables. We find a greater share of impervious surfaces, lower tree cover, and higher land surface temperature, on the side of the boundary with higher regulated density. These results provide suggestive evidence that the location of urban heat islands are, at least in part, driven by zoning regulations.

4.2.1 Data

Comprehensive analysis of zoning at the neighborhood-scale is challenging because cities do not follow standardized zoning practices, and the data, if available, are not often comparable across cities. In addition, in order to carry out a boundary discontinuity analysis, we need both parcel-level geospatial data on the zoning districts and a zoning code that provides sufficient information to calculate regulated density. As a result, we take a case study approach. We start our case study with the Greater Boston area, where complete data on parcel-level land-use zoning regulations are available from digitized zoning maps compiled by the Metropolitan Area Planning Council (MAPC) for their Zoning Atlas project. The Zoning Atlas includes data for 101 towns and municipalities in Greater Boston. The Zoning Atlas was constructed between 2010–2020 and provides a snapshot of zoning regulations. However, most zoning regulations were set during the early to mid-20th century with few zoning changes afterward.

To test whether patterns we see in Boston also apply in other cities, we augment this data by hand collecting geospatial zoning data and zoning codes for three other large cities—Baltimore, Chicago, and Pittsburgh. For each of these cities, we collect the zoning shape files and zoning codes, where available. Zoning shape files are digitized maps which contain information on the zoning codes and regulations that apply to each land parcel. Zoning codes are documents which set out the regulations for various 'codes'. For example, in Chicago, the zoning code 'RS1' refers to districts that allow single-family homes with a minimum lot

size of 6250 sq. ft., a maximum height of 30 feet, and a floor to area ratio of at most 50 percent. From the zoning codes, we collected information to be able to calculate the 'allowed density'—the maximum dwelling units per acre (DUPAC) of residential land. For each city and each residential and zoning codes, we hand collected the following data: minimum lot size, minimum lot size per unit, maximum number of units, maximum height, maximum number of floors, and the maximum floor to area ratio. Note that for Baltimore, Chicago, and Pittsburgh, we only collected data for the central cities, rather than the greater metropolitan area. For these cities, we only collected data for the central cities, rather than the greater metropolitan area. Consequently, parcels included for these cities are characterized by a higher degree of imperviousness, and less tree cover, than the larger Greater Boston area. The quality of hand-collected data is lower; zoning data are missing for non-residential land, and data for some parcels are missing due to incomplete zoning information needed to be able to calculate DUPAC.

DUPAC is constructed by counting the number of lots allowed on one acre following minimum lot size requirements and multiplying this number by the maximum allowable dwelling units for each parcel. This measure captures the zoning restrictions from minimum lot size requirements, as well as the maximum dwelling units allowed. This measure allows for comparisons across municipalities that regulate residential density in slightly different ways.

The outcome variables in our analysis are land-use data from the NLCD—namely tree canopy cover from 2016 and imperviousness data from 2019—at the *pixel*-level. Each pixel represents a 30 meters $\times$ 30 meters space on the surface of the Earth, allowing us to detect sharp changes over a short distance across zoning district boundaries. These data are cross-sectional. For each pixel falling within 300 meters (i.e., 1000 feet) of a zoning boundary, we calculate the distance to the boundary.

We also use Landsat land surface temperature as an outcome. Land surface temperature measures how hot the ground is to touch, and is not an accurate measure of experienced temperature. Furthermore, land surface temperature data is affected by cloud cover. In addition, Landsat data is only available at a temporal frequency of every two weeks. However, despite these issues, we include Landsat land surface temperature as an outcome due to its spatial granularity—the resolution of the data is 30 meters $\times$ 30 meters. For each city, we obtain all images taken during the summer months of June, July, and August. We restrict to images taken on extremely hot days, i.e., days in which the air temperature in the city exceeds 32°C (i.e. 90°F), over the years 2010–2019. We focus on extremely hot days because temperature variations have larger effects on health in the extremes.

Figure 12b presents a map of imperviousness, i.e., the share of the land area covered in

constructed surfaces, at the pixel-level for the 101 municipalities in the Greater Boston area. The urban center is generally more impervious than the outskirts. The pattern is reversed in Figure 12c, which presents a map showing tree cover, i.e., the share of the land area covered in trees for the Greater Boston area. Figure 12d presents a map showing land surface temperature on extremely hot days. Consistent with the map of urban imperviousness and tree cover, areas closer to the city center generally have higher land surface temperature. However, there is substantial variation within municipal boundaries, outlined in black. Figure 12a presents a map of the Greater Boston area depicting parcel-level regulated density across 101 municipalities. In general, regulated density is higher near the city center, but there are also areas of lower regulated density close to the city center. There is more variation in regulated density in cities close to the center, as these regulations are more likely to bind closer to productive amenities. Figures A17, A19, and A21 present similar maps of Baltimore, Chicago, and Pittsburgh, respectively.

4.2.2 Empirical specification and results

We focus on changes in tree cover, imperviousness, and surface temperature along these zoning district boundaries where regulated density changes discontinuously. Following Kulka et al. (2023), we use a spatial regression discontinuity design around the zoning boundaries to study the effect of density regulations on land-use and temperature:

$$Y_{ix} = \beta_0 + \beta_{RD} \cdot 1_{strict} + \beta_1 \cdot Dist_{ix} + \beta_2 \cdot 1_{strict} \times Dist_{ix} + \gamma_x + \varepsilon_{ix}$$

where Y_{ixt} is the share of impervious surfaces, or tree cover, or land surface temperature on hot days for pixel i near zoning boundary x. The running variable, $Dist_{ix}$, is the distance from pixel i to the zoning boundary x, where the regulated density changes discontinuously. For each boundary, we define a 'lax' and a 'strict' side of the boundary, where the lax side has *higher* density. The running variable $Dist_{ix}$ is positive for the strict (i.e., lower density) side of the boundary. 1_{strict} is an indicator which takes on the value 1 if an area is on the strict side of the boundary. The RD estimate is given by the coefficient on the indicator variable, β_{RD}, which measures the difference in Y_{ix} due to zoning regulations. We include boundary fixed effects, and cluster standard errors by municipality.[25]

Many factors change along municipality borders that could affect land-use—for example, local government spending on tree planting could lead to discontinuous changes in land-cover along municipal boundaries. In addition, households tend to sort across school attendance

[25]For the Chicago, Pittsburgh and Baltimore case studies, we do not cluster on municipality, as we only have data for the central city.

area boundaries, which could affect private spending on green spaces. To ensure that major amenities such as schools and local governments do not change at the boundary, we restrict the analysis to boundaries within local government jurisdictions (e.g., Cambridge, Brookline, etc.) and elementary school attendance areas. Furthermore, we exclude boundaries that intersect with highways, major roads, and water ways. However, we are not able to exclude the possibility that boundaries were drawn endogenously. Previous literature has shown that zoning boundaries tend to follow pre-existing land-use and density (Davidoff 2015). Therefore, we interpret the results presented below as reduced form, suggestive evidence that zoning affects the land-use and, therefore, the location of urban heat islands.

We first present results for the Greater Boston area, which has the highest quality data.[26] We identify 6,600 boundaries across 95 municipalities in Greater Boston. For example, there are 375 boundaries in Cambridge, excluding any boundaries that overlap with school attendance zone boundaries. Zoning districts are small; the median area of a district on the lax and strict side of the boundary is 5 and 10 acres, respectively. Therefore, we focus on a narrow bandwidth of 300 meters (i.e., 1000 feet) around the boundary. The final dataset for Greater Boston consists of 1.1 million observations, each of which represents a pixel within 300 meters (i.e., 1000 feet) of a boundary.

Figure 13 and Table 1 present the RD results for Greater Boston. The strict side of the boundary, with lower regulated density, is presented on the right side of the figures. Relative to the strict side of the boundary, the lax side of the boundary has 10 additional residential units per acre. We find that tree cover is 5 p.p. lower and the share of impervious surfaces is 7 p.p. higher on the side of the boundary with lower regulated density. The mean tree cover and share of impervious surfaces across zoning districts are 22 percent and 60 percent respectively, indicating that the estimated effects are economically significant. Correspondingly, land surface temperature on the lax side of the boundary is 0.6°C (i.e., 1.1°F) higher on hot days.

Figures A18, A20, and A22 present the RD results for Baltimore, Chicago, and Pittsburgh, respectively. We find a similar story to Greater Boston in these cities, although the magnitudes vary. In Baltimore, DUPAC changes by 18 units on average at the boundary. We find that tree cover is 4.2 p.p. lower, the share of impervious surfaces is 6.9 p.p. higher, and land surface temperature is 0.6°C (i.e., 1.1°F) higher on the side of the boundary with lower regulated density. In Pittsburgh, we find that DUPAC changes by 44 units at the boundary. Tree cover is 3.4 p.p. lower, the share of impervious surfaces is 6.2 p.p. higher,

[26] We collect comprehensive zoning data for the Greater Boston Area from the Metropolitan Area Planning Council (MAPC), whereas hand collected data for the other three cities are missing information on some parcels.

and land surface temperature is 0.3°C (i.e., 0.5°F) higher on the side of the boundary with lower regulated density. In Chicago, we find that tree cover is 1.9 p.p. lower, and the share of impervious surfaces is 4.9 p.p. higher on the side of the boundary with lower regulated density. DUPAC changes by 18 units across the boundaries on average. We do not find a statistically significant change in land surface temperature in Chicago. Tables 5, 6, and 7 summarize the RD estimates for each of these cities. These results provide suggestive evidence that zoning policies and land-use regulations shape where urban heat islands are located in a city.

4.3 The historical origins of urban heat islands: evidence from the Great Migration

Why do Black individuals live in more impervious neighborhoods? Some neighborhoods may have developed with higher densities and a greater concentration of impervious surfaces for reasons relating to economic productivity, such as proximity to economic activities in the city center. Decentralized residential sorting could have led to the concentration of Black households in higher density neighborhoods. An alternative explanation, however, is that Black neighborhoods developed with greater density as a result of racism embedded in the housing market. A range of formal and informal institutions have historically restricted the choice of neighborhoods of Black households. Examples of such institutions include housing covenants that prohibited sales to Black buyers, racial zoning laws stipulating separation between White and Black neighborhoods, redlining and discriminatory mortgage lending practices, and actual and threatened violence. These forces have been well-documented by historical records (Rothstein 2017) and case studies both in the past (Ondrich et al. 1998, 1999, Yinger 1986) and more recently (Christensen & Timmins 2022, Christensen et al. 2022). Cutler et al. (1999) find that in 1940, 60 percent of all Census tracts had a Black population share of less than one percent. In 1960, the comparable figure was 56 percent—a relatively small change despite the massive increase in Black population, suggesting that neighborhood choices of Black Southern migrants were largely limited to tracts that already had some Black residents. Li (2023) shows that around half of racial segregation could be explained by implicit or explicit constraints on the neighborhood choices of Black households.

In Appendix C, we develop a residential sorting model to illustrate how early constraints on Black households' neighborhood choices result in the development of greater density in Black neighborhoods. Intuitively, Black migrants choose from a restricted set of neighborhoods, driving up housing prices in those neighborhoods (if supply is upward sloping), prompting some White households to leave those neighborhoods in response. If Whites

exhibit distaste for racial diversity, neighborhoods with greater initial Black share will see increases in density in response to a large Black migration shock. We test this model prediction using the Great Migration as a natural experiment. During the Great Migration, between 1940 and 1970, four million Black Americans moved from the U.S. South to urban areas in the North and West. Previous literature has shown that the Great Migration transformed the racial demographics of destination cities, prompting White flight from urban neighborhoods, altering the policies of local governments, and changing access to opportunities in destination cities (Boustan 2010, Derenoncourt 2022, Tabellini 2020). We consider the effect of the Great Migration shocks on the neighborhood-scale distribution of density and imperviousness. Our results show that in response to exogenous shocks to the city-wide Black population, density increases in the neighborhoods with higher initial Black population share. We show that the neighborhoods with higher initial Black population shares are more likely to be zoned for higher density today.

4.3.1 Data

We compiled Census tract-level data on total population, Black and White population, rent, number of housing units, single and multi-family housing units from the 1940, 1950, 1960 and 1970 decennial Censuses. As tract boundaries are changing over time, we normalize boundaries for all years to 2010 tract boundaries. We normalize the data for 1940, 1950, and 1960, to 2010 tract boundaries using area weights. For 1970, we obtain normalized data from the Neighborhood Change Database, which normalizes the Census tract boundaries to 2010 tract definitions using block population weights. Our sample is limited by the availability of neighborhood-level historical data, as only 45 cities were tracted in 1940.

We also hand collect additional modern-day, parcel-level zoning data for 20 of the 45 cities that were tracted in 1940. From the digitized zoning maps and zoning codes, we identify the land parcels within each city that were zoned for residential use, and separately identify land zoned for single-family or multi-family homes. This allows us to calculate the share of a tract's land area that is zoned for single-family housing and residential use.

4.3.2 Empirical specification and results

The model presented in Appendix C predicts that, under certain conditions, Black migration to a city will lead to greater density in neighborhoods with a larger initial Black population share. We test this prediction using the following regression specification:

$$\Delta Y_{j,CZ} = \beta_0 + \beta_1 \cdot \Delta N_{CZ} + \beta_2 s^0_{j,CZ} + \beta_3 \cdot \left(\Delta N_{CZ} \times s^0_{j,CZ}\right) + \epsilon_j \tag{3}$$

where $\Delta Y_{j,CZ}$ is the change in tract outcome over 1940–1970. Tract-level outcomes include changes in population density, housing density, number of housing units, and number of multifamily units. The key dependent variable, N_{CZ}, is the change in the commuting zone's Black population over 1940–1970, expressed in standard deviations. CZ population is calculated based on sum of tract population for all available tracts in the base year. The initial Black share of tract population in the base year, 1940, is given by $s^0_{j,CZ}$ and is expressed in standard deviations. We control for initial CZ total and Black population in 1940, and include state fixed effects.[27] The model presented in Appendix C predicts that as CZ Black populations increase, neighborhoods with larger initial Black population share will see a larger increase in $\Delta Y_{j,CZ}$, i.e., the coefficient of interest, β_3, is expected to be positive.

To isolate exogenous shocks to the cities' Black populations, N_{CZ}, we exploit the Great Migration as a natural experiment. Between 1940–1970, around four million Black Americans moved from the U.S. south to cities in the North and West. The choice of destinations by the Black migrants may be endogenous. Black migrants may have chosen destinations with lower segregation or destinations with greater urban density, which may be correlated with imperviousness. To address this, we instrument for changes in the city-wide Black population, $\Delta N_{B,CZ}$, with a migration shift-share instrument. The instrument is constructed based on the 1940 Black migration rates and economic shocks at origins that are plausibly orthogonal to economic shocks at destination cities (Derenoncourt 2022, Boustan 2010). Derenoncourt (2022) and Boustan (2010) show that Black Southern migrants tended to move where previous migrants from their communities had settled, thus generating correlated origin-destination flows. For example, Detroit drew the plurality of its migrants from Alabama while Baltimore drew the plurality from Virginia. Shocks to migrants' origin locations ('push factors') are plausibly orthogonal to shocks to the destinations ('pull factors'), plausibly satisfying the exclusion restriction criteria for a valid instrument. Push factors used to construct the instrument include defense facility spending in Southern counties during World War II and shocks to cotton and other economic sectors in the South. For example, cotton mechanization contributed to Black outmigration from the South more in some places than others. The instrument is constructed by interacting pre-1940 Black migration rates with these push factors at origin counties of the Black migrations.

$$\widehat{mig}_{B,CZ} = \sum_{s \in S} \omega_{j,CZ} \cdot \widehat{mig}_j$$

Here, $\widehat{mig}_{B,CZ}$ is the predicted number of Black migrants in a commuting zone CZ, calculated as the sum of the interaction of the share of migrants from a Southern origin

[27] These controls do not materially affect the results.

county j that settled in CZ over 1935–1940 and the predicted number of migrants leaving origin county j due to economic push factors over 1940–1970, $\widehat{mig}_j$. We use $\widehat{mig}_{B,CZ}$ as an instrument for $N_{B,CZ}$.[28]

Figure 14 presents the reduced form effects of the interaction between the Great Migration instrument and the initial Black population share on four dependent variables related to density. These include change in population density, change in housing density, change in the number of housing units, and change in the number of multi-family homes at the tract-level over 1940–1970. Tables 2 and 3 present the 2SLS estimates of the effects. These results are based on around 9,000 tracts in 45 CZs containing cities that were tracted in 1940. The IV results presented in Table 3 show that, in response to a one-SD increase in the city-wide Black population, population density increases by 7,998 persons per square mile in tracts with no Black individuals in 1940.[29] In tracts with one-SD higher initial Black population share, population density increased by an additional 1,680 persons per square mile.[30] Mean tract population density is 15,262, meaning that the effect size is over 10 percent of the mean. Similarly, we find that an increase in the city-wide Black population led to a larger increase in housing density and the number of housing units, especially the number of multi-family homes, in tracts with higher initial Black population share.

These results show that, consistent with model predictions, density increased in areas with a high baseline Black share in response to city-wide Black population shock. Results presented above suggest that Black migration, combined with institutions that restricted the choice set of Black individuals, shaped the way that the cities' built environment developed over space and time. As these restrictions began to lift in the latter part of the century, they were replaced by seemingly race-neutral exclusionary zoning policies (Rothstein 2017, Shertzer et al. 2016, Trounstine 2018). Cui (2022) shows that most suburbs adopted minimum lot size restrictions from 1945–1970, coinciding with the period of the second wave of the Great Migration, as central city populations became increasingly more Black (Figure A16).

Using contemporary parcel-level zoning data for about 2,800 tracts in 20 cities that served as destinations during the Great Migration, we present consistent suggestive evidence that zoning codified higher historical density in Black neighborhoods, while keeping density low in other neighborhoods. Descriptively, neighborhoods that had a one-SD higher Black

[28] Derenoncourt (2022) uses the percentile predicted increase in Black population as an instrument, rather than the number of predicted Black migrants. Because we effectively apportion the commuting zone wide migration shocks to Census tracts, by interacting $\widehat{mig}_{B,CZ}$ with Black population share, we do not use percentile predicted increase.

[29] One SD change in CZ Black population corresponds to 466,279 individuals.

[30] One SD increase in 1940 tract Black population share corresponds to a 16 p.p. change.

population share in 1940 have 3.9 p.p. less land zoned for single-family homes today.[31] We then replace the dependent variable in equation 3 with the present day share of land zoned for single-family homes. The results show that in tracts with no Black individuals in 1940, a one-SD increase in the city-wide Black population led to a 4.9 p.p increase in the share of area zoned for single-family homes.[32] In contrast, in tracts with one-SD higher initial Black population share, a one-SD increase in the city-wide Black population led to a decrease of 1.6 p.p. in the share of area zoned for single-family homes. lower.[33] These results suggest that zoning codified higher density in historically Black neighborhoods, while restricting density in other neighborhoods.

Finally, we test whether the Great Migration shocks can predict commuting zone-level Black mortality on hot days. For this analysis, we construct daily Black and White mortality at the commuting zone level for 64 Great Migration commuting zones that experience at least one hot day over the sample period. In each commuting zone, we restrict to the set of Census tracts that experience at least one hot day (i.e., a day over 32°C or 90°F), and calculate the commuting zone-level three-day Black and White mortality rates by aggregating across these Census tracts. We create separate sub-samples for hot days over 32°C (i.e., 90°F) and reference days between 17–22°C (i.e., 63-72°F) for each race. For each of these samples, we regress the mortality rate on the Great Migration instrument.[34] Following Derenoncourt (2022), we include baseline 1940 controls, as well as region fixed effects. Table 4 presents the reduced form results of regressing the Great Migration shocks on contemporary Black and White mortality rates at the commuting zone-level. We find that in cities that served as destinations during the Great Migration, the Great Migration shock can predict Black mortality on hot days (i.e., days over 32°C or 90°F), but not on reference days (i.e., 17–22°C or 63–72°F). One standard deviation of the shock predicts an increase in mortality of 20.5 deaths per 100,000, relative to a mean of 92.65 deaths per 100,000. In contrast, the Great Migration shocks do not predict White mortality on hot or reference days.

Taken together, these results suggest that the built environment and its racial incidence are a product of history, and were perpetuated by policy. These factors have consequences for heat-related mortality and racial health disparities today.

[31] Our sample is restricted based on the 45 Great Migration destination cities that were tracted in the 1940s, and cities for which we were able to obtain digitized zoning maps.

[32] This is consistent with Sahn (2023), who finds that less land is zoned for multi-family housing in cities that saw a larger increase in racial diversity during the Great Migration.

[33] The mean share of land zoned for single-family homes across the tracts is 42 p.p..

[34] Because this regression is at the commuting zone-level, rather than the Census tract level, we directly borrow the instrument from Derenoncourt (2022), constructed as the percentile of the predicted increase in Black population.

5 Conclusion

The lack of fine-scale, ground-truth measures of temperature has posed a challenge in assessing the true impact of the built environment on experienced temperatures and mortality. In this paper, we overcome this challenge by combining random shocks in imputed air temperatures with satellite-derived imperviousness data at the Census tract-level and newly assembled confidential micro-data on mortality and demographics. We show that the population living in urban heat islands, where the built environment elevates experienced temperatures, see the largest increase in mortality on hot days. We find that, relative to Census tracts with median imperviousness, the most impervious Census tracts see an additional six deaths per 100,000 among the elderly on hot days. Using cold and other non-hot days as a placebo, we show that excess mortality rates on cold days do not vary by tract imperviousness conditional on our fixed effects. This suggests that the results cannot be explained by selection alone, as we would expect any selection across deciles to persist on non-hot days. We show that these effects persist even after including county-by-date fixed effects, suggesting much of the effects are driven by within-county variations across tracts on hot days. We rule out several alternative explanations. We show that the effects are not driven by differential composition of the elderly by tract imperviousness. The effects persist in warmer areas that are more likely to have higher adaptation, suggesting that differences in adaptation alone do not explain the results. We do not find evidence of substantial harvesting effects driving our results.

We document substantial racial disparity in the relationship between temperature and mortality. Black individuals over 65 face significantly higher mortality rates following hot days, both in absolute terms and as a percentage increase relative to baseline mortality, compared to their White counterparts. Some of these differences are plausibly due to differences in baseline health or access to resources—such as healthcare and air conditioning. However, some of the racial disparities are due to the fact that the Black population is more likely to live in impervious areas. A Kitagawa–Oaxaca–Blinder style decomposition of the effects suggests that half of the Black-White gap in mortality on hot days can be attributed to the fact that Black individuals live in different Census tracts with higher imperviousness. This points to the role of segregation of Black individuals into more impervious neighborhoods as a potential driver of disparities in temperature-related mortality.

Motivated by this, we investigate what determines the local spatial variation in urban imperviousness within cities, racial disparities in exposure to imperviousness and, ultimately, mortality on hot days. We show that housing market regulations and historical institutions drive the location of density, imperviousness, and urban heat islands. Based on a boundary

discontinuity design along zoning district boundaries in four large U.S. cities, we provide suggestive evidence that zoning leads to the concentration of impervious surfaces, lack of tree cover, and higher surface temperatures on the side of the boundary with greater regulated density. The built environment is also a product of history. We find that exogenous Black population shocks during the Great Migration over 1940–1970 led to an increased density in neighborhoods with higher initial Black population share. We find that these neighborhoods are more likely to be zoned for higher density today. Finally, we show that the Great Migration shocks predict higher Black mortality on hot days, but not on cold days, in the destination city. Taken together, these results suggest that neighborhood imperviousness and its racial incidence have deep historical roots and are affected by policies relating to housing density.

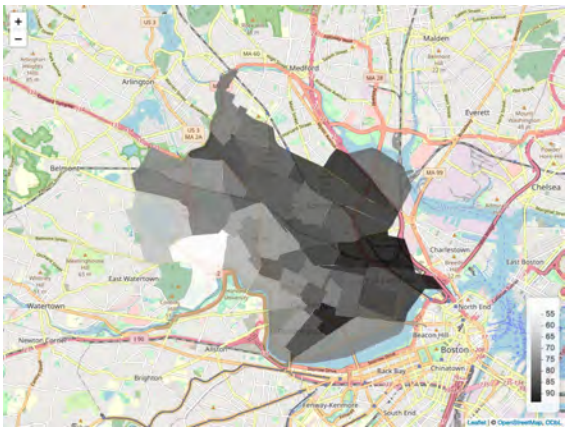
The urban economics literature documents many benefits of increasing density in productive cities, such as more affordable housing, better labor allocation and higher productivity (Hsieh & Moretti 2019, Herkenhoff et al. 2018, Ganong & Shoag 2017, Kulka et al. 2023, Turner et al. 2014). This paper documents that increasing density, to the extent that it increases imperviousness, may come at a cost to public health. Does increasing density inevitably increase imperviousness? Figure 15 plots the relationship between log imperviousness and log population density in the 50 largest counties by population in temperate or continental climates. While the relationship between density and imperviousness is strong, there is some dispersion around the line of best-fit. For example, Alameda county in California and Montgomery county in Maryland have a similar population density of around 2,000 persons per square mile. However, Alameda county is twice as impervious as Montgomery county (i.e., 64 percent versus 32 percent). This suggests that it may be possible to design cities in ways that increase density without increasing imperviousness and creating urban heat islands.

Our results also suggest that local policy makers could play a role in mitigating the health costs of extreme. Cities in the U.S. and globally are hiring more 'Chief Heat Officers' with the goal of creating heat-resilient cities.[35] Our results could inform these local policy makers. For example, city and county governments could more effectively target cooling centers, information campaigns, weatherization programs, and energy subsidies for cooling to communities in urban heat islands, where the mortality effects of extreme heat are concentrated.

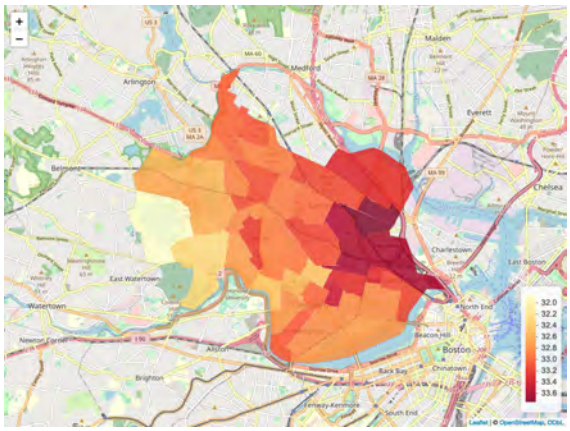
[35]Examples of U.S. counties and cities that have appointed a Chief Heat Officer include Miami-Dade and Los Angeles.

Figures

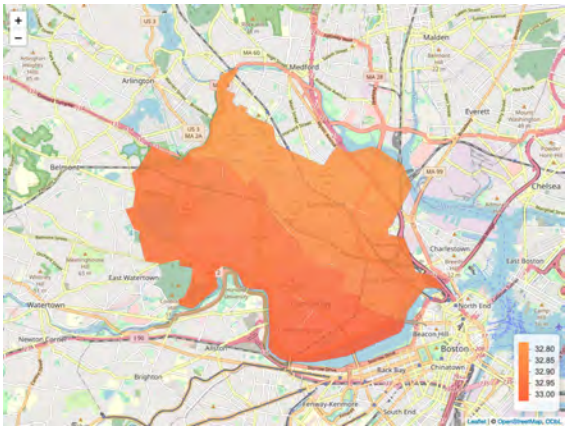
Figure 1: Actual versus imputed temperature in Somerville and Cambridge, MA



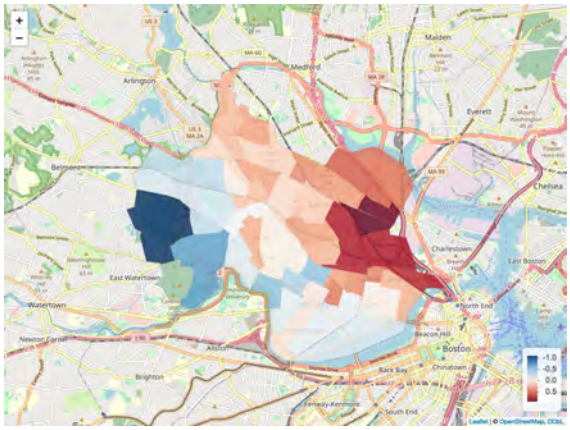
(a) Imperviousness (%)



(b) Actual temperature (°C)



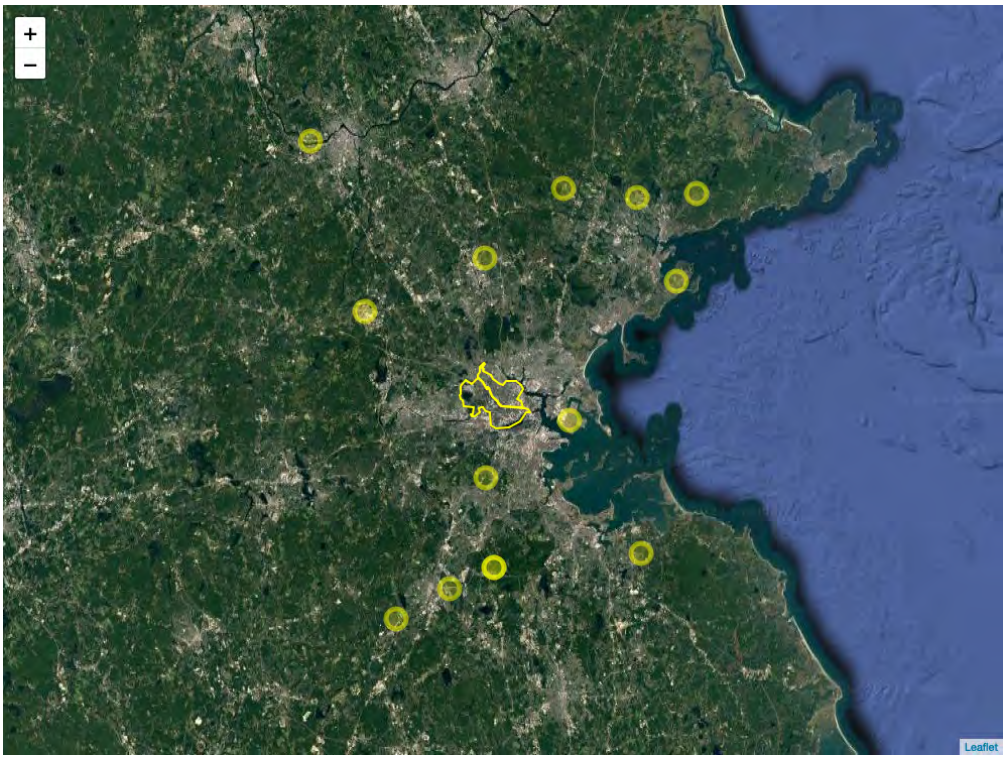
(c) Imputed temperature (°C)



(d) Actual - imputed (°C)

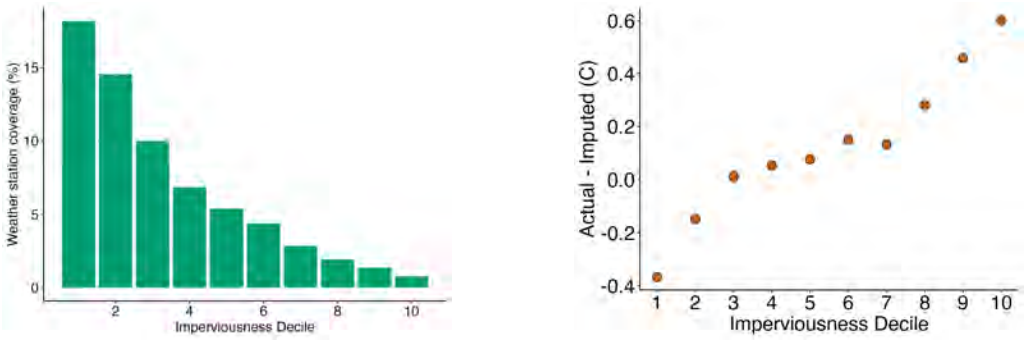
Note: This figure presents a case study related to measuring urban heat islands in the cities of Cambridge and Somerville, MA. Panel (a) presents the Census tract share of impervious surfaces. Panel (b) presents the average ambient temperature at the Census tract level on 29 July 2019, as measured by the Urban Heat Island Mapping Campaign. Panel (c) presents tract-level imputed temperatures based on weather stations located within 20 miles. Panel (d) presents the measurement error—the difference between actual and imputed temperatures.

Figure 2: Weather stations within 20 miles of Cambridge and Somerville, MA



Note: This map shows the location of weather stations located within 20 miles of the cities of Cambridge and Somerville, MA. The yellow circles mark the location of the weather stations. Cambridge and Somerville city borders are outlined in yellow. The weather station locations are overlaid on top of a satellite image of the Greater Boston area, depicting that weather stations are more likely to be located in the outskirts of the city.

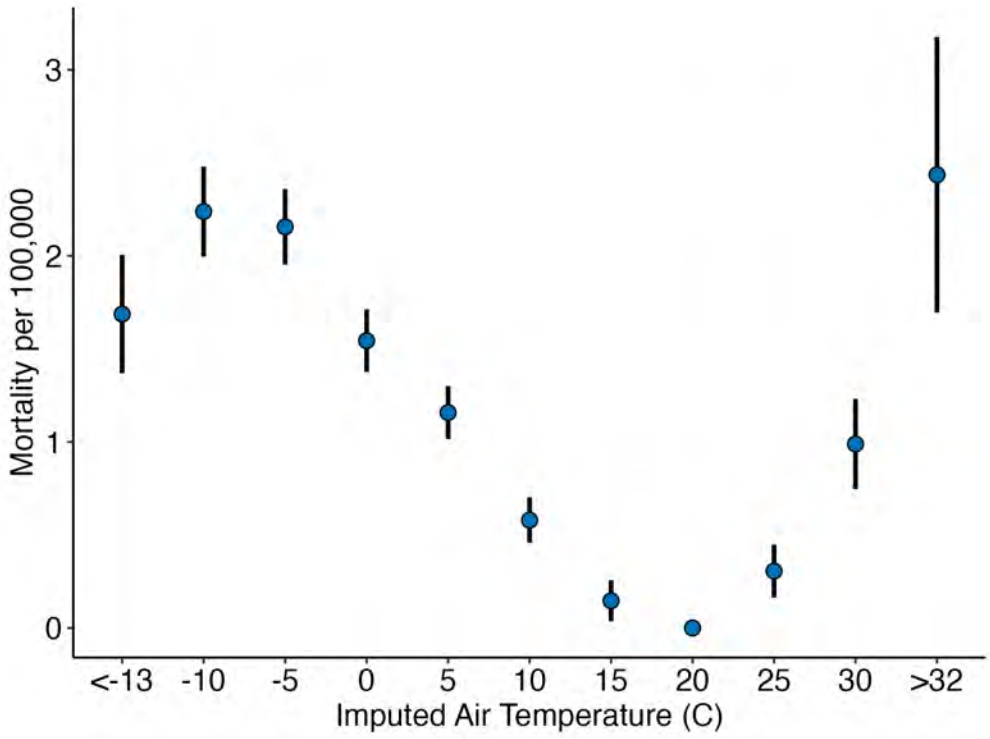
Figure 3: Measurement error in tract air temperature imputed from weather stations



(a) Station coverage by tract imperviousness (b) Measurement error by imperviousness

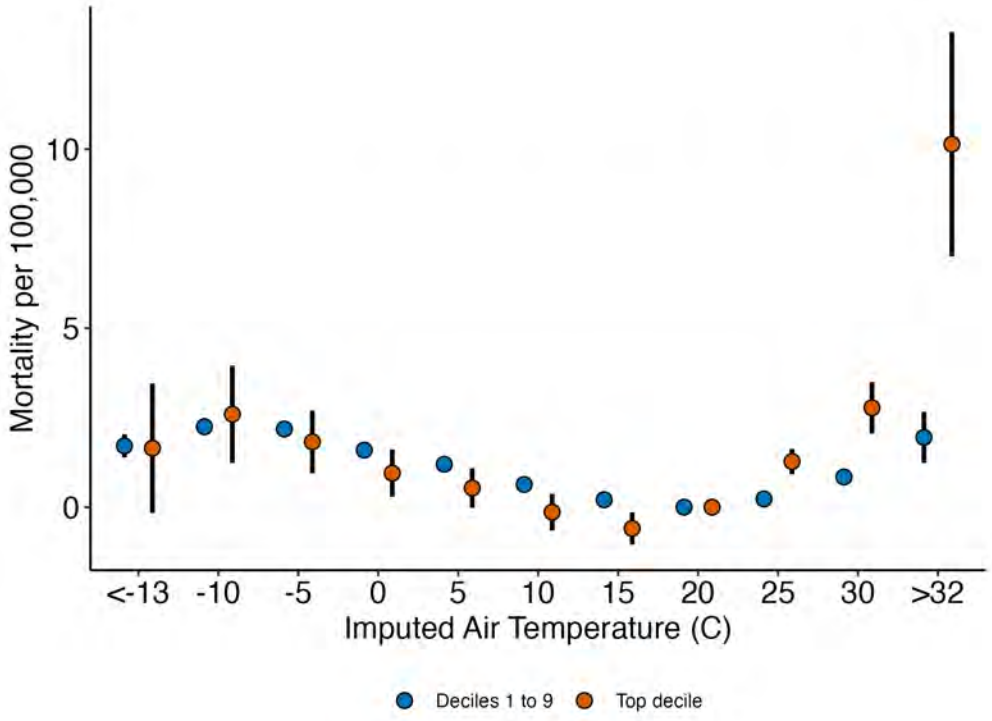
Note: Panel (a) shows the percent of Census tracts in temperate and continental climates that contain one or more weather stations, by deciles of imperviousness. Panel (b) presents mean measurement errors, defined as actual air temperature minus imputed air temperature, for each decile of imperviousness. This analysis is restricted to Census tracts that contain at least one weather station that is included in the GHCN database. Actual air temperatures are based on weather stations located in the highly impervious tracts. Imputed air temperatures are inverse-distance weighted means based on other weather stations located within 20 miles of the highly impervious Census tract.

Figure 4: Baseline temperature–mortality relationship: over 65



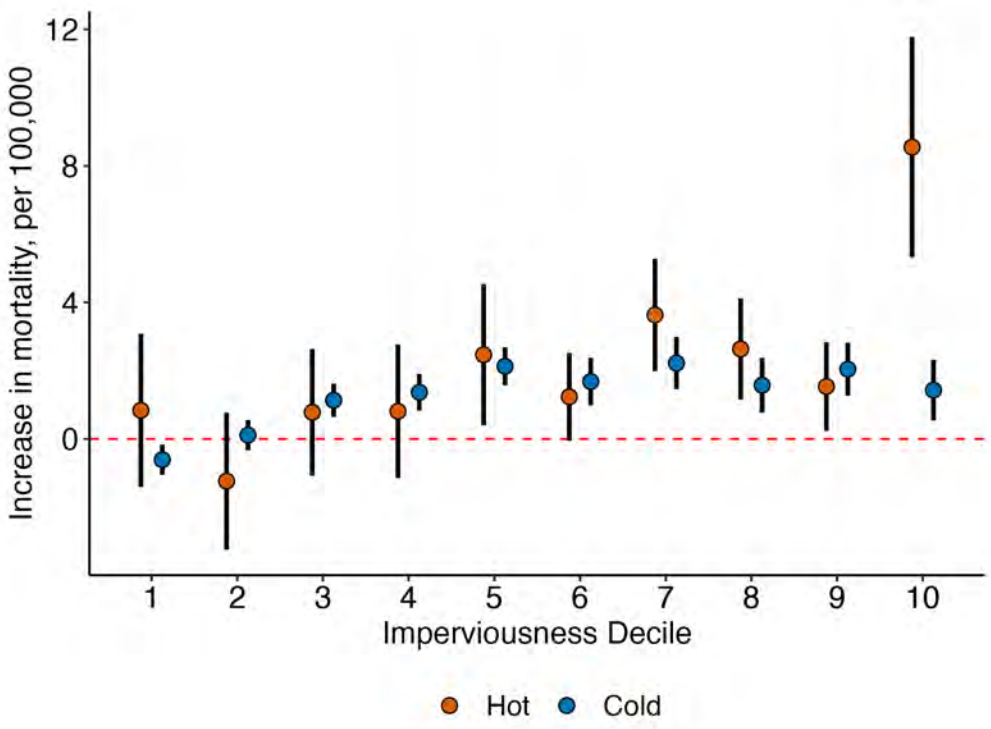
Note: This figure plots estimated three-day mortality effects of temperature for the over-65 population living in temperate or continental climates. 85 percent of the U.S. population live in temperate or continental climates. The effects reflect excess mortality on a day with a given average temperature relative to a day with an average temperature of 17–22°C. Imputed temperature is calculated based on an inverse distance-weighted average from weather stations within 20 miles of the Census tract. 95 percent confidence intervals are presented based on standard errors clustered at the county-level.

Figure 5: Temperature–mortality relationship: tracts in the top decile versus other tracts



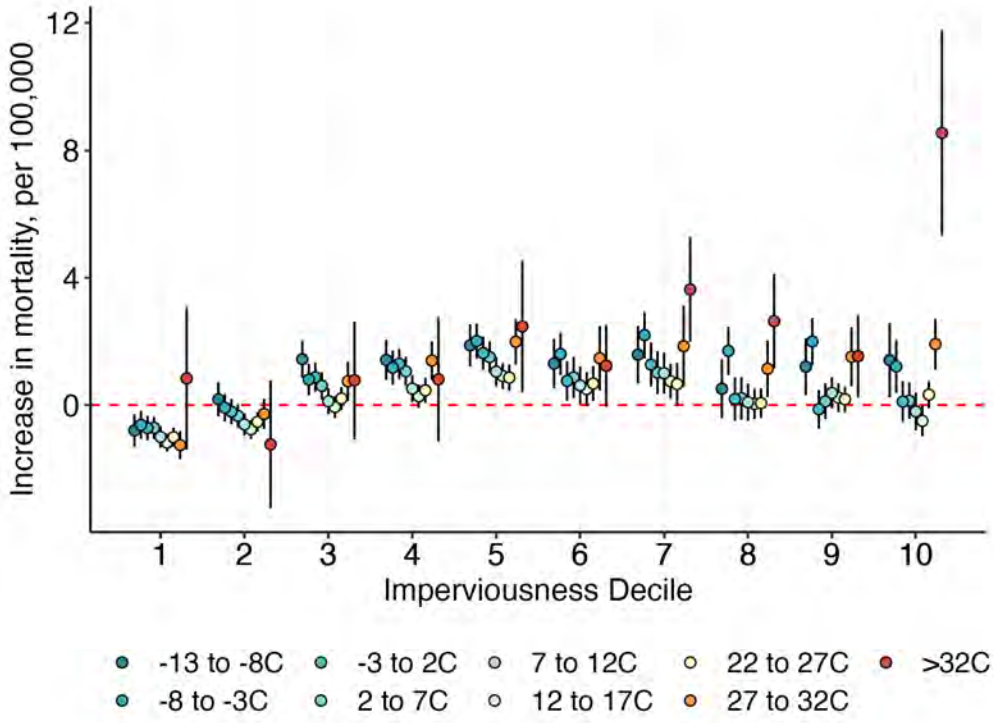
Note: This figure plots estimated three-day mortality effects of temperature separately for tracts in the top decile of imperviousness and all other tracts, for individuals living in temperate or continental climates. The effects reflect excess mortality on a day with a given average temperature relative to a day with an average temperature of 17–22°C. Imputed temperature is calculated based on an inverse distance-weighted average from weather stations within 20 miles of the Census tract. Imperviousness is calculated from satellite-derived data from the National Land Cover Database (NLCD). 95 percent confidence intervals are presented based on standard errors clustered at the county-level.

Figure 6: Increase in over-65 mortality rates on hot and cold days by imperviousness decile



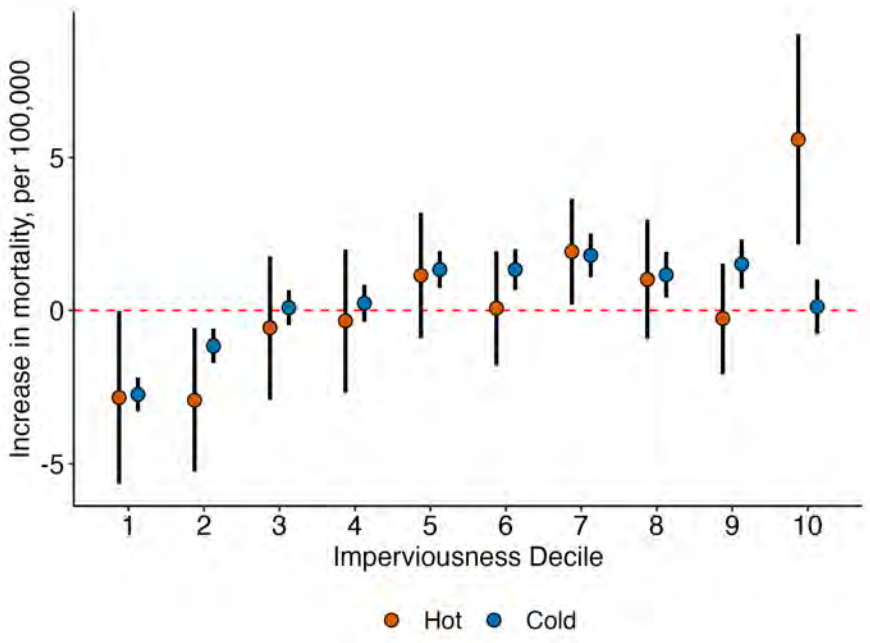
Note: This figure plots estimated three-day mortality effects of a hot day, as well as a cold day, for tracts in the temperate or continental climate zones for each decile of imperviousness. Imperviousness deciles are calculated based on the national distribution of tract imperviousness i.e., the share of the tract's area covered in impervious surfaces. Imperviousness is calculated from satellite-derived data from the National Land Cover Database (NLCD). The hot day coefficients reflect excess mortality on a day over 32°C (i.e., over 90°F) relative to a 17–22°C day. The cold day coefficients reflect excess mortality on a day between -13°C to -8°C (i.e., 9–18°F) relative to a 17–22°C (i.e., 63–72°F) day. 95 percent confidence intervals are presented based on standard errors clustered at the county-level.

Figure 7: Increase in over-65 mortality rates on hot and non-hot days by imperviousness decile



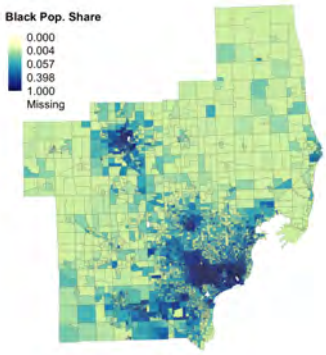
Note: This figure plots estimated three-day mortality effects of a day in one of 9 temperature bins in increments of 5°C (i.e., 9°F), for tracts in the temperate or continental climate zones for each decile of imperviousness. Imperviousness deciles are calculated based on the national distribution of tract imperviousness i.e., the share of the tract's area covered in impervious surfaces. Imperviousness is calculated from satellite-derived data from the National Land Cover Database (NLCD). The coefficients reflect excess mortality relative to a 17–22°C (i.e., 63–72°F) day. 95 percent confidence intervals are presented based on standard errors clustered at the county-level. We exclude the coldest bin because of very wide confidence intervals. Coefficients for this bin do not vary by imperviousness.

Figure 8: Increase in over-65 mortality rates on hot and non-hot days by imperviousness decile, including county-date fixed effects

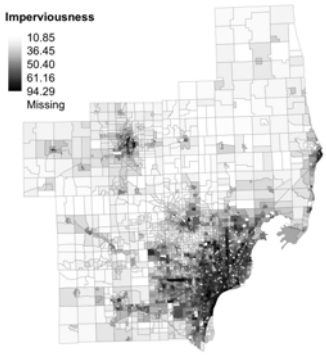


Note: This figure plots estimated three-day mortality effects of a hot day, as well as a cold day, for tracts in the temperate or continental climate zones for each decile of imperviousness, including county-date fixed effects in addition to tract-day-of-year and state-year fixed effects. Imperviousness deciles are calculated based on the national distribution of tract imperviousness i.e., the share of the tract's area covered in impervious surfaces. Imperviousness is calculated from satellite-derived data from the National Land Cover Database (NLCD). The hot day coefficients reflect excess mortality on a day over 32°C (i.e., over 90°F) relative to a 17–22°C day. The cold day coefficients reflect excess mortality on a day between -13°C to -8°C (i.e., 9–18°F) relative to a 17–22°C (i.e., 63–72°F) day. 95 percent confidence intervals are presented based on standard errors clustered at the county-level.

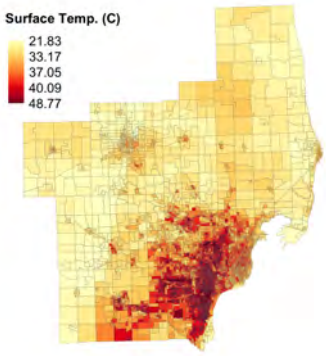
Figure 9: Illustrative example of Detroit and Flint in 2019



(a) Black Population Share



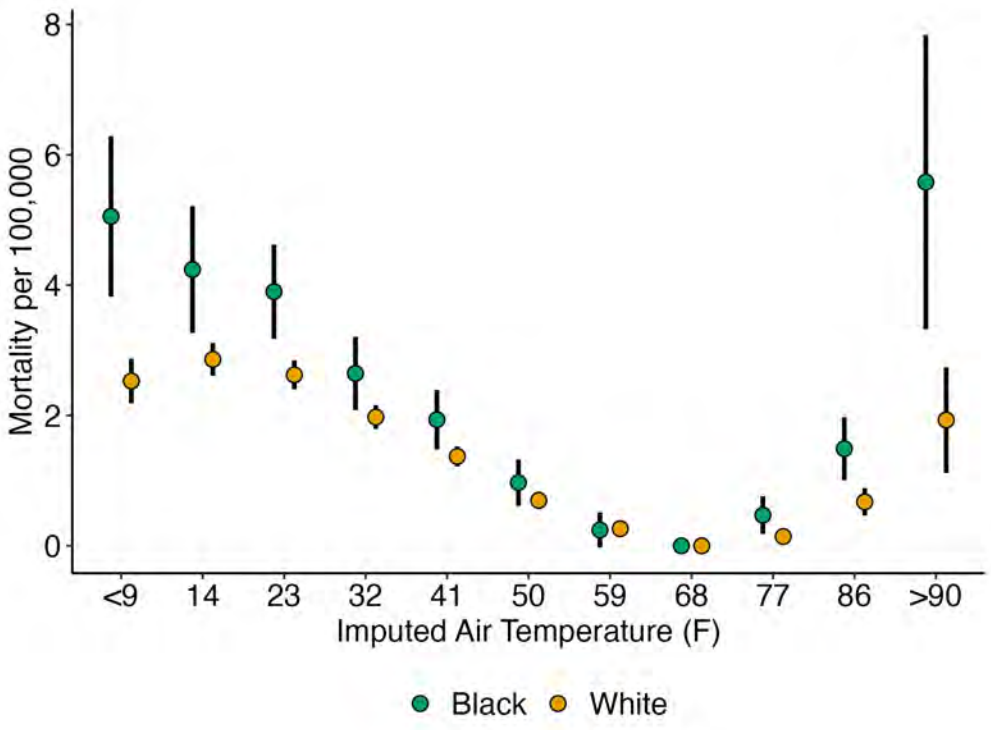
(b) Imperviousness



(c) Land Surface Temperature

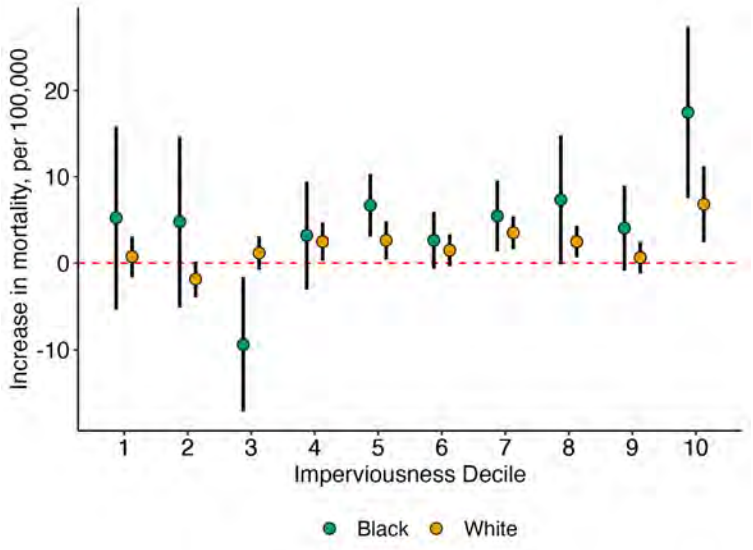
Note: panels (a), (b), and (c) present block-group level data on black population share, imperviousness (i.e., share of land area covered in impervious surfaces), and mean summer land surface temperature, for the Detroit-Warren-Ann Arbor Combined Statistical Area in 2019. Black population share is calculated based on the 2015–19 American Community Survey (ACS). Imperviousness is calculated based on satellite data from the National Land Cover Database (NLCD). Mean summer land surface temperature is calculated based on Landsat data.

Figure 10: Mortality Effects of Air Temperature: above 65, by race

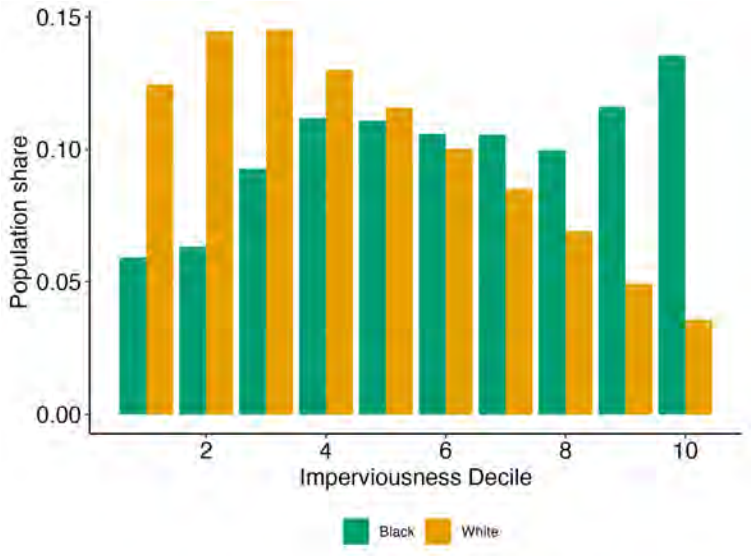


Note: This figure plots estimated three-day mortality effects of temperature for the Non-Hispanic Black and White population over 65. The effects reflect excess mortality on a day with a given average temperature relative to a day with an average temperature of 17–22°C. Imputed temperature is calculated based on an inverse distance-weighted average from weather stations within 20 miles of the Census tract. 95 percent confidence intervals are presented based on standard errors clustered at the county-level.

Figure 11: Heterogeneity by race: Black vs. White



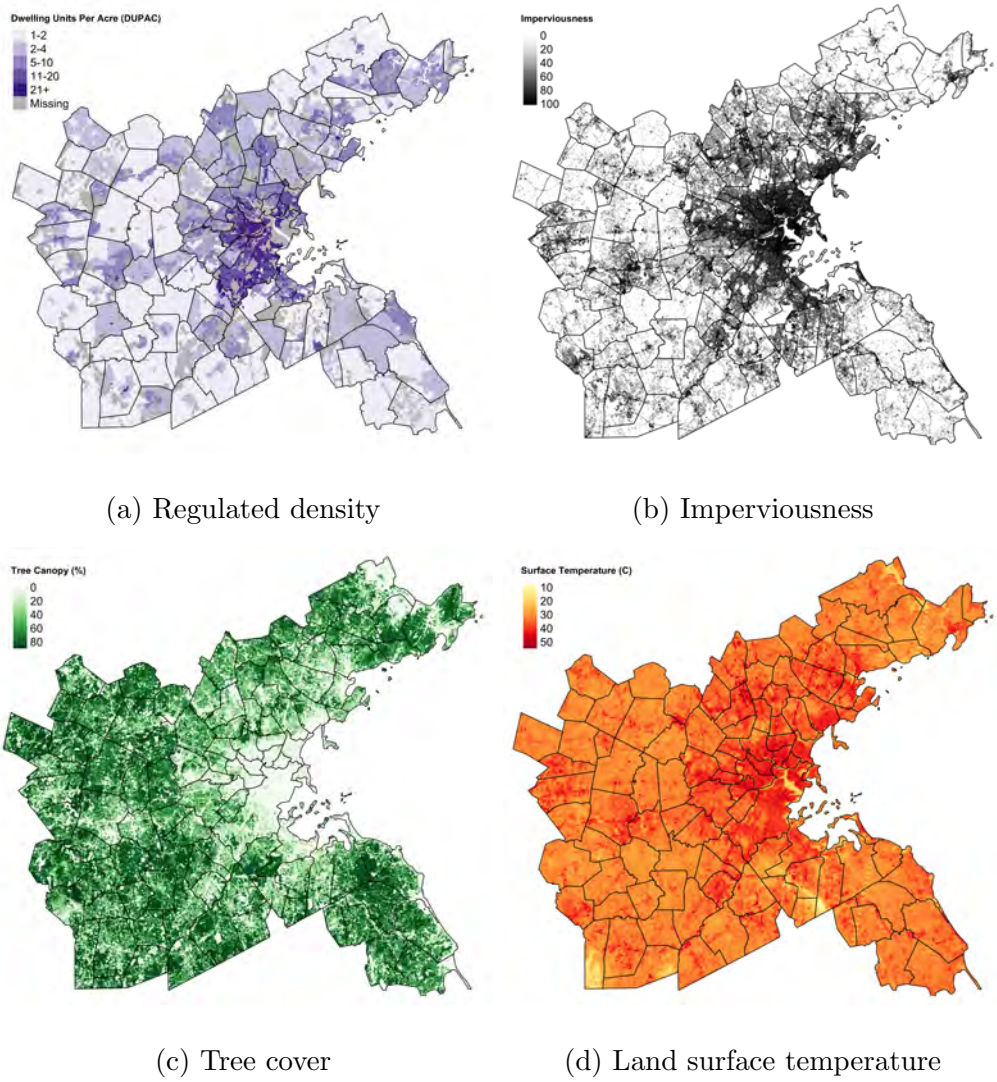
(a) Increase in over-65 mortality rates on hot days by imperviousness decile, by race



(b) Population distribution across imperviousness decile: above 65, by race

Note: Panel (a) plots estimated three-day mortality effects of a hot day for temperate or continental climate zones for the Non-Hispanic Black and White populations over 65 living in each decile of imperviousness. Imperviousness is calculated from satellite-derived data from the National Land Cover Database (NLCD). The effects reflect excess mortality on a day over 32°C relative to a 17–22°day. 95 percent confidence intervals are presented based on standard errors clustered at the county-level. Panel (b) presents the share of the Non-Hispanic Black and Non-Hispanic White population over 65 in temperate or continental climate zones that live in each decile of imperviousness. Imperviousness deciles are calculated based on the national distribution of tract imperviousness, i.e., the share of the tract's area covered in impervious surfaces.

Figure 12: Greater Boston case study



(a) Regulated density

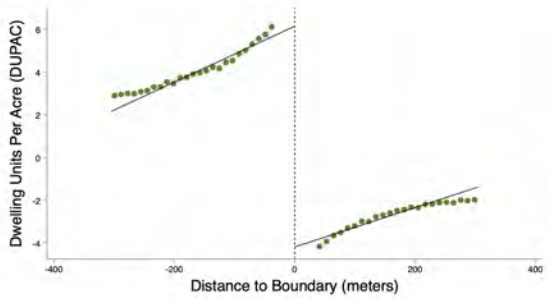
(b) Imperviousness

(c) Tree cover

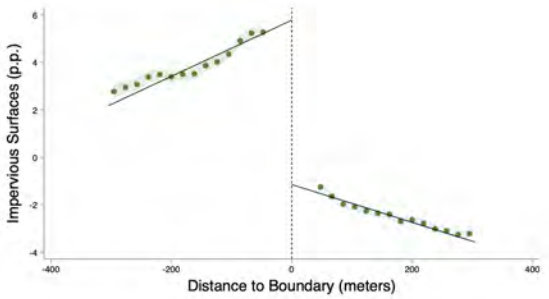
(d) Land surface temperature

Note: These figures present maps of the Greater Boston area. The shading corresponds to parcel-level Dwelling Units per acre (DUPAC) in panel (a), pixel-level imperviousness in 2019 in panel (b), pixel-level tree cover in 2016 in panel (c), and pixel-level land surface temperature in panel (d) for hot days over 2010–19. Imperviousness data at a 30 meter $\times$ 30 meter resolution are obtained from the National Land Cover Database (NLCD). Land surface temperature at a 30 meter $\times$ 30 meter resolution are based on Landsat data.

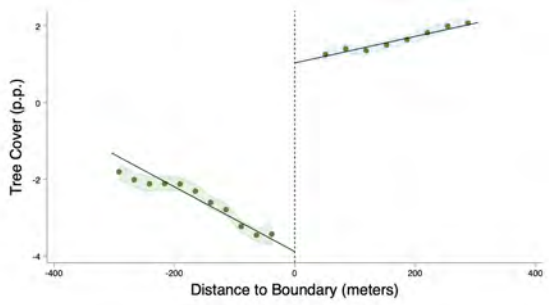
Figure 13: Greater Boston: Regression discontinuities at regulation boundary



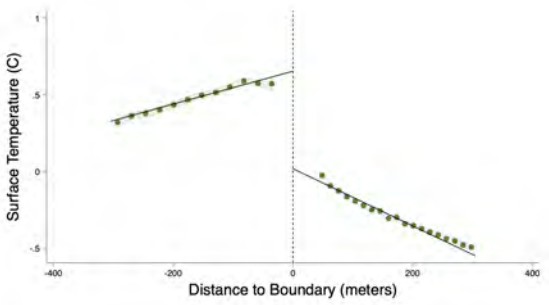
(a) Change in regulated density



(b) Change in imperviousness



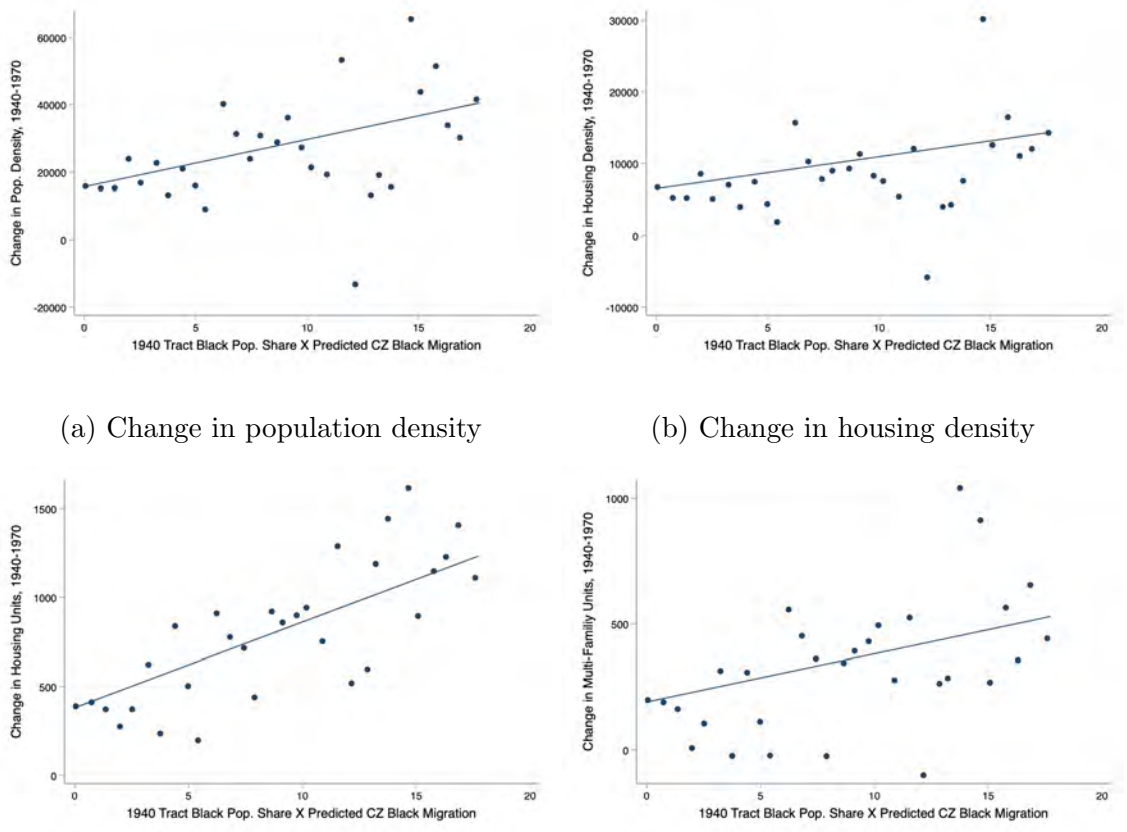
(c) Change in tree cover



(d) Change in land surface temperature

Note: These figures present RD plots of Dwelling Units per Acre (DUPAC), imperviousness (share of land area covered in impervious surfaces), tree cover (share of land area covered in tree canopy), and land surface temperature on hot days at the pixel level for Greater Boston. Negative distances indicate the side of the boundary with higher regulated density. 95 percent confidence intervals are shown with standard errors clustered at the municipality level.

Figure 14: Effect of Great Migration shock on density



(a) Change in population density

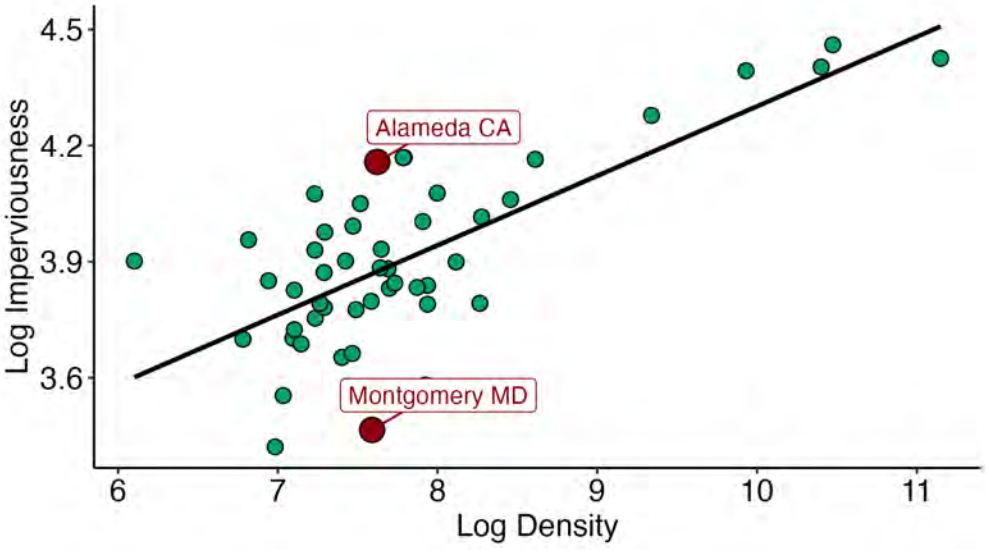
(b) Change in housing density

(c) Change in housing units

(d) Change in multi-family Units

Note: This binned scatterplot depicts the relationship between increase in tract level density over 1940–70, and interaction between the instrument for Black population increases during the Great Migration and 1940 Black tract population share. The instrument is predicted Black population increase at the commuting zone level, defined as the interaction between pre-1940 Black migration patterns and post-1940 outflows of migrants as predicted by southern economic factors. Both variables have been residualized on 1940 Black population share and the instrument, as well as 1940 commuting zone Black and total populations.

Figure 15: Density versus imperviousness in 50 largest counties



Note: This scatterplot depicts the relationship between log imperviousness and log population density in the 50 largest counties by population in temperate or continental climates. Imperviousness is calculated based on satellite data from 2019 the National Land Cover Database (NLCD). Population density is calculated based on data from the 2010 decennial Census.

Tables

Table 1: RD estimates: Greater Boston case study

	DUPAC	Tree Cover	Imperviousness	Temperature
β_{RD}	-10.33^{***}	4.919^{***}	-6.925^{***}	-1.144^***
	(1.893)	(0.749)	(0.991)	(0.173)
Observations	1,103,014	1,103,014	1,103,014	1,103,299
Mean of Dep. Var.	16	22	60	99

Note: This table presents the estimates of the RD coefficients from regressing the dependent variable on distance to the zoning boundary for Greater Boston. Negative distances indicate the side of the boundary with higher regulated density. The dependent variables include Dwelling Units per Acre (DUPAC), imperviousness (share of land area covered in impervious surfaces), tree cover (share of land area covered in tree canopy), and land surface temperature on hot days. The specification includes boundary fixed effects and standard errors clustered at the municipality level.

Table 2: Effect of city's Black population change on tract density, 1940–1970

	(1) Δ Pop. Density	(2) Δ Housing Density	(3) Δ Housing Units	(4) Δ Multifamily Homes
Panel A. First stage on Δ CZ Black Population (SD) × Black Share (SD)				
$\widehat{mig}$ × Black Share (SD)	0.882	0.882	0.882	0.882
	(0.218)	(0.218)	(0.218)	(0.218)
F-stat	64.4	64.4	64.4	64.4
Panel B. OLS				
Δ CZ Black Population (SD)	1129.184*	417.215**	24.700***	13.594**
× Black Share (SD)	(441.778)	(202.307)	(7.297)	(5.783)
Panel C. Reduced form				
$\widehat{mig}$ × Black Share (SD)	1402.132*	443.222	48.027***	19.094**
	(718.059)	(333.407)	(8.897)	(9.600)
Panel D. 2SLS				
Δ CZ Black Population (SD)	1679.717***	537.245*	54.174***	21.575 **
× Black Share (SD)	(504.257)	(280.749)	(12.597)	(12.353)
Observations	9,027	9,027	9,027	9,027
Mean of Dep. Var.	15,252	6,298.3	401.3	192.4

Specifications include controls for 1940 CZ black population and total population, and state fixed effects. Standard errors are clustered at the Commuting Zone level. These results are based on around 9,000 tracts in 45 CZs containing cities that were tracted in 1940. One SD change in CZ Black population corresponds to 466,279 individuals. One SD increase in 1940 tract Black population share corresponds to a 16 p.p. change. * $p < 0.10$, ** $p < 0.05$, *** $p < 0.01$

Table 3: Effect of city's Black population change on tract density, 1940–1970, IV

	(1) Δ Pop. Density	(2) Δ Housing Density	(3) Δ Housing Units	(4) Δ Multifamily Homes
Δ CZ Black Population (SD),	7997.525***	3085.263***	-24.431	-6.334
1940-1970	(983.111)	(434.880)	(23.295)	(15.873)
Black Share (SD), 1940	-2315.192**	-957.591*	-190.972***	-54.457**
	(1090.485)	(503.664)	(41.312)	(26.980)
Δ CZ Black Population (SD)	1679.717***	537.245*	54.174***	21.575*
× Black Share (SD)	(504.257)	(280.749)	(12.597)	(12.354)
CZ Black Population, 1940	-0.795*	-0.023	0.056	-0.000
	(0.436)	(0.158)	(0.035)	(0.039)
CZ Total Population, 1940	0.330	0.293	-0.157***	-0.088***
	(0.575)	(0.263)	(0.010)	(0.017)
Observations	9,027	9,027	9,027	9,027
Mean of Dep. Var.	15,252	6,298	401.3	192.4

Specifications include state fixed effects. Standard errors are clustered at the Commuting Zone level. These results are based on around 9,000 tracts in 45 CZs containing cities that were tracted in 1940. One SD change in CZ Black population corresponds to 466,279 individuals. One SD increase in 1940 tract Black population share corresponds to a 16 p.p. change. * $p < 0.10$, ** $p < 0.05$, *** $p < 0.01$

Table 4: Reduced form effects of Great Migration shocks on Black and White mortality

	(1) Black, hot	(2) Black, reference	(3) White, hot	(4) White, reference
GM shock	20.48	-5.12	0.68	-1.57
	(7.97)	(3.51)	(3.40)	(1.55)
Observations	300	1200	300	1200
Mean mortality	92.65	92.65	91.87	91.87

Note: This table presents the reduced form effects of the Great Migration shock on Black and White mortality on hot days over 32°C (i.e., 90°F) and reference days (17–22°C or 63–72°F) over the sample period. There are 64 unique commuting zones in the sample. Each observation represents a commuting-zone-date. Columns (1) and (2) present the reduced form effects of the Great Migration shock on Black mortality on a hot day and a reference day, respectively. Columns (3) and (4) present the reduced form effects of the Great Migration shock on White mortality on a hot and a reference day, respectively. We control for the 1940 share of urban population made up of recent Black migrants, educational upward mobility and the share of the labor force in manufacturing. We include Census region fixed effects. Standard errors are clustered by commuting zone.

References

Akbar, P. A., Hickly, S. L., Shertzer, A. & Walsh, R. P. (2019), 'Racial segregation in housing markets and the erosion of black wealth', *The Review of Economics and Statistics* pp. 1–45.

Alsan, M., Garrick, O. & Graziani, G. (2019), 'Does diversity matter for health? experimental evidence from oakland', *American Economic Review* **109**(12), 4071–4111.

Andrews, R., Casey, M., Hardy, B. L. & Logan, T. D. (2017), 'Location matters: Historical racial segregation and intergenerational mobility', *Economics Letters* **158**, 67–72.

Arias, E., Heron, M. & Xu, J. (2017), 'United states life tables, 2014', **66**, 4.

Bailey, Z. D., Feldman, J. M. & Bassett, M. T. (2021), 'How structural racism worksâracist policies as a root cause of us racial health inequities'.

Banzhaf, S., Ma, L. & Timmins, C. (2019), 'Environmental justice: The economics of race, place, and pollution', *Journal of Economic Perspectives* **33**(1), 185–208.

Barreca, A., Clay, K., Deschênes, O., Greenstone, M. & Shapiro, J. S. (2015), 'Convergence in adaptation to climate change: Evidence from high temperatures and mortality, 1900–2004', *American Economic Review* **105**(5), 247–251.

Barreca, A., Clay, K., Deschênes, O., Greenstone, M. & Shapiro, J. S. (2016), 'Adapting to Climate Change: The Remarkable Decline in the US Temperature-Mortality Relationship over the Twentieth Century', *Journal of Political Economy* **124**(1), 105–159. Publisher: The University of Chicago Press.

Basu, R. & Samet, J. M. (2002), 'Relation between elevated ambient temperature and mortality: a review of the epidemiologic evidence', *Epidemiologic reviews* **24**(2), 190–202.

Bayer, P. & Timmins, C. (2005), 'On the equilibrium properties of locational sorting models', *Journal of Urban Economics* **57**(3), 462–477.

Beatty, T. K. & Shimshack, J. P. (2014), 'Air pollution and children's respiratory health: A cohort analysis', *Journal of Environmental Economics and Management* **67**(1), 39–57.

Benz, S. A. & Burney, J. A. (2021), 'Widespread race and class disparities in surface urban heat extremes across the united states', *Earth's Future* **9**.

Boustan, L. P. (2010), 'Was postwar suburbanization âwhite flightâ? evidence from the black migration', *The Quarterly Journal of Economics* **125**(1), 417–443.

Brock, W. A. & Durlauf, S. N. (2002), 'A multinomial-choice model of neighborhood effects', *American Economic Review* **92**(2), 298–303.

Card, D., Mas, A. & Rothstein, J. (2008), 'Tipping and the dynamics of segregation', *The Quarterly Journal of Economics* **123**(1), 177–218.

Carleton, T., Jina, A., Delgado, M., Greenstone, M., Houser, T., Hsiang, S., Hultgren, A., Kopp, R. E., McCusker, K. E., Nath, I. et al. (2022), 'Valuing the global mortality consequences of climate change accounting for adaptation costs and benefits', *The Quarterly Journal of Economics* **137**(4), 2037–2105.

Census Bureau (2022), 'Nation's urban and rural populations shift following 2020 census'. **URL:** *https://www.census.gov/newsroom/press-releases/2022/urban-rural-populations.html*

Chakma, T., Colmer, J. & Voorheis, J. (2023), 'Individual-level heat disparities in the united states'.

Chakraborty, T., Hsu, A., Manya, D. & Sheriff, G. (2020), 'A spatially explicit surface urban heat island database for the united states: Characterization, uncertainties, and possible applications', *ISPRS Journal of Photogrammetry and Remote Sensing* **168**, 74–88.

Christensen, P., Sarmiento-Barbieri, I. & Timmins, C. (2022), 'Housing discrimination and the toxics exposure gap in the united states: Evidence from the rental market', *Review of Economics and Statistics* **104**(4), 807–818.

Christensen, P. & Timmins, C. (2022), 'Sorting or steering: The effects of housing discrimination on neighborhood choice', *Journal of Political Economy* **130**(8), 2110–2163.

Colmer, J., Hardman, I., Shimshack, J. & Voorheis, J. (2020), 'Disparities in pm2. 5 air pollution in the united states', *Science* **369**(6503), 575–578.

Cui, T. (2022), 'The emergence of exclusionary zoning across american cities'.

Currie, J. & Neidell, M. (2005), 'Air pollution and infant health: what can we learn from california's recent experience?', *The Quarterly Journal of Economics* **120**(3), 1003–1030.

Currie, J., Voorheis, J. & Walker, R. (2020), What caused racial disparities in particulate exposure to fall? new evidence from the clean air act and satellite-based measures of air quality, Technical report, National Bureau of Economic Research.

Curriero, F. C., Heiner, K. S., Samet, J. M., Zeger, S. L., Strug, L. & Patz, J. A. (2002), 'Temperature and mortality in 11 cities of the eastern united states', *American journal of epidemiology* **155**(1), 80–87.

Cutler, D. M., Glaeser, E. L. & Vigdor, J. L. (1999), 'The rise and decline of the american ghetto', *Journal of political economy* **107**(3), 455–506.

Davidoff, T. (2015), 'Supply constraints are not valid instrumental variables for home prices because they are correlated with many demand factors', *Available at SSRN 2400833* .

Derenoncourt, E. (2022), 'Can you move to opportunity? evidence from the great migration', *American Economic Review* .

Deryugina, T. & Molitor, D. (2021), 'The causal effects of place on health and longevity', *Journal of Economic Perspectives* **35**(4), 147–170.

Deschênes, O. (2014), 'Temperature, human health, and adaptation: A review of the empirical literature', *Energy Economics* **46**, 606–619.

Deschênes, O. & Greenstone, M. (2011), 'Climate Change, Mortality, and Adaptation: Evidence from Annual Fluctuations in Weather in the US', *American Economic Journal: Applied Economics* **3**(4), 152–185.

Deschênes, O. & Moretti, E. (2009), 'Extreme weather events, mortality, and migration', *The Review of Economics and Statistics* **91**(4), 659–681.

Ganong, P. & Shoag, D. (2017), 'Why has regional income convergence in the us declined?', *Journal of Urban Economics* **102**, 76–90.

Grimmond, S. (2007), 'Urbanization and global environmental change: Local effects of urban warming', *The Geographical Journal* **173**(1), 83–88.

Gronlund, C. J. (2014), 'Racial and socioeconomic disparities in heat-related health effects and their mechanisms: a review', *Current epidemiology reports* **1**, 165–173.

Herkenhoff, K. F., Ohanian, L. E. & Prescott, E. C. (2018), 'Tarnishing the golden and empire states: Land-use restrictions and the us economic slowdown', *Journal of Monetary Economics* **93**, 89–109.

Heutel, G., Miller, N. H. & Molitor, D. (2021), 'Adaptation and the mortality effects of temperature across us climate regions', *Review of Economics and Statistics* **103**(4), 740–753.

Howard, L. (1818), *The climate of London: deduced from meteorological observations, made at different places in the neighbourhood of the metropolis*, Vol. 1, W. Phillips, George Yard, Lombard Street, sold also by J. and A. Arch â¦.

Hsieh, C.-T. & Moretti, E. (2019), 'Housing constraints and spatial misallocation', *American Economic Journal: Macroeconomics* **11**(2), 1–39.

Hsu, A., Sheriff, G., Chakraborty, T. & Manya, D. (2021), 'Disproportionate exposure to urban heat island intensity across major us cities', *Nature Communications* **12**(2721).

Huynen, M.-M., Martens, P., Schram, D., Weijenberg, M. P. & Kunst, A. E. (2001), 'The impact of heat waves and cold spells on mortality rates in the dutch population.', *Environmental health perspectives* **109**(5), 463–470.

IOM (2003), 'Unequal treatment: Confronting racial and ethnic disparities in health care'.

IPCC (2021), 'Climate change 2021: The physical science basis. contribution of working group i to the sixth assessment report of the intergovernmental panel on climate change'.

Kulka, A., Chiumenti, N. & Sood, A. (2023), 'How to increase housing affordability: Understanding local deterrents to building multifamily housing'.

Li, N. Y. (2023), 'Racial sorting, restricted choices, and the origins of racial segregation in the us'.

Mohai, P., Pellow, D. & Roberts, J. T. (2009), 'Environmental justice', *Annual review of environment and resources* **34**, 405–430.

Monarrez, T. & Schönholzer, D. (2022), 'Dividing lines: Racial segregation across local government boundaries', *Journal of Economic Literature* .

Murphy, S. L., Xu, J., Kochanek, K. D., Curtin, S. C. & Arias, E. (2017), 'Deaths: Final data for 2015', *National Vital Statistics Reports* **66**(6).

Ondrich, J., Stricker, A. & Yinger, J. (1998), 'Do real estate brokers choose to discriminate? evidence from the 1989 housing discrimination study', *Southern Economic Journal* **64**(4), 880–901.

Ondrich, J., Stricker, A. & Yinger, J. (1999), 'Do landlords discriminate? the incidence and causes of racial discrimination in rental housing markets', *Journal of Housing Economics* **8**(3), 185–204.

Rothstein, R. (2017), *The color of law: A forgotten history of how our government segregated America*, Liveright Publishing.

Sahn, A. (2023), Racial diversity and exclusionary zoning: Evidence from the great migration, Technical report, Working paper.

Shandas, V., Voelkel, J., Williams, J. & Hoffman, J. (2019), 'Integrating satellite and ground measurements for predicting locations of extreme urban heat', *Climate* **7**(1), 5.

Shanks, B. (2021), 'Land use regulations and housing development'.

Shertzer, A., Twinam, T. & Walsh, R. P. (2016), 'Race, ethnicity, and discriminatory zoning', *American Economic Journal: Applied Economics* **8**(3), 217–246.

Song, J. (2021), 'The effects of residential zoning in us housing markets', *Available at SSRN 3996483* .

Tabellini, M. (2020), 'Racial heterogeneity and local government finances: Evidence from the great migration', *Available at SSRN 3526044* .

Thompson, A. (2023), 'Why hot overnight temperatures are so dangerous'.
URL: *https://www.scientificamerican.com/article/why-hot-overnight-temperatures-are-so-dangerous/*

Trounstine, J. (2018), *Segregation by design: Local politics and inequality in American cities*, Cambridge University Press.

Turner, M. A., Haughwout, A. & Van Der Klaauw, W. (2014), 'Land use regulation and welfare', *Econometrica* **82**(4), 1341–1403.

Voorheis, J., Colmer, J., Houghton, K., Lyubich, E., Munro, M., Scalera, C. & Withrow, J. (2023), 'Building the prototype census environmental impacts frame', *US Census Bureau Center for Economic Studies Working Paper Series* (CES-23-20).

Williams, D. R. & Cooper, L. A. (2019), 'Reducing racial inequities in health: using what we already know to take action', *International journal of environmental research and public health* **16**(4), 606.

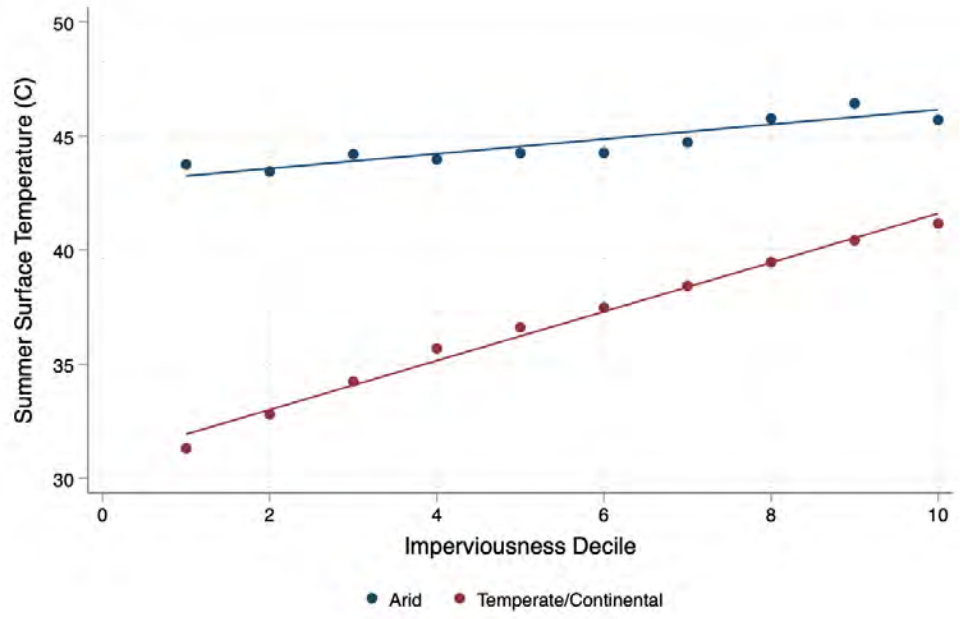
Yinger, J. (1986), 'Measuring racial discrimination with fair housing audits: Caught in the act', *The American Economic Review* pp. 881–893.

Zhao, L., Lee, X., Smith, R. B. & Oleson, K. (2014), 'Strong contributions of local background climate to urban heat islands', *Nature* **511**(7508), 216–219.

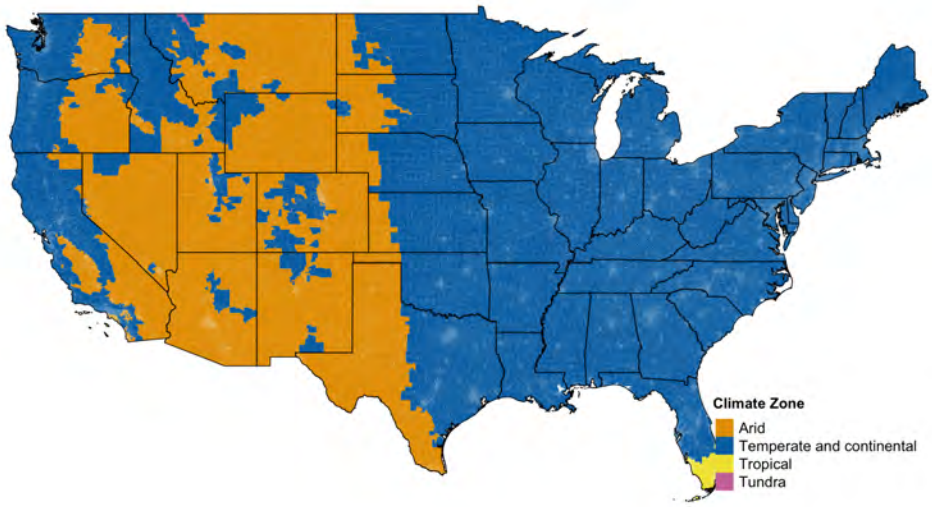
Appendices

A Additional figures and tables

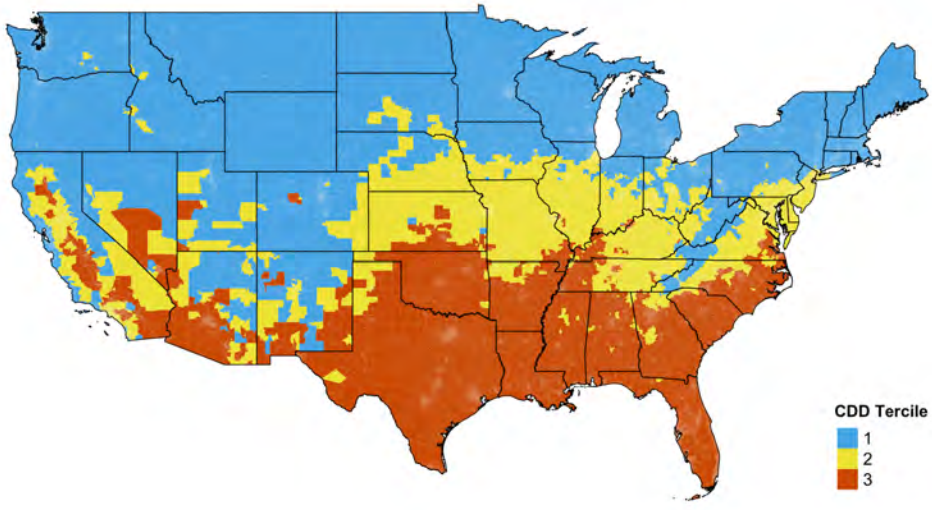
Figure A1: Relationship between summer land surface temperature and imperviousness, by climate zone



Note: This figure presents a binscatter of mean summer land surface temperature in 2019 by deciles of tract imperviousness (i.e., share of the land area covered in impervious surface) for arid and temperate or continental climate zones. The correlation between mean summer land surface temperature and imperviousness decile are 0.7 and 0.2, respectively, in temperate/continental and arid climates. Climate zones are defined based on the Köppen climate classification. Mean summer land surface temperature is calculated based on Landsat data.



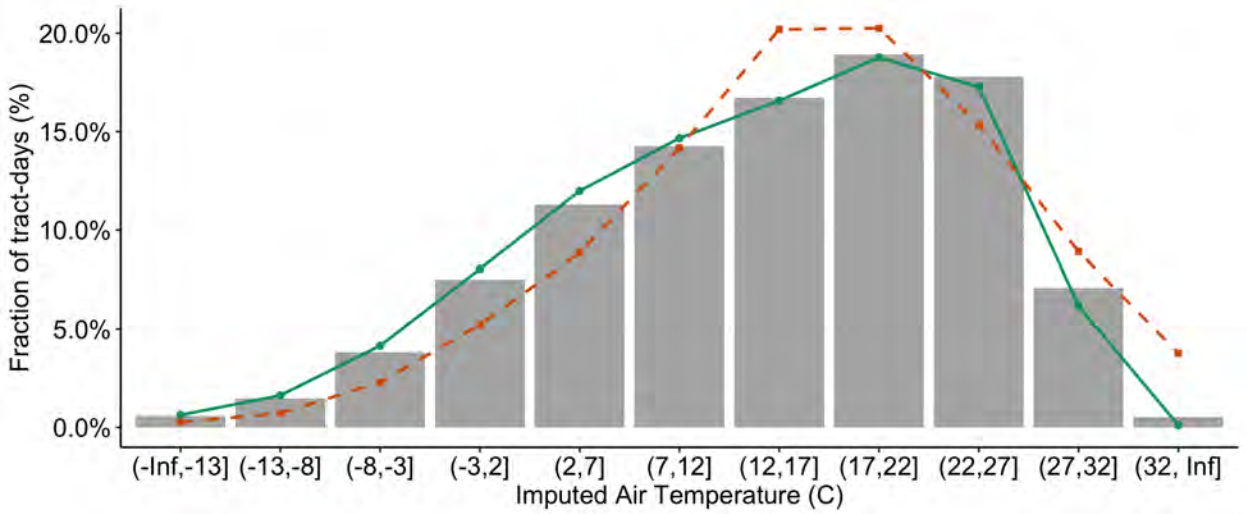
(a) Climate zones



(b) Average annual CDD

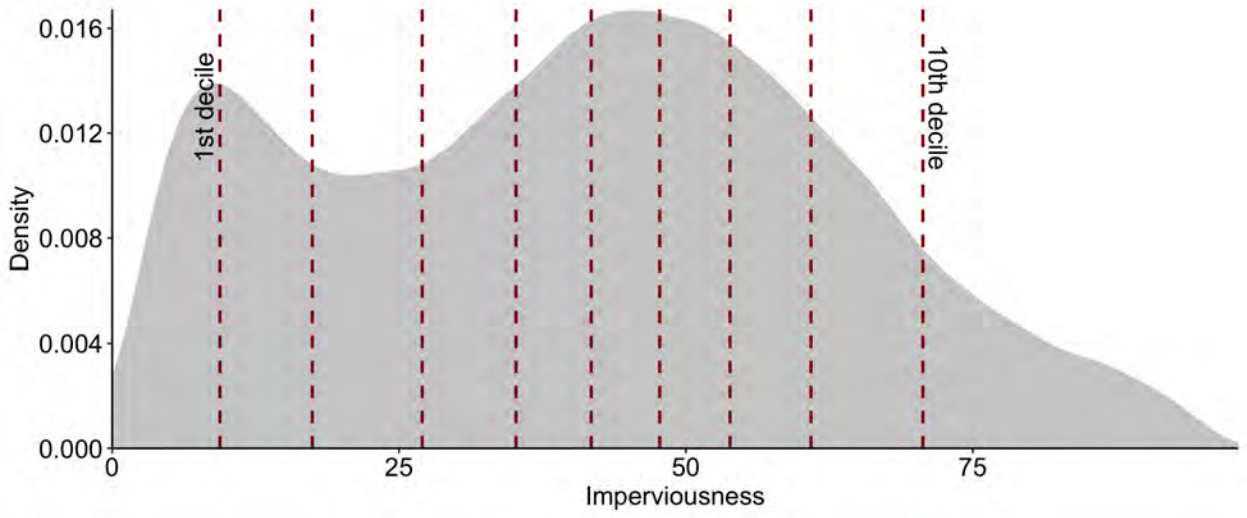
Note: Panel (a) presents a map of climate zones in contiguous United States under the Köppen climate classification system. Panel (b) presents a map of US census tracts by terciles of annual average Cooling Degree Days (CDD) over 2000–19.

Figure A3: U.S. Daily Average Temperature Distribution



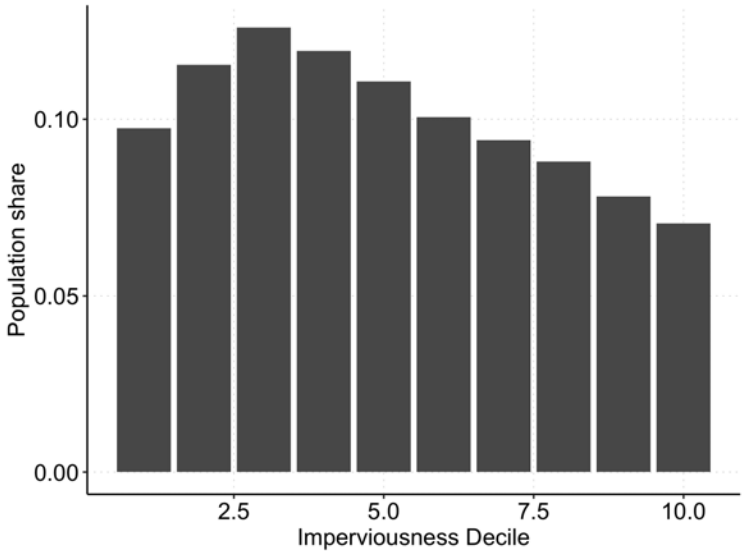
Notes: This figure summarizes the distribution of daily average temperature in the United States from 2000–2019. Distributions are reported separately for the entire United States and for arid and temperate or continental climates. The grey bars represent the distribution for all climates. The green solid line represents the distribution for temperate and continental climates. orange dashed line represents the distribution for arid climate zones. Daily temperature data come from the Global Historical Climatology Network (GHCN) land surface station database.

Figure A4: U.S Census Tract Imperviousness Distribution

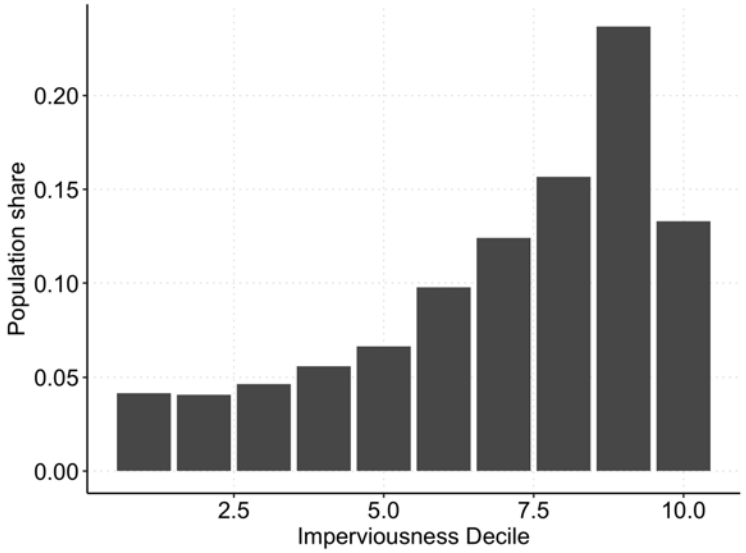


Notes: this figure summarizes the distribution of Census tract imperviousness for contiguous United States in 2019. Tract imperviousness is defined as the share of the tract's land area covered in impervius surfaces. This is calculated based on gridded data on imperviousness obtained from National Land Cover Database (NLCD). The red dashed lines present the deciles of the national distribution.

Figure A5: Population distribution across deciles of tract imperviousness, by climate zone

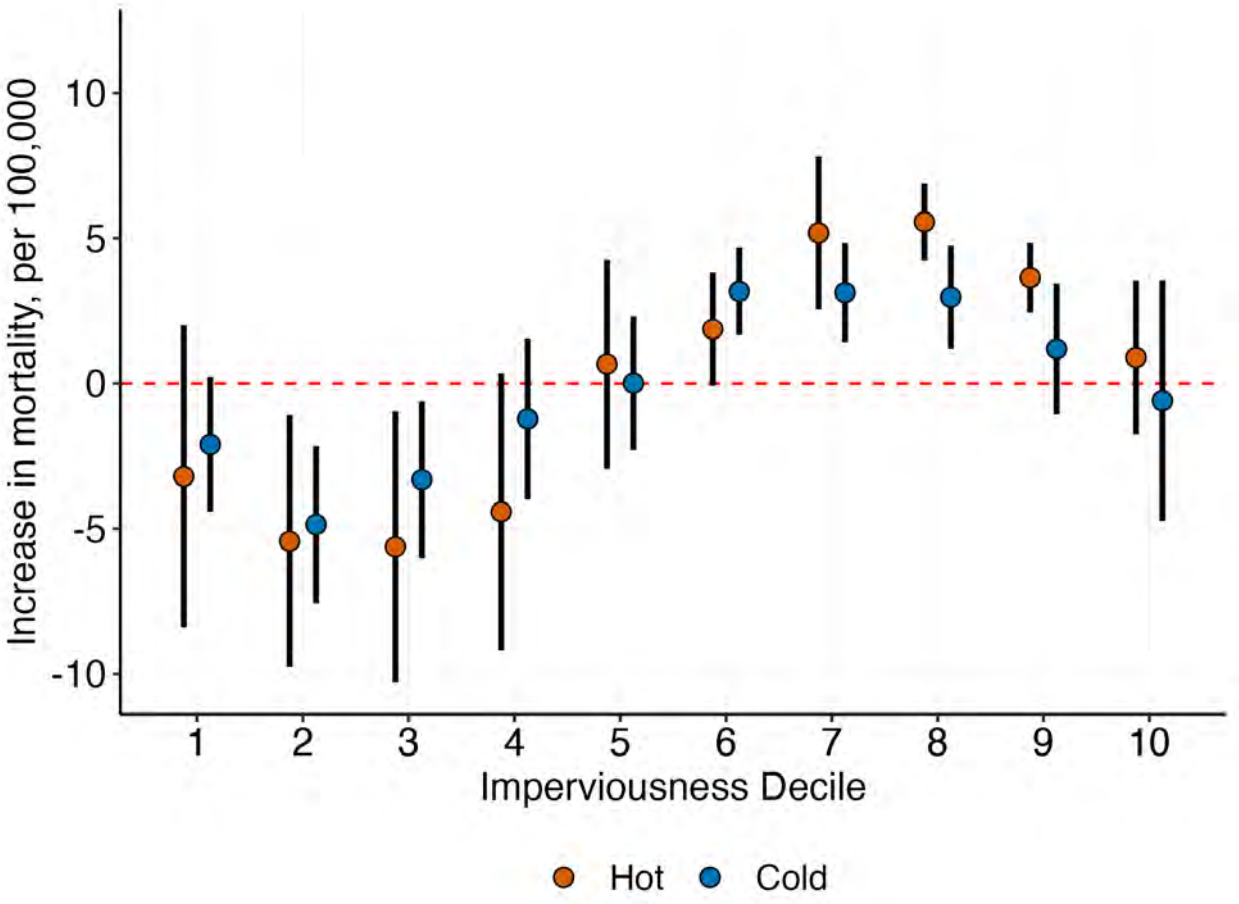


(a) Temperate and continental



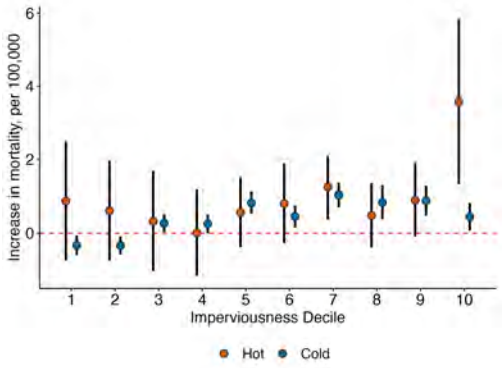
(b) Arid

Figure A6: Increase in over-65 mortality rates in hot days, arid climates

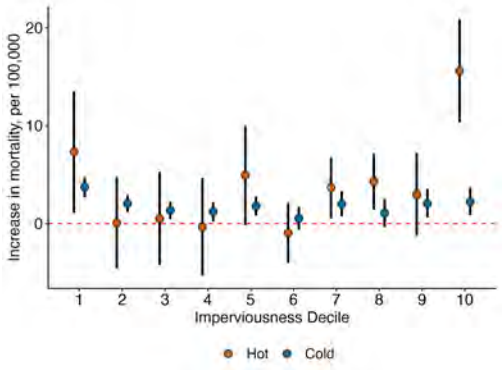


Notes: This figure plots estimated three-day mortality effects of a hot day for tracts in the arid climate zones for each decile of imperviousness. Imperviousness deciles are calculated based on the national distribution of tract imperviousness i.e., the share of the tract's area covered in impervious surfaces. The effects reflect excess mortality on a day over 32°C relative to a 17–22°C day. 95 percent confidence intervals are presented based on standard errors clustered at the county-level.

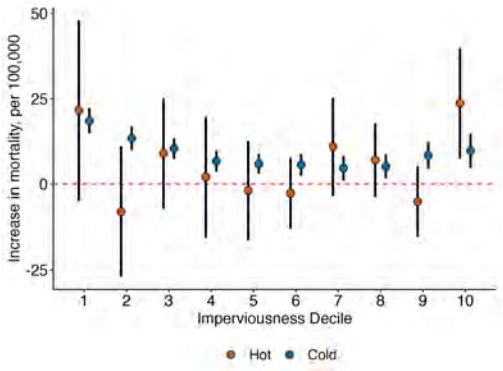
Figure A7: Increase in mortality rates on hot days by imperviousness decile: age bins above 65



(a) Age 65–74



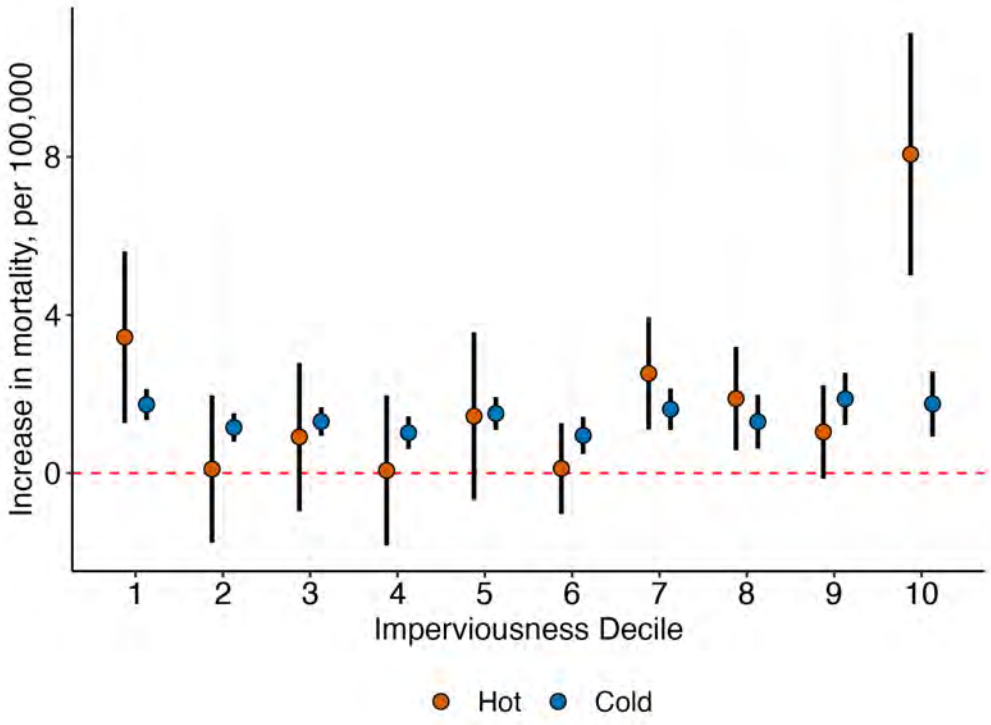
(b) Age 75–84



(c) Over 85

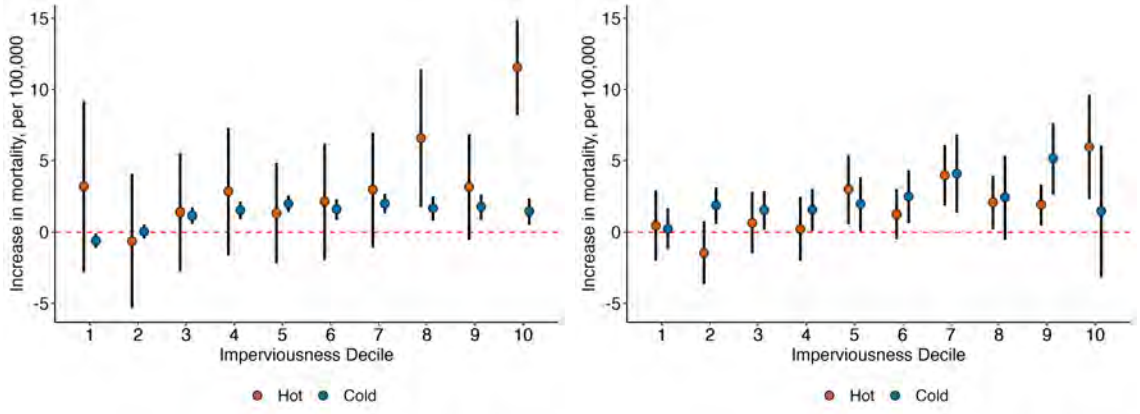
Note: This figure plots estimated three-day mortality effects of a hot day for temperate and continental climates for each decile of imperviousness. The effects reflect excess mortality on a day over 32°C relative to a 17–22°C day. 95 percent confidence intervals are presented based on standard errors clustered at the county-level.

Figure A8: Increase in over-65 mortality rates in hot days, pooled



Notes: This figure plots estimated three-day mortality effects of a hot day for tracts in the temperate and continental for each decile of imperviousness for the over 65 population, pooling three age bins over 65. The three age bins are 65–74. 75–84, and over 85. Imperviousness deciles are calculated based on the national distribution of tract imperviousness i.e., the share of the tract's area covered in impervious surfaces. The effects reflect excess mortality on a day over 32°C relative to a 17–22°C day. 95 percent confidence intervals are presented based on standard errors clustered at the county-level.

Figure A9: Increase in mortality rates on hot days by imperviousness decile: by CDD

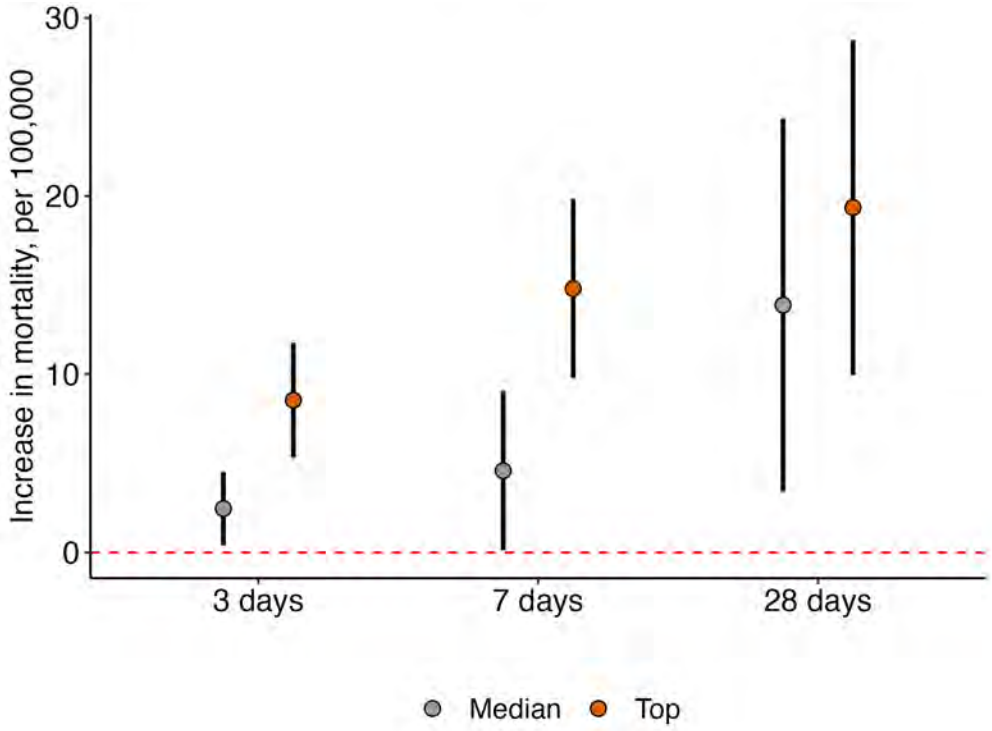


(a) Cooler terciles

(b) warmest terciles

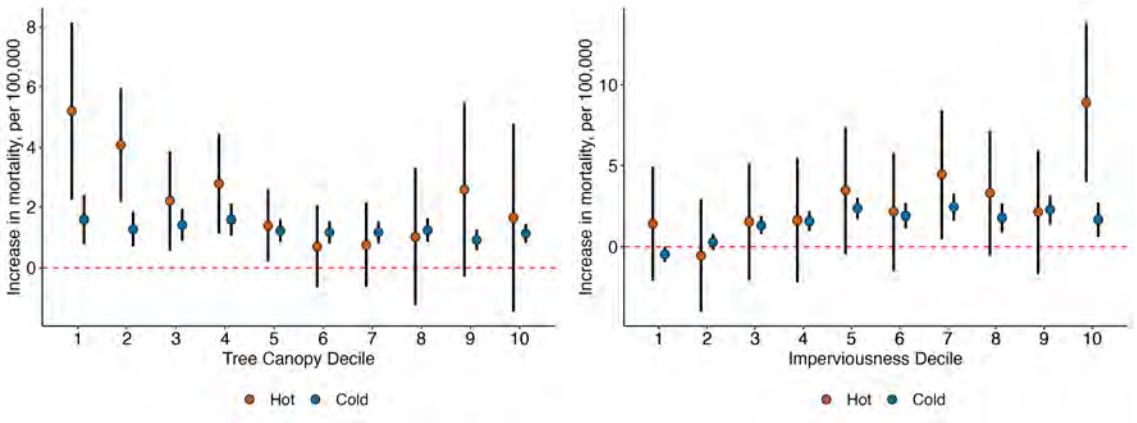
Note: This figure plots estimated three-day mortality effects of a hot day for temperate and continental climates for each decile of imperviousness by CDD. Panel (a) presents the estimates for tracts in the first and second terciles of CDD. Panel (b) presents the estimates for tracts with the warmest tercile of CDD. The effects reflect excess mortality on a day over 32°C relative to a 17–22°C day. 95 percent confidence intervals are presented based on standard errors clustered at the county-level.

Figure A10: Increase in mortality rates on hot days: three-, seven-, and 28-day mortality



Note: This figure plots estimated three-day, seven-day and 28-day mortality effects of a hot day for temperate and continental climates for the median and top decile of imperviousness. The effects reflect excess mortality on a day over 32°C relative to a 17–22°C day. 95 percent confidence intervals are presented based on standard errors clustered at the county-level.

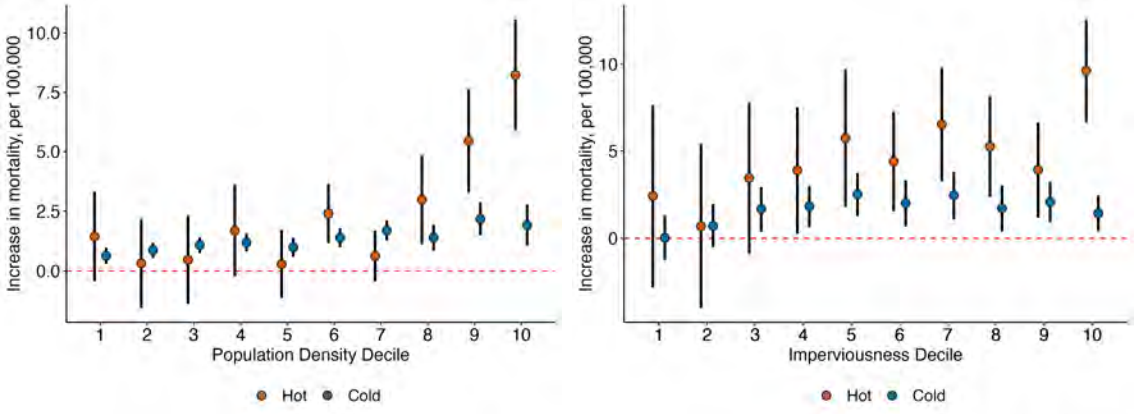
Figure A11: Increase in mortality rates: tree canopy



(a) By tree canopy decile (b) Controlling for tree canopy

Note: Panel (a) plots the estimated three-day mortality effects of a hot day for the over-65 population living in each decile of tree canopy cover. Panel (b) plots the estimated three-day mortality effects of a hot day for the over-65 population living in each decile of imperviousness, controlling for the effect of a hot day by deciles of tree canopy cover. The effects reflect excess mortality on a day over 32°C relative to a 17–22°C day. 95 percent confidence intervals are presented based on standard errors clustered at the county-level.

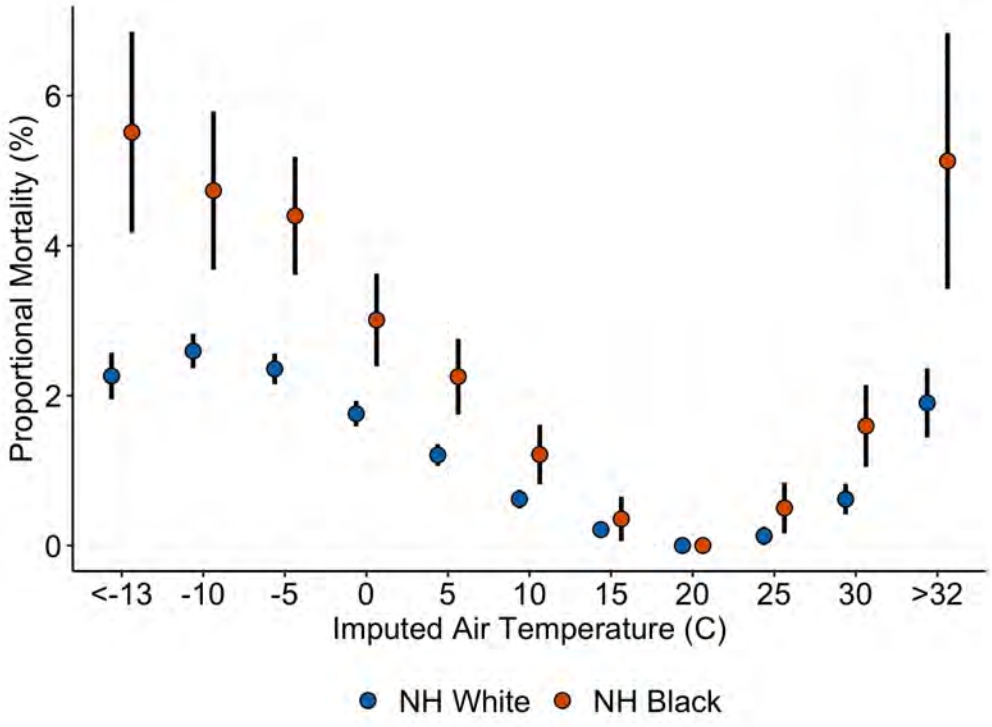
Figure A12: Increase in mortality rates: population density



(a) By pop. density decile (b) Controlling for pop. density

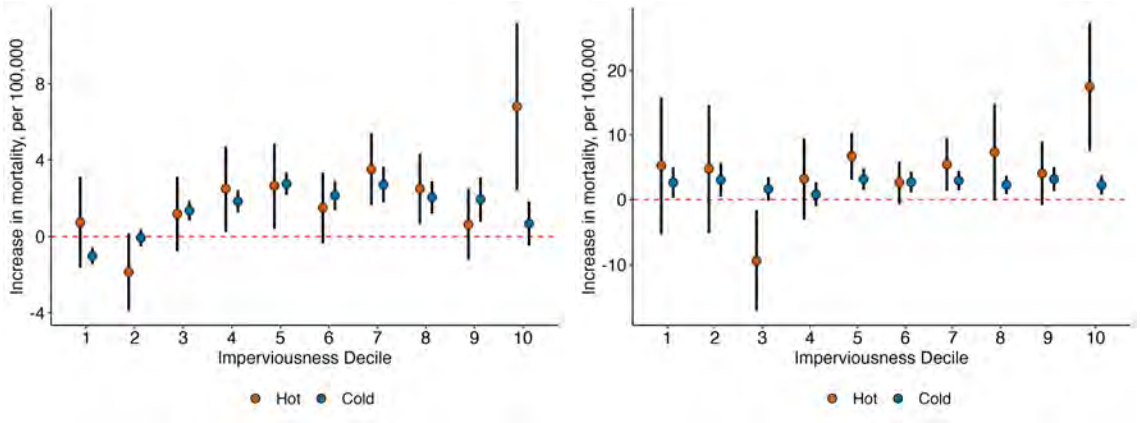
Note: Panel (a) plots the estimated three-day mortality effects of a hot day for the over-65 population living in each decile of population density. Panel (b) plots the estimated three-day mortality effects of a hot day for the over-65 population living in each decile of imperviousness, controlling for the effect of a hot day by deciles of population density. The effects reflect excess mortality on a day over 32°C relative to a 17–22°C day. 95 percent confidence intervals are presented based on standard errors clustered at the county-level.

Figure A13: Proportional Mortality Effects of Air Temperature: above 65, by race



Note: This figure plots estimated three-day mortality effects, as a percentage increase relative to baseline mortality, of temperature for the Non-Hispanic Black and White population over 65. The effects reflect excess proportional mortality on a day with a given average temperature relative to a day with an average temperature of 17–22°C. 95 percent confidence intervals are presented based on standard errors clustered at the county-level.

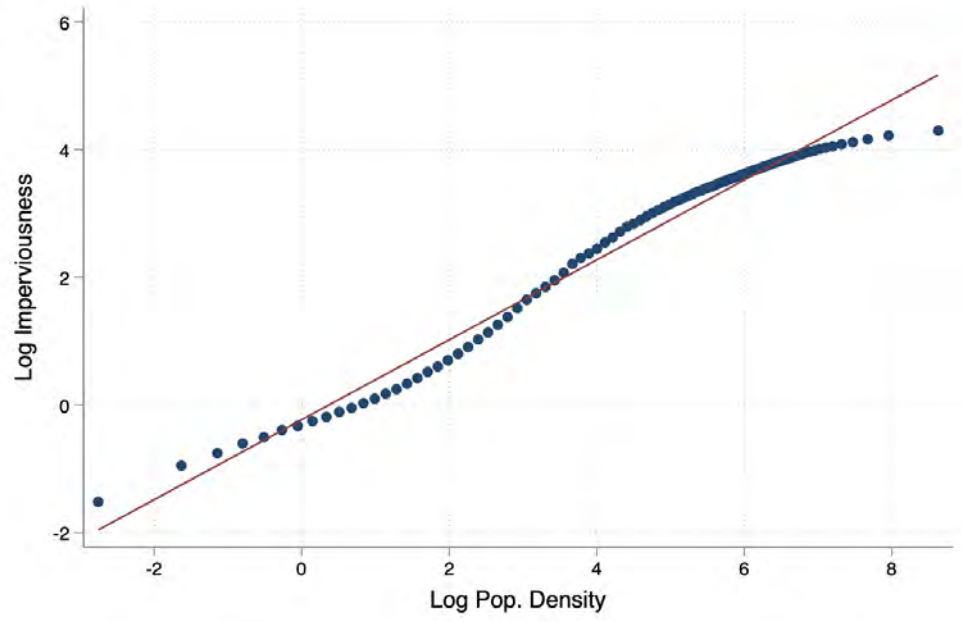
Figure A14: Increase in mortality rates on hot days by imperviousness decile: by race



(a) White (b) Black

Note: This figure plots estimated three-day mortality effects of a hot day for the over-65 Black and White population living in each decile of imperviousness by CDD. Panel (a) presents the estimates for White individuals over 65. Panel (b) presents the estimates for Black individuals over 65. The effects reflect excess mortality on a day over 32°C relative to a 17–22°C day. 95 percent confidence intervals are presented based on standard errors clustered at the county-level.

Figure A15: Relationship between Census-block log imperviousness and log population density



Note:

Figure A16: Trends in minimum lot size adoption from Cui (2023)

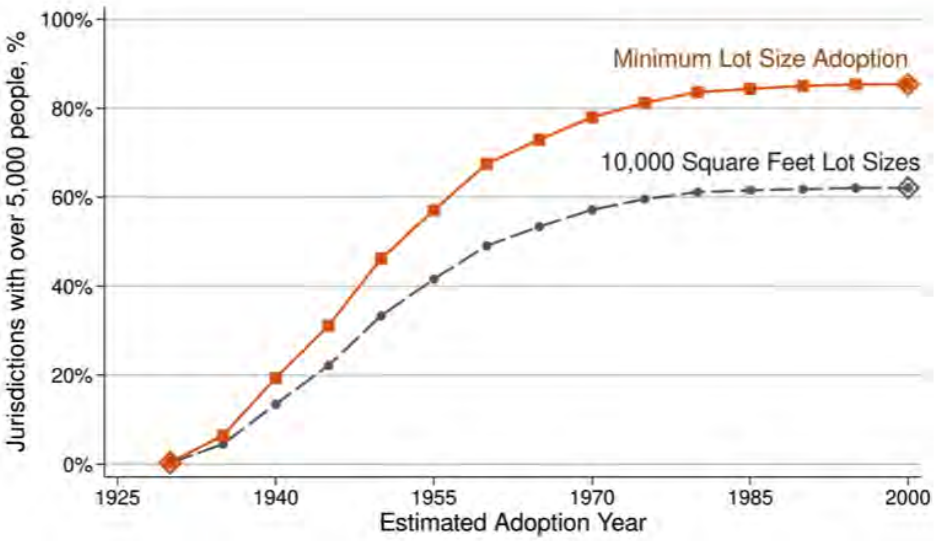
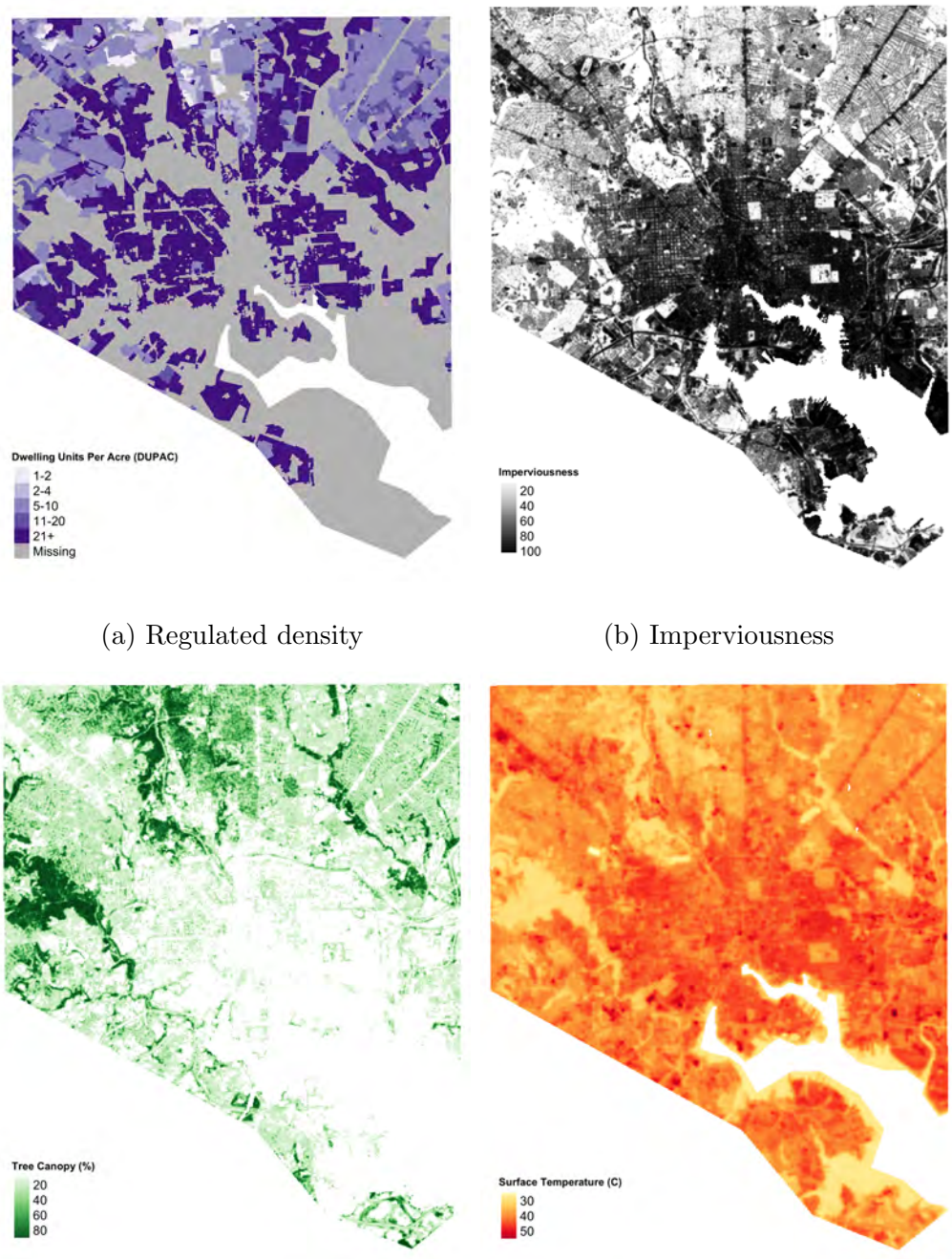


Figure A17: Baltimore case study



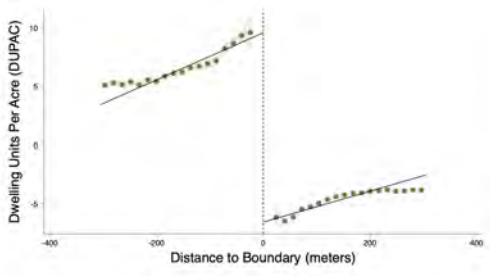
(a) Regulated density

(b) Imperviousness

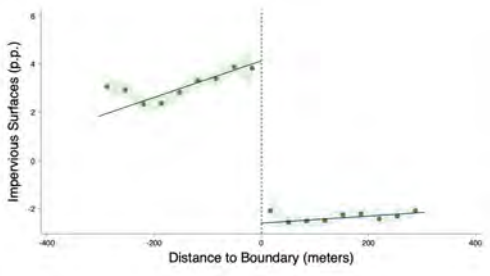
(c) Tree cover

(d) Land surface temperature

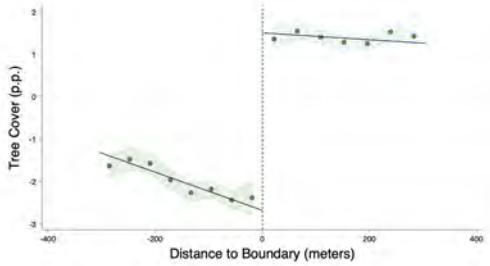
Figure A18: Baltimore: Regression discontinuities at regulation boundary



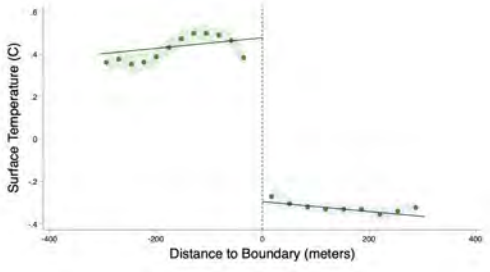
(a) Change in regulated density



(b) Change in imperviousness

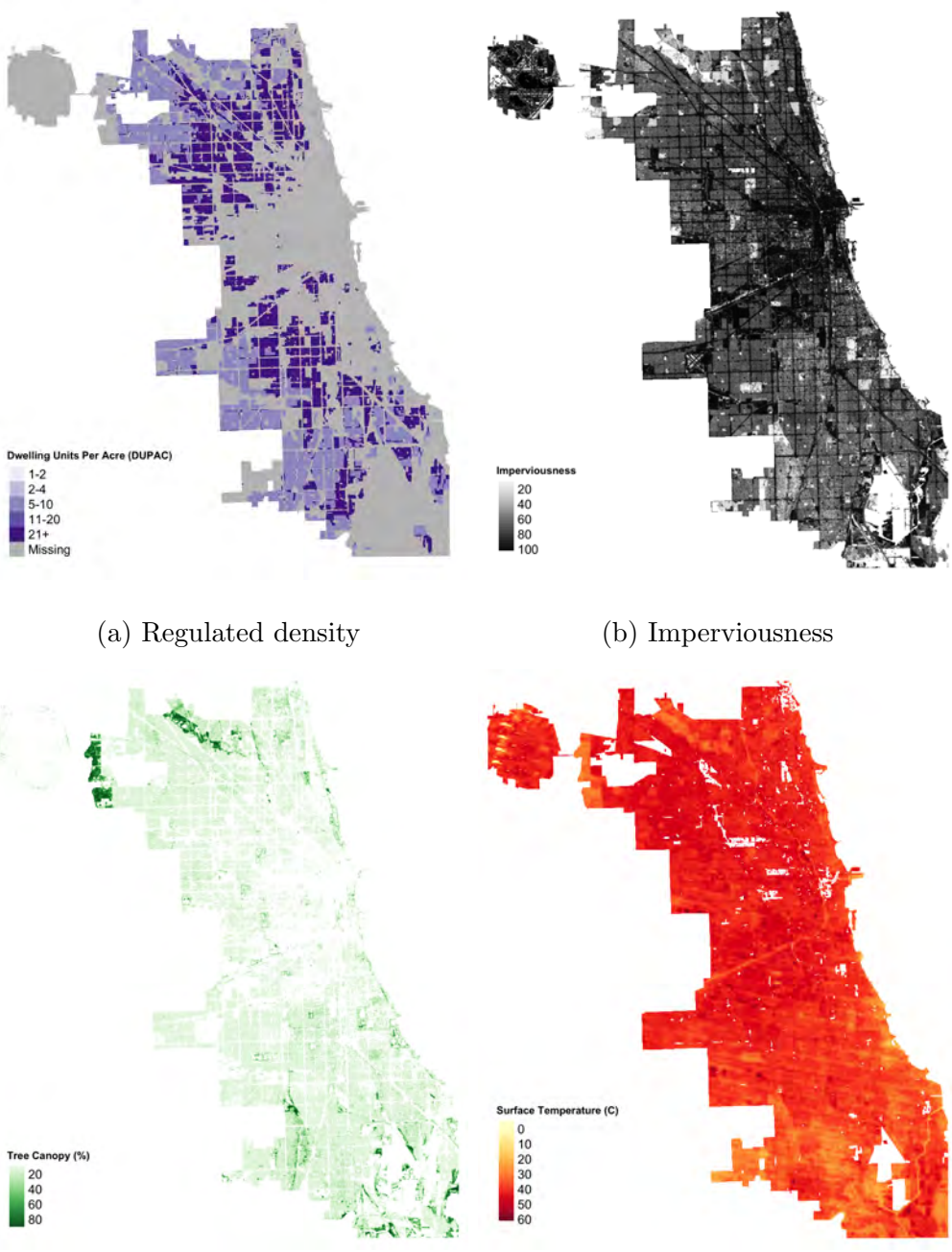


(c) Change in tree cover



(d) Change in land surface temperature

Figure A19: Chicago case study



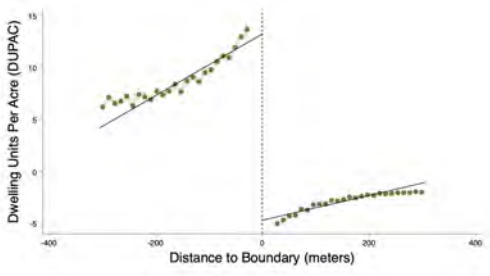
(a) Regulated density

(b) Imperviousness

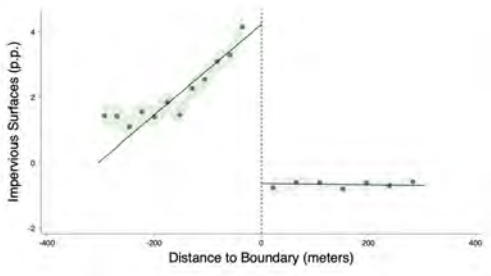
(c) Tree cover

(d) Land surface temperature

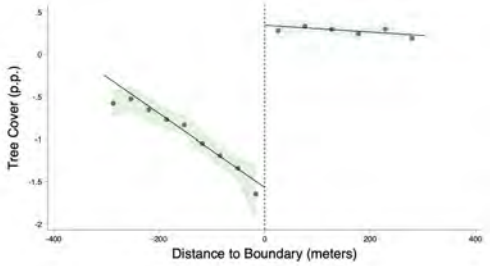
Figure A20: Chicago: Regression discontinuities at regulation boundary



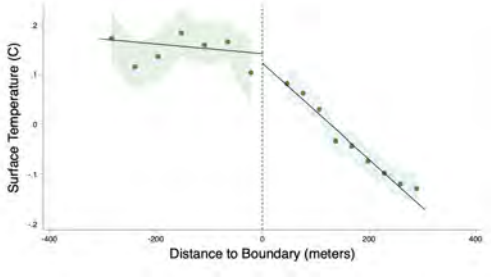
(a) Change in regulated density



(b) Change in imperviousness

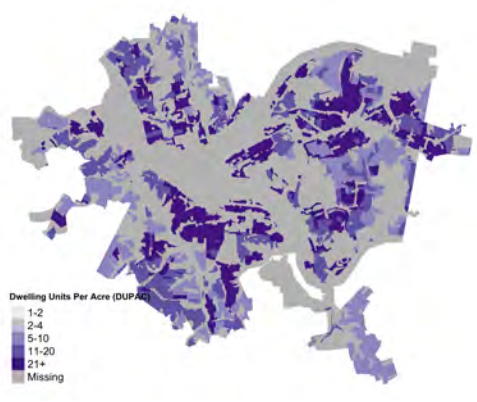


(c) Change in tree cover



(d) Change in land surface temperature

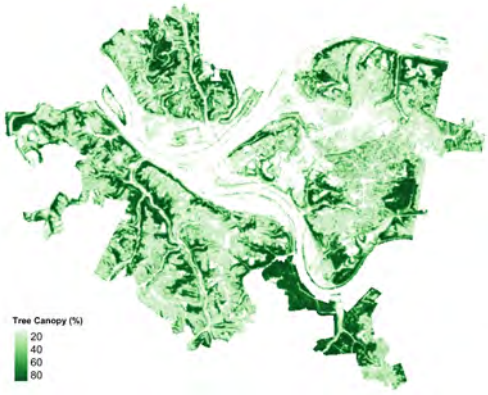
Figure A21: Pittsburgh case study



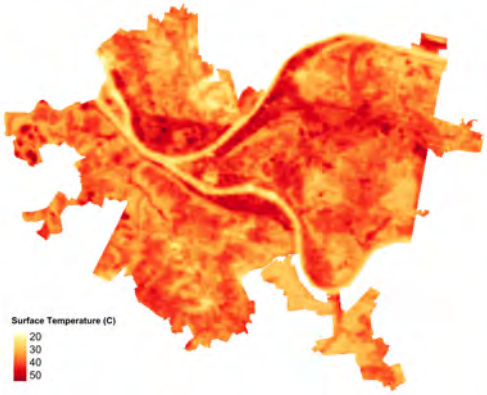
(a) Regulated density



(b) Imperviousness

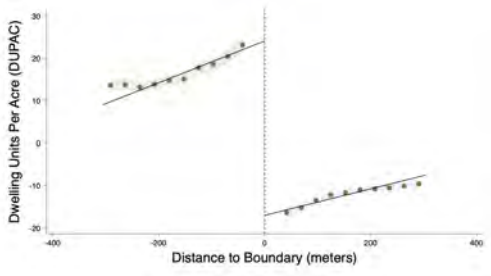


(c) Tree cover

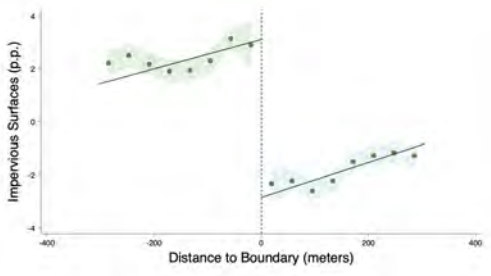


(d) Land surface temperature

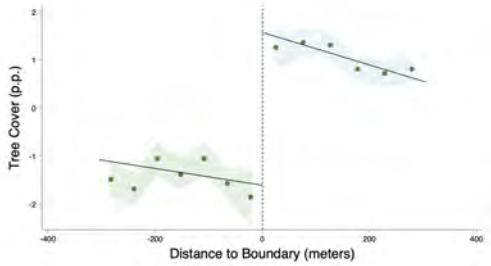
Figure A22: Pittsburgh: Regression discontinuities at regulation boundary



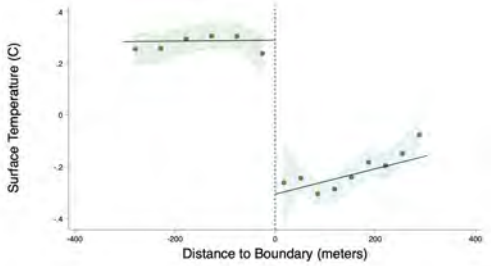
(a) Regulated density



(b) Imperviousness



(c) Tree canopy cover



(d) Land surface temperature

Table 5: RD estimates: Baltimore case study

	DUPAC	Tree Cover	Imperviousness	Temperature
β_{RD}	-18.29***	4.22***	-6.91***	-0.58***
	(0.450)	(0.264)	(0.313)	(0.042)
Observations	235378	229378	229378	235378
Mean of Dep. Var.	27.5	32.2	40.1	38.0

Table 6: RD estimates: Chicago case study

	DUPAC	Tree Cover	Imperviousness	Temperature
β_{RD}	-18.73***	1.91***	-4.86***	-0.02
	(0.216)	(0.138)	(0.267)	(0.046)
Observations	183596	164971	183596	183400
Mean of Dep. Var.	15.9	14.5	61.6	39.1

Table 7: RD estimates: Pittsburgh case study

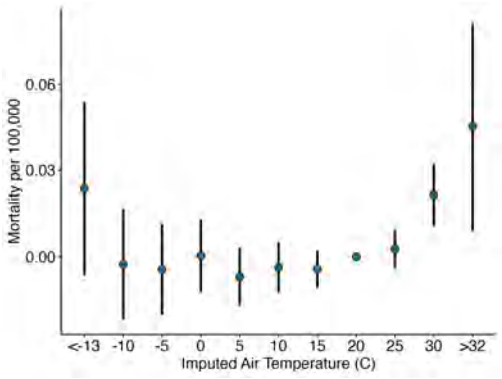
	DUPAC	Tree Cover	Imperviousness	Temperature
β_{RD}	-44.1***	3.40***	-6.16***	-0.29***
	(2.060)	(0.521)	(0.611)	(0.123)
Observations	81500	81500	87251	88094
Mean of Dep. Var.	32.4	14.5	58.8	39.1

B Results for under 5 and age 5–64

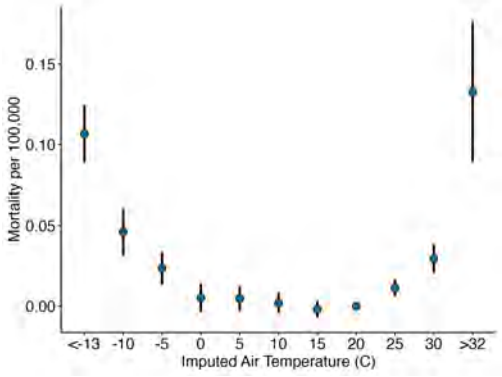
Figure B1 presents the effects of imputed temperature on mortality for the populations below 5 and age 5–64. A hot day increases the mortality rates by 0.05 and 0.13 deaths per 100,000 for those below 5 and those aged 5–64, respectively. Mean mortality rates for these age groups are 0.2 and 2.3 per 100,000, respectively.

Figure B2 presents the estimates of $\beta_{d,hot}$ from equation 2 for the 5–64 age group. A hot day increases the mortality by 0.24 deaths per 100,000 in the median decile and 0.06 deaths per 100,000 in the top decile of Census tracts by imperviousness. The mean mortality rate for the 5–64 age group is 2.3 deaths per 100,000. For this age group, a hot day also increases mortality in the lowest decile of imperviousness. We hypothesize that agricultural workers, who are exposed to outdoor temperature, but work on land that is not impervious, may explain this. Figure B3 presents the estimates of $\beta_{d,hot}$ from equation 2 for the under 5 age group. We are not able to detect any relationship between imperviousness and excess mortality for children under 5. One plausible explanation is that parents of young children may be likely to engage in adaptation behavior, and excess deaths on hot days may be driven by co-morbidities rather than differences in exposure due to imperviousness.

Figure B1: Baseline Temperature–Mortality Relationship



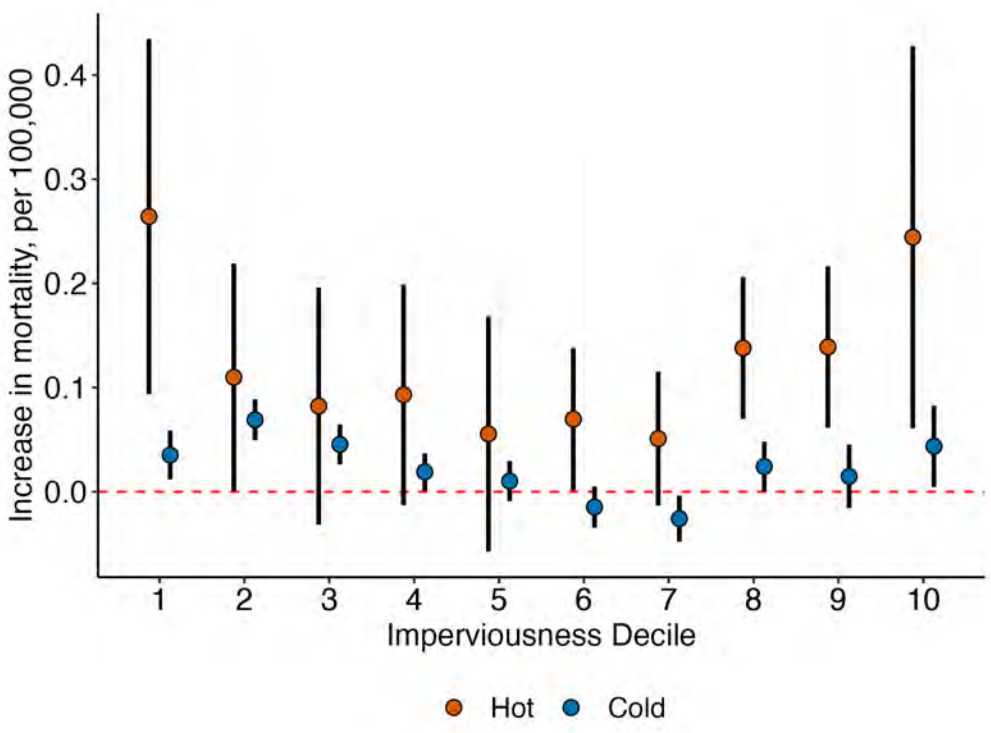
(a) Below 5 years



(b) 5–64 years

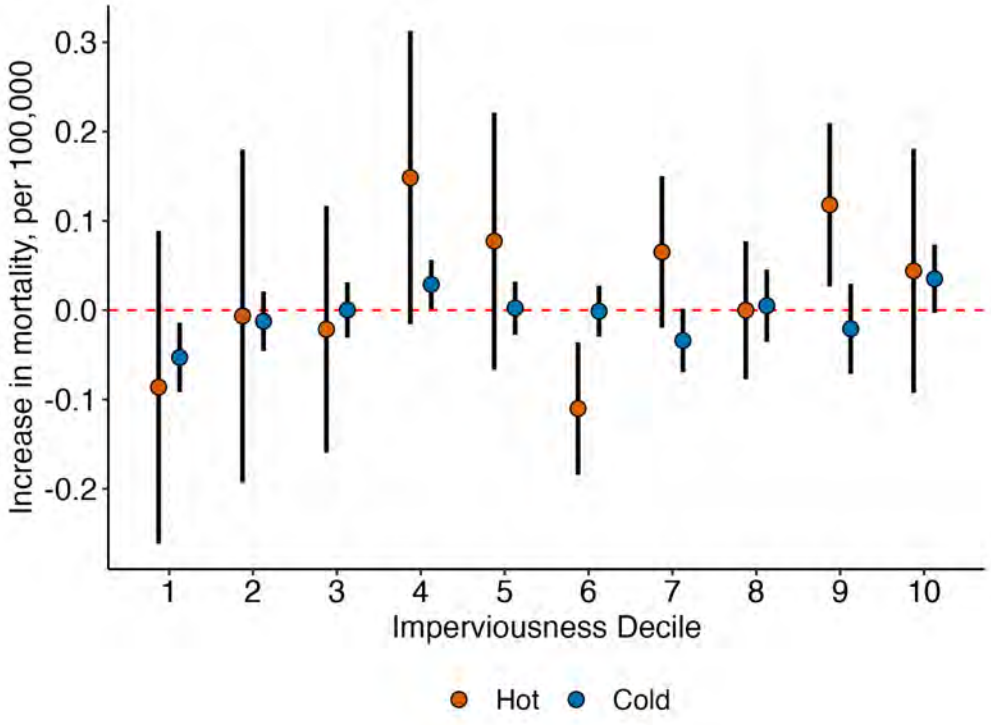
Note: This figure plots estimated three-day mortality effects of temperature by age group for individuals living in temperate or continental climates. 85 percent of the U.S. population live in temperate or continental climates. The effects reflect excess mortality on a day with a given average temperature relative to a day with an average temperature of 17–22°C. Panels (a) and (b) present the coefficients for the below 5 and 5–64 populations, respectively. 95 percent confidence intervals are presented based on standard errors clustered at the county-level.

Figure B2: Increase in mortality rates on hot and cold days by imperviousness decile, age 5–64



Note: This figure plots estimated three-day mortality effects of a hot day, as well as a cold day, for tracts in the temperate or continental climate zones for each decile of imperviousness. Imperviousness deciles are calculated based on the national distribution of tract imperviousness i.e., the share of the tract's area covered in impervious surfaces. The hot day coefficients reflect excess mortality on a day over 32°C (i.e., over 90°F) relative to a 17–22°C day. The cold day coefficients reflect excess mortality on a day between -13°C to -8°C (i.e., 9–18°F) relative to a 17–22°C (i.e., 63–72°F) day. 95 percent confidence intervals are presented based on standard errors clustered at the county-level.

Figure B3: Increase in mortality rates on hot and cold days by imperviousness decile, below 5



Note: This figure plots estimated three-day mortality effects of a hot day, as well as a cold day, for tracts in the temperate or continental climate zones for each decile of imperviousness. Imperviousness deciles are calculated based on the national distribution of tract imperviousness i.e., the share of the tract's area covered in impervious surfaces. The hot day coefficients reflect excess mortality on a day over 32°C (i.e., over 90°F) relative to a 17–22°C day. The cold day coefficients reflect excess mortality on a day between -13°C to -8°C (i.e., 9–18°F) relative to a 17–22°C (i.e., 63–72°F) day. 95 percent confidence intervals are presented based on standard errors clustered at the county-level.

C A simple spatial model of neighborhood choice under restricted choices

Black migrants choose from a restricted set of neighborhoods, driving up housing prices in those neighborhoods (if supply is upward sloping), prompting some White households to leave those neighborhoods in response. If Whites exhibit distaste for racial diversity, neighborhoods with greater initial Black share will see increases in density in response to a large Black migration shock.[36] Individual i of race $r \in \{B, W\}$ chooses neighborhood $j \in J_c$ from a set of neighborhoods in city c. Indirect utility is given by $\nu_{ij} = \delta_{rj} + \varepsilon_{ij}$, where δ_{rj} is a race-specific mean and ε_{ij} refers to idiosyncratic deviations from the race-specific mean for an individual i. Black individuals choose from a restricted choice set, i.e., from a subset of neighborhoods $J_{cB} \in J_c$, whereas White individuals choose from the entire set of neighborhoods, J_c.

Let $\delta_{ij} = \beta_r lnR_j + \gamma_r s_j + \xi_{rj}$ where R_j is local housing prices and s_j is the neighborhood share of Black population. Assuming that ε_{ij} follows a type 1 extreme value distribution, the choice probabilities, i.e., the probability that a person of race r chooses neighborhood j, are given by:

$$\pi_{rj} = \frac{exp(\delta_{rj})}{\sum_{k \in J_{cr}} exp(\delta_{rk})}$$

The log of the choice probabilities can be written as:

$$\ln \pi_{rj} = -\theta_{rc} + \beta_r lnR_j + \gamma_r s_j + \xi_{rj}$$

where $\theta_{Bc} = \sum_{k \in J_{cB}} exp(\delta_{Bk})$ and $\theta_{Wc} = \sum_{k \in J_c} exp(\delta_{Wk})$ are the race-specific intercepts.

Let total population in the neighborhood Q_j be the sum of the neighborhood's Black and White populations: $Q_j = Q_{Bj} + Q_{Wj}$ so that the neighborhood Black population share is $s_j = \frac{Q_{Bj}}{Q_j}$. Let the total population of the city be the sum of the city's Black and White population: $N = N_B + N_W$. Therefore, $Q_{rj} = N_r \cdot \pi_{rj}$. Holding land area constant, the density of a neighborhood is simply Q_j. Housing supply is defined by elasticity $\lambda_j = \frac{\partial \ln R_j}{\partial \ln Q_j}$ where $\lambda = 0$ implies perfectly elastic supply. Now consider the arrival of a Black migrant in city c. What happens to the population of neighborhood j when a Black migrant arrives in the city c? The effect on the total population in neighborhood j is the sum of the effect on

[36] The model presented in this section is adapted from Li (2023) and related to the models presented by Bayer & Timmins (2005) and Brock & Durlauf (2002).

the Black and White populations:

$$\frac{\partial Q_j}{\partial N_B} = \frac{\partial Q_{Bj}}{\partial N_B} + \frac{\partial Q_{Wj}}{\partial N_B}$$

$$\frac{\partial Q_j}{\partial N_B} = \pi_{Bj} + Q_{Bj}\frac{\partial \ln \pi_{Bj}}{\partial N_B} + Q_{Wj}\frac{\partial \ln \pi_{Wj}}{\partial N_B}$$

Assume weak homophily, i.e., $\gamma_B \geq 0$ and $\gamma_W \leq 0$. Whites display some distaste for racial diversity. The effect of a Black migrant on log choice probabilities is:

$$\frac{\partial \ln \pi_{rj}}{\partial N_B} = \frac{1}{Q_j}\left[(\beta_r \lambda_j - \gamma_r s_j)\frac{\partial Q_{Wj}}{\partial N_B} + (\beta_r \lambda_j + \gamma_r(1-s_j))\frac{\partial Q_{Bj}}{\partial N_B}\right]$$

Re-writing the effect of a Black migrant on neighborhood population for $j \in J_{cB}$:

$$\frac{\partial Q_j}{\partial N_B} = \pi_{Bj} + s_j \cdot \left(a_B \frac{\partial Q_{Wj}}{\partial N_B} + b_B \frac{\partial Q_{Bj}}{\partial N_B}\right) + (1-s_j) \cdot \left(a_W \frac{\partial Q_{Wj}}{\partial N_B} + b_W \frac{\partial Q_{Bj}}{\partial N_B}\right)$$

where $a_r = \beta_r \lambda_j - \gamma_r s_j$ and $b_r = \beta_r \lambda + \gamma_r(1-s_j)$ are decreasing in s_j. The first-term is a first order demand response from Black migrants, the second term is a second order response from Black residents and migrants, the third term captures the White departure effects. The White departure effect depends on both demand and supply elasticities, as well as on White distaste for racial diversity, γ_W.

Li (2023) shows that if White distaste for racial diversity is sufficiently small, then neighborhood population decreases in response to Black migrants regardless of the initial black share, i.e., $\frac{\partial Q_j}{\partial N_B} \geq 0 \ \forall s_j$. This result is intuitive—if White individuals do not exhibit strong distaste, then the magnitude of the White departure effect depends only on rent increases. With strong White distaste for racial diversity, the White outmigration effect depends on the initial Black-share of the neighborhood. The White outmigration effect is small if s_j is sufficiently large, i.e., $\frac{\partial Q_j}{\partial N_B} \geq 0$ for $s_j > \bar{s}$, for some threshold $\bar{s}$. Mechanically, in the extreme case, if the initial White population is zero and the neighborhood Black population share, $s_j = 1$, then the White departure effect is zero.

In general, if the Black population share s_j is large, then the positive effect on Black population will dominate the negative effect on White population, leading to greater density in neighborhoods with positive initial Black population share. From this reasoning, we can conclude that *if Whites exhibit distaste for racial diversity, Black migration to a city will lead to greater density in neighborhoods with a larger initial Black population share, while the effect on neighborhoods with small Black population share is ambiguous.*